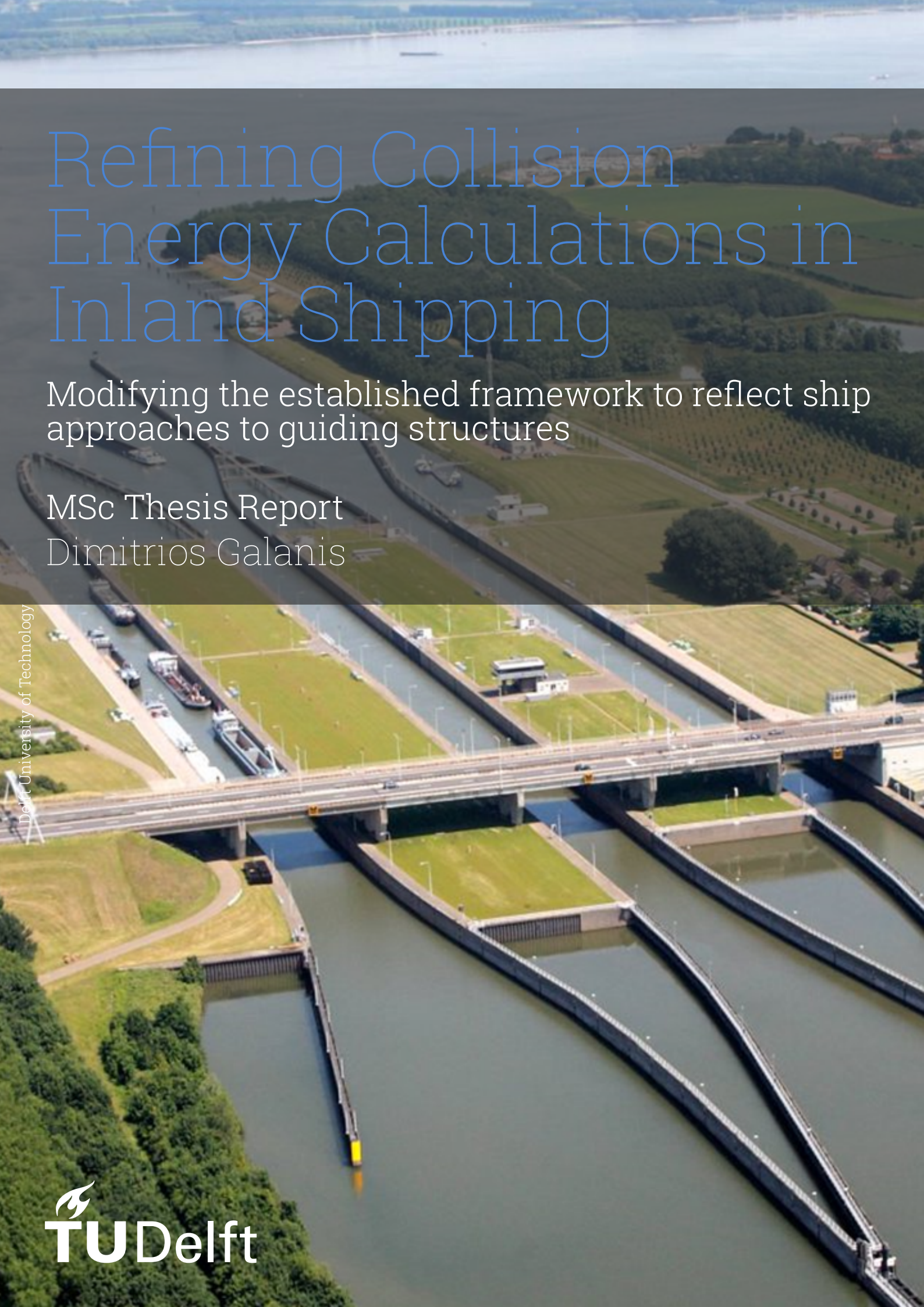

Refining Collision Energy Calculations in Inland Shipping

Modifying the established framework to reflect ship approaches to guiding structures

MSc Thesis Report

Dimitrios Galanis

Delft University of Technology

TU Delft

Refining Collision Energy Calculations in Inland Shipping

Modifying the established framework to reflect ship approaches to guiding structures

by

Dimitrios Galanis

to obtain the degree of Master of Science

at the Delft University of Technology,

to be defended publicly on Thursday September 12th, 2024 at 16:00 PM.

Student number:	5366569	
Project duration:	June 9th, 2023 – September 12th, 2024	
Thesis committee:	Prof. dr. ir. Mark van Koningsveld,	TU Delft
	Ir. Bas Horsten,	Witteveen+Bos
	Ir. Lex de Boom,	Witteveen+Bos / TU Delft
	Ir. Arne, J., van der Hout	TU Delft
	Dr. ir. Bas Hofland,	TU Delft

TU Delft

Witteveen + Bos

Preface

This thesis report serves as my final academic obligation before obtaining my MSc degree in Civil Engineering at Delft University of Technology. This research is carried out under a graduation internship agreement involving myself, the university, and Witteveen+Bos

Starting with the acknowledgements, I would like to first thank my daily supervisor at Witteveen+Bos, Bas Horsten, for his steadfast support and availability throughout my final academic endeavor. I am also deeply grateful to the rest of my committee members: Lex de Boom, for providing me with feedback and acting as first audience along with Bas before I presented to the entire committee; Arne van der Hout, who took the time for long and insightful conversations about my thesis topic; Bas Hofland, for his enthusiasm about my research and valuable advice; and Mark van Koningsveld, who chairs the committee and has consistently provided me with insightful feedback at every meeting.

Dimitrios Galanis
Rotterdam, September 2024

Abstract

The key parameters governing collision energy calculation are the velocity of the vessel, its mass, and the angle of approach. The conventional method outlined in the Recommendations of the Committee for Waterfront Structures Harbours and Waterways (EAU, 2012), which was specifically developed for berthing ships, relies on an overly simplistic model that fails to capture the dynamics of ship-to-guiding structure collisions. Nevertheless, in the Netherlands, the Guidelines for Civil Engineering Structures (Richtlijnen Ontwerp Kunstwerken, ROK) suggest that the EAU 2012 method be applied unmodified for guiding structures. This report introduces a methodological approach aimed at refining the calculation of collision energy by addressing specific deficiencies in the existing framework, particularly regarding its application to guiding structures.

The kinetic energy approach used in the EAU 2012 method requires, as inputs, the mass of the ship, its velocity vector normal to the structure, a virtual mass coefficient accounting for water mass moving with the ship, and an eccentricity coefficient accounting for energy loss due to rotation when the ship does not approach the structure parallel.

The literature review identifies critical gaps in the EAU 2012 approach to calculating collision energy for guiding structures. An unsuitable application of the eccentricity coefficient and assumptions about the velocity vector direction, which do not align with actual conditions in ship-to-guiding structure collisions, are discovered. Moreover, the review reveals that the framework does not differentiate between berthing and guiding approaches, resulting in a one-size-fits-all approach that fails to account for the unique characteristics and requirements of guiding structures. The framework only partially includes the ship's angle of approach to the structure in the kinetic energy calculation. Although the recommendation is to calculate the kinetic energy using the normal ship speed to the structure—thus indirectly accounting for the approach angle—when it comes to the eccentricity coefficient, which relies on approach geometry, the recommendation is to consider the total velocity vector. This practice results in exaggerated collision energy when a ship maintains forward speed near guiding structures while passing through the lock.

The theoretical refinement proposed in this thesis focuses on the scenario where the ship approaches a guiding structure with purely longitudinal speed. Specifically, a new definition for the angle variable in the eccentricity coefficient expression is proposed, which directly reflects the effect of the approach angle of the ship linked to the contributing velocity vector and not only laterally through the magnitude of the contributing vector. This proposed change is validated through comparative analysis.

The comparative analysis is performed using historical data cases from model research published by Rijkswaterstaat (Ministry of Infrastructure and Water Management). The data consist of experiments with ship approaches to structures that have characteristics fitting guiding structure approaches. The ships are of lengths commonly found in lock passages, maintain forward speed, and approach structures similar to those at lock entrances. The historical data provide the maximum force exerted on the tested structure and the resulting deflection. This information is used to derive the energy absorbed by the structure. The published reports valuable to this research resulted in the Virtual Water Mass method. This method is reproduced to provide benchmark values for the kinetic energy absorbed, which are compared to both the EAU 2012 collision energy calculation and the proposed refined calculation for the historical data cases.

The findings of the comparative analysis suggest that the proposed refined calculation provides results closer to the benchmark values than the EAU 2012 calculation. However, a consistent improvement was not discovered. Although the refined calculation is significantly closer to the benchmark value in every case compared to the EAU 2012 calculation, this improvement cannot be quantified as a universal percentage, as it varied for each case. Despite this, the comparative analysis still supports the main objective of demonstrating the exaggeration in the EAU 2012 collision energy calculation.

A case study, as part of this research, explores the potential effect of the refined calculation on an actual structure design. In the case study, the design vessel, velocity, and angle of approach are sourced from the Waterway Guidelines (2011, 2020) and ROK 2.0 (all documents published by Rijkswaterstaat). After calculating the impact energy using the two methods compared in this research, the design of the mono-pile follows the Blum method. The structure is modeled as a series of piles connected by a main girder, with the girder having the same diameter as the piles to ensure uniformity and strength.

The case of the Volkerak locks is chosen, and calculations using both the standard EAU 2012 method and the proposed refined one are executed. Two designs are produced and compared. With the refined calculation, a design with a smaller pile diameter of 1,620 mm and a longer in-between pile distance of 6.5 m is achieved, compared to the EAU 2012 design, where the pile diameter is 2,020 mm and the distance between piles is 3 m. These results demonstrate the potential for material savings if the refined calculation is adopted.

The study concludes that a refined approach is indeed necessary and that focus should be placed on specific definitions and descriptions in the guidelines. Ambiguity in such definitions leaves decision-making subject to individual interpretations, creating inconsistency among the designs of structures with the same purpose. Although this inconsistency may not be inherently dangerous, as it usually results in an overly conservative design, it contributes to excess material usage and resource waste.

Contents

1

Introduction

1.1. Relevance

Guiding structures are essential components of inland waterway navigation, especially around locks and narrow channels. Their primary function is to guide vessels safely into position, reducing the risk of collisions with infrastructure, nearby vessels, or the lock itself. The proper alignment of vessels is critical, as even slight misalignments can result in significant structural damage and economic losses. By ensuring the safe passage of ships, guiding structures prevent both operational disruptions and environmental hazards such as fuel spills and contamination, which can occur in the event of collisions.

In regions like the Netherlands, where inland waterways are vital transportation routes, the importance of these structures is even greater. According to Rijkswaterstaat, over 150,000 cargo vessels pass through the Volkerak locks annually, highlighting the sheer volume of traffic that relies on these structures to function smoothly. Inland waterway networks such as these play a key role in connecting major European ports like Rotterdam and Antwerp with inland industrial centers across the continent (Wongnitchakul, 2023). The economic significance of maintaining safe and efficient inland waterways cannot be overstated, as disruptions due to structural failure or accidents could have substantial ripple effects on supply chains.

Furthermore, the design and performance of guiding structures are crucial for ensuring the longevity of critical infrastructure. Current design standards, such as those outlined in the Recommendations of the Committee for Waterfront Structures Harbours and Waterways (EAU, 2012), do not fully account for the differences between berthing and guiding structure collisions. This leaves room for investigation of the suitability of the standards to describe guiding structure collisions, as they are specifically tailored for berthing.

1.2. Problem Statement

The design of guiding structures (figure 1.1) as part of the leading jetties to a lock in the Netherlands follows the same principles as the berthing structures in the mooring area, since both are designed according to the same clauses included in the ROK-2.0, 2021. Both structures are part of the complete lock approach, but the skipper uses each one of them for a different purpose. While both structures can be used for guidance, only the mooring area structures are used for berthing. Whereas, the guiding structures in the mouth of the lock only have a guiding and protection purpose.

The ROK 2.0 with reference to the EAU, 2012, does not distinguish between these two different structure designs. For both structures a kinetic energy of the ship that is to be absorbed by the structure is used, named berthing energy in the framework. This is because, while berthing, the ship is impacting the face of the structure as part of its mooring manoeuvring. Thus, it has been generally accepted by the engineering community for practical purposes that this calculation applies broadly to impacts and should be used for both structures of the lock approach, berthing and guiding ones. But, the kinetic energy approach introduced in the EAU, 2012 seems to produce exaggerated values of the ship's kinetic

energy absorbed by the structure when the framework is applied on guiding structure approaches.

Although there is an impact in both situations, the circumstances under which these impacts happen are subject to differences. The distinctive use these structures have, means that ships move differently close to each one of them while they are approaching the lock entrance. In figure 1.1, two stills of a ship approaching a guiding structure and a berthing structure are depicted along with orientation information about the ship's velocity.

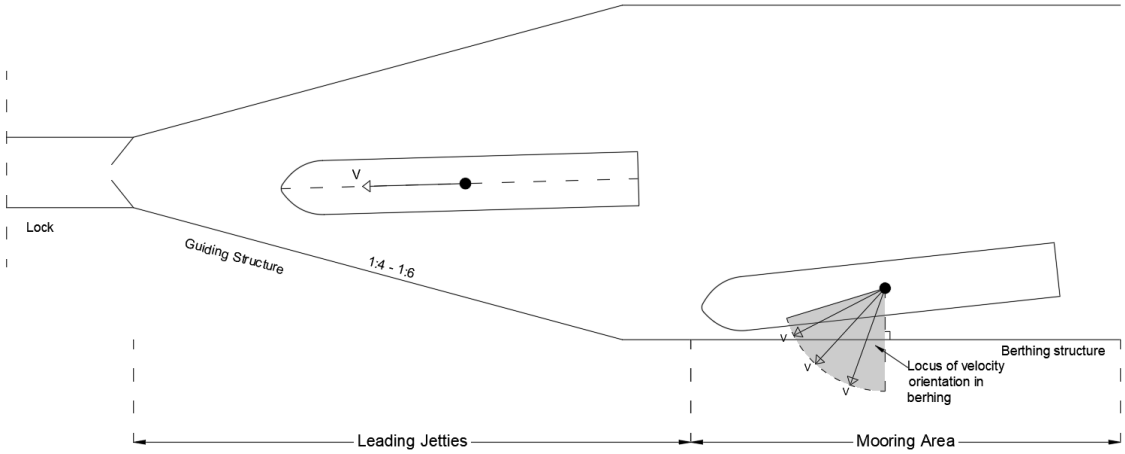

Figure 1.1: Lock Approach

When a ship approaches the berthing structure the orientation of its velocity vector generally falls within the area between the distance r, joining the center of mass and the impact point, and the perpendicular to the structure imaginary line, joining the center of mass and the face of the structure (figure 1.2). The reason behind this is that, the orientation of the ship speed is determined by the bow thrusters that a ship may carry so that berthing maneuvers are performed. Hence, the ship maintains a lateral movement rather than a forward one in order to berth.

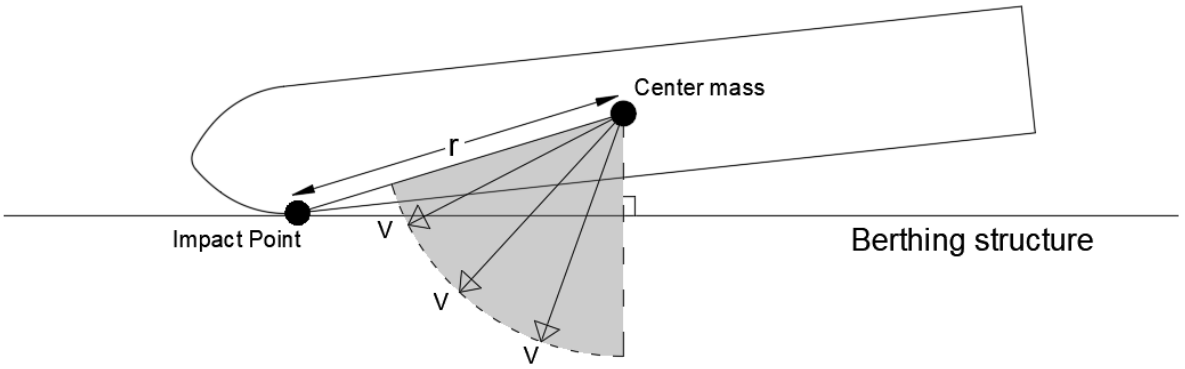

Figure 1.2: Berthing Approach

The guiding structures are positioned symmetrically right before the lock entrance and their horizontal angle with the waterway axis is between 1:4 to 1:6 (figure 1.1) depending on the waterway class (Vrijburcht, 2000). When a ship approaches the guiding structure it maintains a required sailing speed to enter and then pass through the lock. This means that the ship is performing a forward movement with its velocity vector orientated close to or exactly on its longitudinal axis. For the purpose of this research, the forward movement of the ship approaching the lock entrance is considered an outcome of a strictly longitudinal velocity vector. The situation is presented in figure 1.3.

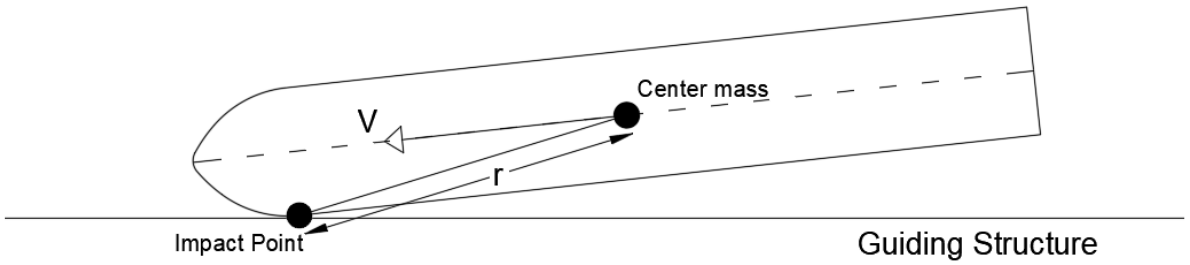

Figure 1.3: Guiding Approach

The existing EAU, 2012 framework for berthing structures falls short in producing realistic collision energy values, when applied to guiding structure approaches. This is due to the inability of the framework to account correctly for the eccentricity of the impact when it involves the ship and the guide. The eccentricity effect in the kinetic energy approach is introduced through a coefficient accounting for energy loss due to rotation when the ship does not approach the structure parallel, the range of which spans $0 < C_e \leq 1$. The coefficient takes the maximum value of unity when the velocity vector direction coincides with the distance r and the impact is considered central. For all other cases, the coefficient depends on the orientation of the velocity vector in respect to the distance r.

Although the EAU, 2012 framework clearly instructs to consider the perpendicular component of the ship's velocity as the design velocity in the kinetic energy calculations, when it comes to accounting for its orientation in the eccentricity coefficient, it considers the ship's total velocity vector. This leads to trivial errors when berthing is considered as the ship's total velocity direction is usually very close to the imaginary perpendicular line joining the center mass and the face of the structure. But, when a guiding structure approach is considered and the velocity vector direction coincides with the longitudinal axis of the ship, the error is significant and produces a result for the eccentricity coefficient that would be expected from a central impact rather than a lateral guiding structure approach impact. Thus, the eccentricity coefficient value, instead of describing the motion of the ship that is usually observed at the lock entrance (figure 1.4, Left), the framework returns an eccentricity coefficient result that would be caused by a central impact situation as presented in figure 1.4, Right.

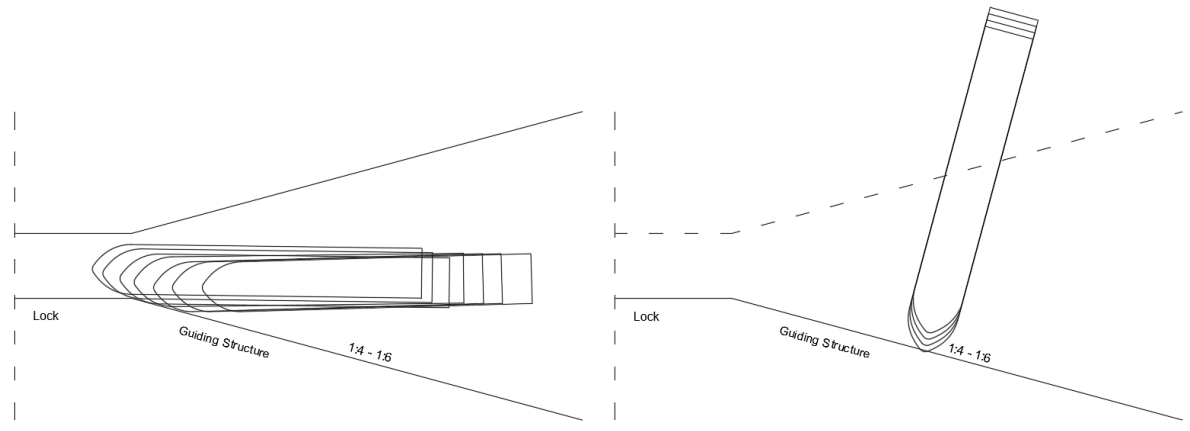

Figure 1.4: Left: Observed ship motion at lock entrance, Right: Motion described by the EAU, 2012 eccentricity

1.3. Research Objective: Questions and goals

This research investigates the differences between the berthing and the guiding structure approach and propose a refining of the standard EAU, 2012 method to accurately represent the approach of a ship to a guiding structure.

This section of the report introduces the research questions, which have been formulated based on a preliminary review of existing literature. The collision energy methodology is carefully examined, and gaps within the literature review are identified. The research questions are structured in a hierarchical manner, beginning with the primary research question and subsequently expounding upon it with related sub-questions.

How can the EAU, 2012 berthing energy calculation method be adjusted to describe collision on guiding structures and produce a realistic calculation of the collision energy?

In order to assess the feasibility of the main question there are sub-questions that arise in the process:

- What is the level of conservatism in the established energy calculation method based on berthing?
- How do collision dynamics in guiding structure approaches differ from berthing dynamics, and what are the underlying reasons that call for a distinct methodology for quantifying collision energy?
- How does the refined method compare to the existing one and what is the impact of application on the design of the new guiding structures? Is it possible that the suggested method by this research leads to a more economical design regarding material usage?

1.4. Research methodology

The methodology employed in this thesis was carefully designed to address the research question, *How can the berthing energy calculation method be adjusted to describe collision on guiding structures and produce a realistic calculation of the kinetic energy?*. The process follows a systematic approach to refine the existing EAU 2012 framework, ultimately leading to a modified method for calculating collision energy specific to guiding structures. The methodology is divided into several key steps:

- Problem Definition

The research begins with a clear definition of the problem related to collision energy calculations in guiding structures. It was identified that the current method (EAU 2012) used for calculating collision energy, which was originally developed for berthing ships, produces unrealistic results when applied to guiding structures. The primary issue lies in the eccentricity coefficient, which does not account for the different dynamics between berthing and guiding approaches, especially in the angle of impact. This miscalculation leads to overestimation of collision energy, resulting in overly conservative designs that require unnecessary material use and increase costs.

- Literature Review

A review of existing literature is conducted to assess the limitations of current collision energy calculation methods and identify gaps in their application to guiding structures. This review includes standards such as EAU 2012, which provides the conventional method for kinetic energy calculations, and comparisons with alternative methods like the **Virtual Water Mass method**, which incorporates additional factors such as water movement during ship impacts. The literature review also explores research on guiding structure design and collision dynamics to understand how velocity vectors, eccentricity coefficients, and impact angles are treated in existing frameworks. The insights from this review serve as the foundation for the theoretical improvements proposed later in the thesis.

- Proposing Refined Calculation Method

The core of the thesis lies in the development of a refined collision energy calculation method. This method focuses on redefining the angle used in the eccentricity coefficient within the EAU 2012 kinetic energy approach. The new angle definition directly reflects the ship's approach angle relative to the guiding structure. By modifying this angle, the method addresses the specific dynamics of guiding structure impacts, where sliding motions dominate rather than perpendicular berthing impacts. This

refinement is designed to provide a more realistic calculation of collision energy, better suited to guiding structures' operational context.

- Applying the Refined Calculation Method on Historical Data

To validate the refined method, historical data from previous model research, particularly from Rijkswaterstaat reports, is used. This data includes real-world cases of ship impacts on structures that fit the characteristics of guiding structure approaches. These cases provide a benchmark for comparing the results of the refined calculation with those produced by the established EAU 2012 method. The historical data allows for a direct comparison of collision energy values and helps demonstrate how the refined method corrects the overestimation issues of the existing framework.

- Comparing Results

A key part of the methodology involves a detailed comparison of the results from both the EAU 2012 method and the newly developed refined method. This comparative analysis focuses on several case studies to highlight the discrepancies in energy calculations between the two methods. The findings from this step are crucial in validating the suitability of the refined method and proving its ability to produce less conservative but equally safe designs for guiding structures.

- Case Study

A comprehensive case study is conducted on the **Volkerak lock**, a critical part of the Netherlands' inland waterway infrastructure. This case study applies both the EAU 2012 method and the refined method to the design of guiding structures at the lock entrance. The case study evaluates the impact of both methods on structural design, particularly in terms of material usage. By simulating different ship impact scenarios and applying the proposed method, the study demonstrates that the refined method leads to smaller pile diameters and longer pile distances. This results in significant material savings while maintaining the structural integrity of the guiding structures.

The final step in the methodology is the modeling of the guiding structure using the refined collision energy calculation method. This involves optimizing the structural design for material efficiency without compromising safety. The modeled structure is compared to the original design derived from the EAU 2012 method to quantify the material savings and cost reductions achieved through the refined method. The optimization process takes into account the loads, pile dimensions, and soil interactions to ensure that the guiding structure can absorb the calculated kinetic energy from ship impacts. The results from the modeling phase confirm the refined method's potential to deliver both economic and environmental benefits.

1.5. Report Outline

Structure of the Report

This report is structured as follows:

- Chapter 2 - Literature Review: This chapter provides a comprehensive review of existing methodologies for calculating collision energy, with a critical examination of their limitations. It highlights the theoretical and practical gaps in current approaches and sets the stage for the proposed methodological improvements.
- Chapter 3 - Refined Calculation Method: This chapter details the development of the new methodology, beginning with the theoretical basis for the redefinition of the angle variable that is used as input in the eccentricity coefficient expression and followed by practical implementation steps.
- Chapter 4 - Results and Validation: This chapter focuses on the validation of the new refined calculation method. It presents the results of applying the refined collision energy calculation method to historical data cases from model research, and compares it the calculations performed with the standard EAU, 2012 method and the Virtual Water Mass method.
- Chapter 5 - Case Study - Volkerak Lock: A detailed case study applying the new methodology to the Volkerak Lock guiding structure.

- Chapter 6 - Discussion: A synthesis of the findings, addressing the research questions posed in the introduction. This chapter discusses the implications of the new methodology for inland water engineering practices and offers recommendations for future research.

2

Literature Review

2.1. Definitions

In inland waterway and maritime engineering, understanding the specific terminology related to guiding structures is essential for accurately assessing and addressing the challenges associated with ship collisions. In this section the relevant definitions are presented, followed by the problem statement of this research project.

A guiding structure is part of the leading jetties at the entrance of a lock. The leading jetty serves to advance rapid and safe entry, and this is why it is bordered by guiding structures (figure 2.1). The mouth of the leading jetty needs to provide both guiding structures with sufficient length and a suitable angle with regard to the lock axis. Given the function and positioning of the leading jetty, it is not the intention that vessels use the leading jetty structure for mooring during the locking process (Glerum and Vrijburcht, 2000).

In the 1991, ”Loads on fender structures and dolphins by sailing ships” study, for Rijkswaterstaat, the author, Vrijburcht, refers to all the preceding structures to a lock as fender structures. The function of the fender structures is to guide and slow down the ships, to protect adjacent structures against ship impacts, to protect ships against structures and to act as a boundary for berthing or waiting space for ships (Vrijburcht, 1991).

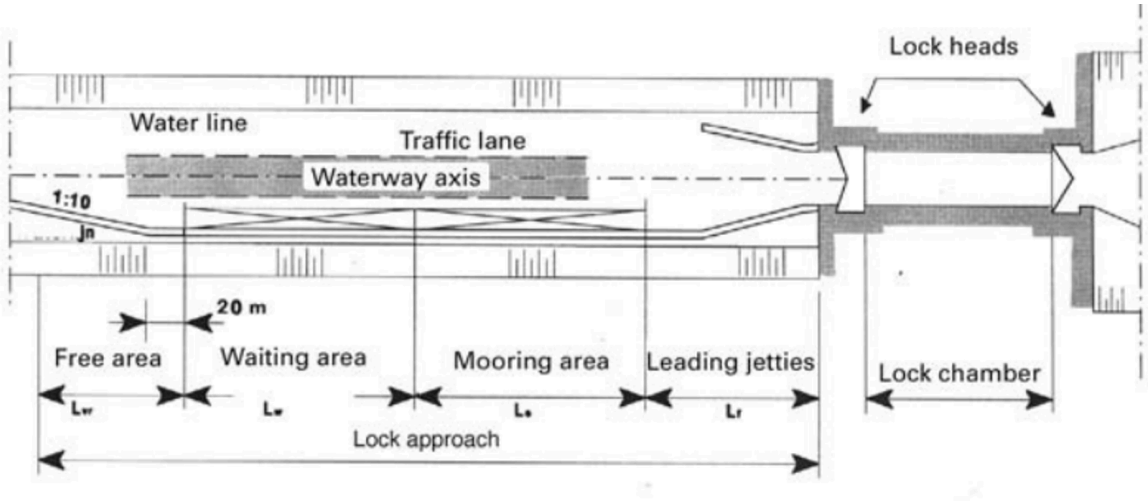

Figure 2.1: Lock and lock approach layout (Vrijburcht, 2000)

It is important to derive clear definitions of the structures in the layout of the lock from the available literature. Usually, the guidelines and the engineering handbooks refer to the structures with broad terms

implying inclusion of sub-categories. For example, the ROK 2.0 uses the word ”resilient structures” and ”collision energy” to present design clauses for guiding and berthing structures with reference to the EAU 2012 method which specifically presents a method for ”berthing energy” calculation. Later in the chapter the consequence of this practice is discussed.

Breaking down the relevant definitions appearing in literature:

- Fender structures: Structures that guide and slow down ships. They must protect structures against impacts from ships, and must protect ships from these structures. In addition, they must act as berthing or waiting place for ships. They are installed where one or more of these functions are required, generally nearby locks, bridges, harbour entrances. (Vrijburcht, 1991)
- Fender: A fender is, in principle, an intermediate layer between a vessel and the waterfront structure which absorbs part of the kinetic energy of a berthing ship. In the case of fenders attached to waterfront structures, the energy absorbed by the fender is transferred to the structure (EAU, 2012).
- Guiding structures: The structures at the mouth of the lock used for guidance by the entering ships. Not suitable for mooring. (Richtlijnen-Vaarwegen, 2020). In a translated version of the Richtlijnen-Vaarwegen, 2011 these structures are referred to as ”guide fenders” (Brolsma and Roelse, 2011).
- Breaking structures (translation of the Dutch term ”remmingwerken”): Structures used in the waiting and mooring area in figure 2.1 (Richtlijnen-Vaarwegen, 2020). Since there is no equivalent English definition, in this report they will be treated as berthing structures due to the similar use and based on the description in the translated Richtlijnen-Vaarwegen, (2011) that refers to them as fender with mooring facilities (Brolsma and Roelse, 2011).
- Berthing structures (Berth): Any dock, pier, jetty, quay, wharf, marine terminal or similar structure (whether floating or not) at which a ship may moor.(IMO MSC.1/Circ.1216)

2.2. EAU,2012 Framework: The kinetic energy approach

The basic assumption of the kinetic energy approach is that an amount of the kinetic energy of the ship right before the moment of the first contact with the structure is to be absorbed by the structure itself. In this way, the loads on the structure are separated from the reaction of the structure (Demenet, 2018). In its simplest form the energy transferred by the ship to the berthing structure through the impact is expressed by the following equation (EAU, 2012) :

$$E_d = \frac{1}{2} * \ G * v^2 * C_e * C_m * C_s * C_c \tag{2.1}$$

where:

- E_d: berthing energy to be absorbed [kNm]
- G: mass of ship. The mass of the fully laden ship should always be used – even when operational conditions dictate that only unloaded ships usually berth at the dolphin concerned – in order to cover the case of an unscheduled re-berthing of a ship
- v: berthing velocity, i.e. translational movement speed of centre of mass at time of first contact with fender/dolphin [m/s]
- C_e: eccentricity coefficient
- C_m: virtual mass factor
- C_s: softness coefficient
- C_c: waterfront structure attenuation factor.

The equation presented is the generally accepted form widely used for the design of the berthing and guiding structures. The discussion that follows breaks down the inputs of this equation.

The square of the **berthing velociy** (v) is included in the equation for calculating the berthing energy to be absorbed and is therefore one of the main parameters to consider when designing fender structures. Measured values for the berthing velocity are not usually available (EAU, 2012). The velocity at which a vessel approaches a berth is the most significant of all factors in the calculation of the energy to be absorbed by the fendering system. The designer should determine, where possible, the characteristic berthing velocities that should be adopted for the design from statistical data at the berth location or at a location that has the same berthing conditions and range of vessels. In the absence of berthing velocity data, characteristic velocities for alongside berthing with the use of tugs or thrusters may be estimated from the Brolsma et al., 1977 curves corresponding to navigation conditions (BS-6349-4, 2014). Brolsma collected field measurements from shore-based docking systems at three berths in Rotterdam and one in Scotland. The proposed mean design values of the berthing velocities were called normal berthings and represent a return period of 30 years based on 100 arrivals per year. Over time, Brolsma's original curves were reproduced, slightly modified and published in PIANC, 2002 and BS-6349-4, 2014. The German recommendations for waterfront structures EAU, 2012 and the Spanish ROM, 2011 both provide recommendations for characteristic values of berthing velocities. Three categories of navigation conditions were distinguished instead of five in the Brolsma curves (Figure 2.2) (Roubos et al., 2017).

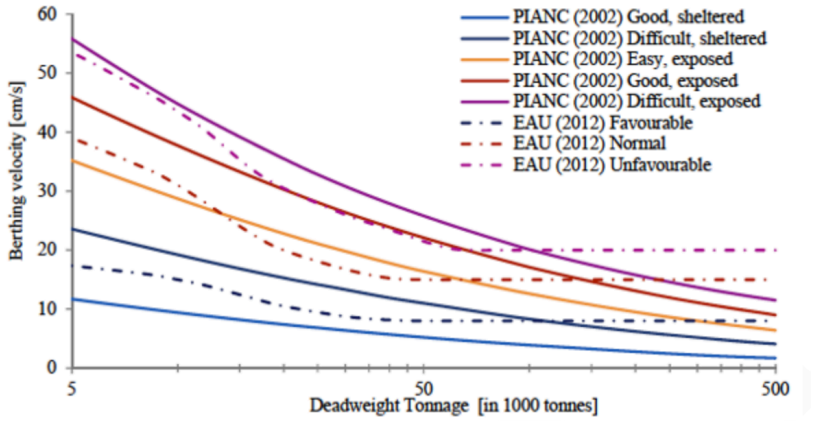

Figure 2.2: Mean design value of berthing velocity PIANC, 2002 and characteristic berthing velocity EAU, 2012(Roubos et al., 2017)

The **eccentricity coefficient** (C_e) considers the energy loss due to the rotation caused by the approaching vessel not coming in parallel with the structure and by a part of the hull coming into contact with the structure (Kang et al., 2022). The coefficient is related to the geometry of the approach and is a function of the radius of gyration of the ship in the rotation about the longitudinal axis and the direction of the vector of berthing velocity (Neşer and Ünsalan, 2006). Typical values for the coefficient lie between the range 0.5 - 0.8 (Atiq, Shajib, et al., 2023).

The **virtual mass factor** (C_m) takes into account the fact that a considerable quantity of water is moved together with the ship, and this must be included in the mass of the ship in the energy calculation. Recommended values for this coefficient are between 1.45 and 2.18 (EAU, 2012). The Cm coefficient depends on the draft of the ship and the water depth (PIANC, 2002).

The **softness coefficient** (C_s) takes into account the ratio of elasticity of the fender system to that of the ship's hull because part of the berthing energy is absorbed by the latter (EAU, 2012). The softness coefficient accounts for the ship's compliance to account for 10% of the elastic energy absorption (PIANC, 2002). In the new document by PIANC, 2024, that is report WG 211 the softness coefficient is no longer part of the calculation citing Berendsen, 2022.

2.3. Identifying Literature Gap: The eccentricity coefficient

In this section the eccentricity coefficient is put under the **microscope**. The expression for eccentricity in the framework by the EAU, 2012 is studied and conclusions are shaped regarding the suitability of

the eccentricity coefficient expression to describe the geometry of the guiding structure approach.

For the berthing energy calculation the EAU, 2012 recommendations suggest the following expression for the situation of no rotation:

$$E_d = \frac{1}{2} * G * v^2 * \frac{k^2 + r^2 * \cos a^2}{k^2 + r^2} * C_m * C_s * C_c = \frac{1}{2} * \ G * v^2 * C_e * C_m * C_s * C_c \tag{2.2}$$

In the expression with substitution for the C_e coefficient, the following variables are introduced:

- k: radius of gyration of ship [m], generally taken as $0.25L$ for large ships with a high block coefficient
- L: length of ship between perpendiculars [m]
- r: distance of ship's centre of mass from point of impact on fender/dolphin [m]
- ω: ship's rotational speed at time of first contact with fender/dolphin [rad/s]
- α: angle between velocity vector and distance r [°]

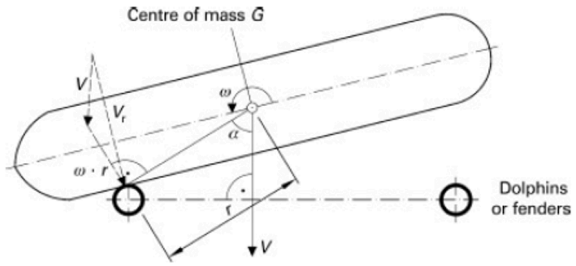

Figure 2.3: Berthing geometry (EAU, 2012)

2.3.1. The eccentricity coefficient expression

The eccentricity coefficient C_e accounts for the fact that the first contact between ship and fender is not normally in the middle of the ship's side and therefore not in line with the vessel's centre of mass either. According to EAU, 2012 with reference to PIANC, 2002, the eccentricity factor is calculated as proposed by Vasco Costa, 1965 using the parameter defined for equations (2.1), (2.2):

$$C_e = \frac{k^2 + r^2 \cos a^2}{k^2 + r^2} \tag{2.3}$$

And for a berthing angle equal to zero, meaning $\alpha = 90^o$ then the coefficient is:

$$C_e = \frac{k^2}{k^2 + r^2} \tag{2.4}$$

The radius of gyration k for large ships with a high block coefficient can usually be taken as 0.25 L, where L is the length between perpendiculars. When designing fenders alongside quay walls, $C_e = 0.5$ can be assumed if more accurate data is not available and for rough calculations, or $C_e = 0.7$ for dolphin fenders. At ro-ro berths, $C_e = 1.0$ should be assumed for the end fenders for ro-ro ships that dock with bow or stern.

In the approach towards a guiding structure, the velocity vector is different than the one in the approach to the berthing structure, as explained in paragraph 1.2. When a ship approaches the berthing structure the orientation of its velocity vector falls within the area between the line joining the center of mass and the impact point, and the perpendicular to the structure imaginary line, joining the center of mass and the face of the structure (figure 2.4, left). Whereas, when a ship approaches the guiding structure it maintains a required sailing speed to enter and then pass through the lock. This means that the ship

is performing a forward movement with its velocity vector orientated close or exactly on its longitudinal axis. For the purpose of this research, the forward movement of the ship approaching the lock entrance is considered an outcome of a strictly longitudinal velocity vector (figure 2.4, right).

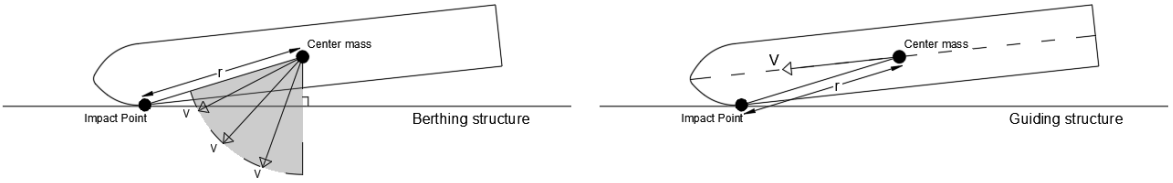

Figure 2.4: Ship approach to berthing and guiding structures

The proposed eccentricity coefficient in the EAU, 2012 recommendations is covering sufficiently the berthing situation, but is inadequate in describing the approach to a guiding structure. The longitudinal berthing velocity component in the fender selection process for side-berthing conditions is not consistent with modern fender selection practice. The longitudinal component of the kinetic energy in side-berthing scenarios is assumed to be conserved as longitudinal motion and not absorbed by the fenders. The eccentricity coefficient in side-berthing scenarios only modifies the normal component of the total kinetic energy and therefore the input values used in the eccentricity coefficient equation (2.3) must reflect the condition in which the velocity vector is normal to the fender base (Cajiao and Phelan, 2022). The same should apply for guiding structure approach scenarios as well, as it is instructed by the ROK 2.0 that the guiding as well as the berthing structures should be designed for the perpendicular to the face of the structure component of the ship approach velocity .

This is where the first complications appear. When applied to the guiding structure approach, the framework introduces input values to the eccentricity coefficient equation (2.3) that don't reflect the condition in which the velocity vector is normal to the structure. This happens because the definition of angle α in the eccentricity equation is vaguely defined as the angle between the velocity vector of the ship and distance r. The framework is not clear at to what is to be considered as the velocity vector for the angle definition. Although there is literature suggesting that the input should be the normal to the structure component (Cajiao and Phelan, 2022), the EAU, 2012 framework does not clarify this. The same goes for other standards like PIANC, 2024 and BS-6349-4, 2014.

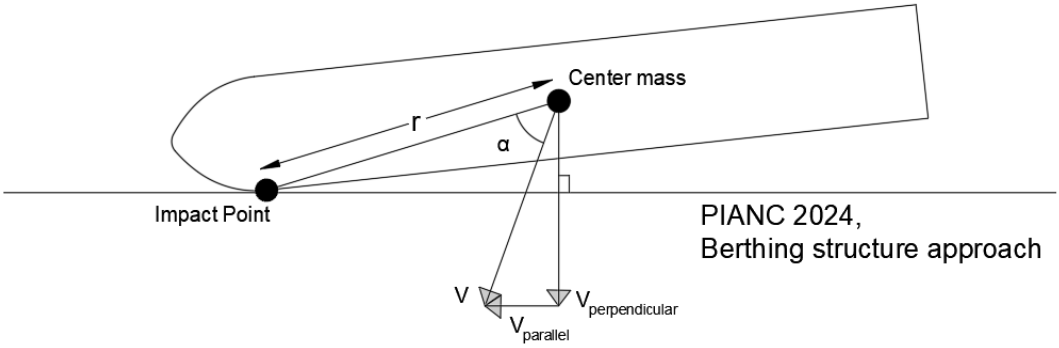

Figure 2.5: PIANC 2024, WG211, Berthing Geometry

Although the standards are specifically stating that the input velocity in the kinetic energy expression calculation should be the normal to the structure component, when it comes to the definition of angle α they present graphs where the angle is defined using the total velocity vector, see figure 2.5. This does not seem to interfere with providing realistic results in berthing as the ship's total velocity direction is usually almost perpendicular to the structure. But, when a guiding structure approach is considered, and the ship maintains purely longitudinal velocity, then an error is produced by the framework and an eccentricity coefficient almost equal to unity is returned.

2.3.2. Angle α in berthing structures

In berthing, the ship slows down almost to a halt before being self-propelled or tugged to berth. This means that the position of the velocity vector in respect to distance r shows variability that depends each time on the way the ship is assisted to berth. For every berth case a unique direction of the velocity is possible, falling within the area shown in figure 2.4, Left. Thus, a unique angle α value is derived for each approach.

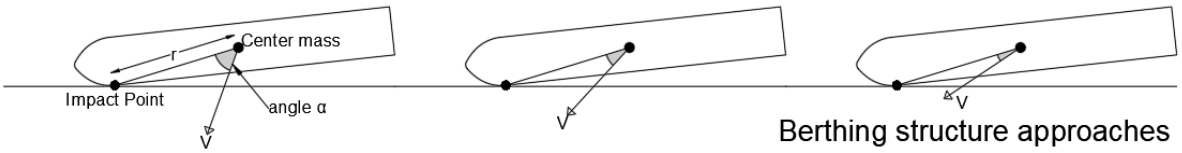

Figure 2.6: Berthing approaches for constant angle of approach

In figure 2.6 for the same angle of approach three possible berthing approaches are presented. The purpose of this figure is to demonstrate that in berthing, the approach angle of the ship is irrelevant regarding the orientation of its total velocity vector as it is determined by the bow thrusters. Although, it stays relevant for the perpendicular to the structure velocity component.

The way that the eccentricity coefficient expression is tuned, the angle of approach in berthing becomes relevant only when the impact point assumptions change. For example, if the ship is to impact the structure with a point very close to its midpoint on its side, then this directional change of the ship is directly reflected on the distance r which becomes significantly smaller and shifts to being almost perpendicular to the structure. This is reflected in the C_e value which will be almost equal to unity as the impact would be almost central.

Thus, the framework works realistically for berthing because the directional change of the ship is reflected on the distance r that shows variability in berthing scenarios due to the many possible impact point locations. In combination with the small velocities and the common almost perpendicular direction of the approach velocity vectors, the overlooking of the direct link of angle α to the approach angle does not produce as significant errors as it does when the framework is applied in guiding structures.

2.3.3. Angle α in guiding structures

When the definition of angle α as introduced by the framework is applied to a ship approaching a guiding structure with purely longitudinal speed, then the value of the angle becomes constant. Unlike in berthing, at the guiding structure approach the ship is sailing with a longitudinal velocity vector. This means that the orientation of the velocity vector in respect to distance r is constant. This gives a constant value of angle α for a specific ship regardless of its angle of approach to the structure. And this is where the blind spot of the framework is identified by this research. The approaches presented in figure 2.7, are all equal to the existing framework since they all produce the same value for the eccentricity coefficient, a value almost equal to unity that falsely resembles a central impact, due to the constant angle α [1].

[1] Of course, depending on the shape of the ship's hull a small change of the distance r is expected since the impact point moves closer to the longitudinal axis of the ship the more a situation resembles a central impact. But this still does not link the angle of approach directly to the eccentricity coefficient expression. The C_e values for all these approaches are almost equal to unity even when the small change of the impact point is taken into account.

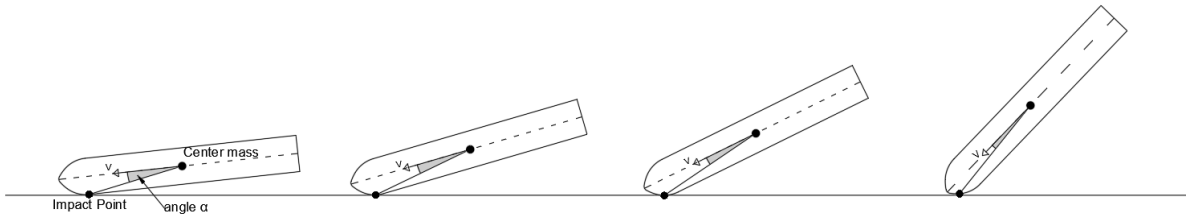

Figure 2.7: Demonstrating the framework's blind spot

2.3.4. Conclusions on the eccentricity coefficient equation

Looking into the eccentricity coefficient equation, what becomes clear is that the approach angle of the ship as it closes on the structure is overlooked by the framework regarding eccentricity. The only way the effect of the approach angle is present, is only realised through the variations of distance r and, on the value of the perpendicular component of the velocity vector. The direct link of angle α to the approach angle is absent. While this does not produce unrealistic results for berthing, it gives significant errors when collision on guiding structures is studied.

In the collision energy calculation of the kinetic energy approach, the framework instructs to use the normal to the structure component of the ship's velocity, but, in the definition of angle α in the eccentricity coefficient present graphs that consider the total ship velocity vector. This is paradoxical, and it is what causes the blind spot discussed in the guiding structure approaches.

In the guiding structure approaches, the framework ignores the approach angle of the ship when it accounts for the eccentric impact. This brings out an erroneous result where, regardless of the approach angle of a ship, the impact is always considered almost central. This happens because the angle α in the eccentricity coefficient expression (2.3) ignores the direction of the ship in respect to the structure, as it considers the longitudinal component of the ship's velocity. Fact that contradicts the purpose of the eccentricity coefficient which is to modify the normal component of the total kinetic energy.

Finally, these collision energy calculations coming from the framework are not linked to the structure properties. This practice is adopted because it gives tangible results as a first hand calculation for the load on the structure when berthing is considered. But, if property structures were considered, like the friction between the ship and the structure, then the energy to be absorbed would be calculated more accurately. Further in this chapter, analytical methods that take into account the response of the structure to an impacting ship are studied.

2.4. Available calculation methods

In his 1983 report for Rijkswaterstaat, Vrijer goes over the available methods to calculate the collision forces on the vessel and the structure. The methods that are presented are the following:

- Virtual water mass method
- Method with constant hydrodynamic coefficients
- Impulse response function method
- Long wave method

Out of the four methods laid down in the report, Vrijer concludes that the virtual water mass method and the impulse response function method with hydrodynamic coefficients could be of use depending on the case one tries to design for, and the expected accuracy on the outcome of those.

The impulse response function method with hydrodynamic coefficients very accurately gives the entire course of the impact force with a universal application and is therefore the recommended one to determine collision forces on fender structures. Whereas, the virtual water mass method while reliable to derive the maximum impact force, one has to take into account that the progression of the impact force in time is not properly represented and that the case investigated should fall within the range of the provided model research results.

2.4.1. Choosing a suitable calculation method

In this research project, the replication of the Impulse Response Function (IRF) method using the BOTS program, originally developed for Rijkswaterstaat, was initially pursued. An application of the impulse response function method is presented in Vrijburcht's 1991 report "Loads on fender structures and dolphins by sailing ships". To break down the method and its calculations, Vrijburcht is referencing studies by Fontijn, 1975, Lindijer, 1981 and Vrijer, 1983a. When the hydrodynamic coefficients are known (either through the 2-dimensional potential flow theory or the 1-dimensional long wave theory for shallow water) then with the impulse response function method the collision force can be calculated as function of time with an uncertainty of 2 % (Vrijer, 1983a). The attempt to reproduce this program for this research was based on Rijkswaterstaat reports; however, this was ultimately deemed impractical for several reasons. First, the IRF method parameters require substantial computational resources, presenting a significant challenge. Although the calculation steps are outlined in the Rijkswaterstaat reports, direct application of these steps failed to yield the same results as those documented. This discrepancy can be attributed to multiple factors:

- Understanding of Calculation Steps: There was difficulty in fully grasping the intricate calculation steps described in the reports.
- Numerical Schemes: The numerical schemes applied to derive converging solutions for spectral analysis differed from those used in the original reports, mainly due to insufficient details provided about these schemes.
- Accuracy of Reports: The precision and reliability of the information in the reports were questionable, affecting the outcome of the reproduced results.

Each of these factors individually and collectively contributed to the impracticality of replicating the BOTS program accurately.

For the purpose of this research, a simplified version of the Virtual Water Mass method will be used. This method allows for deriving the maximum impact force reliably with simpler and more straightforward calculations. Thus, it is suitable for fast calculations in the design phase and could be potentially integrated in the tools the engineers have for preliminary designs.

This simplified version is suggested by Vrijer, 1978 in a model research report for TOW (Applied research for water management). The most important conclusion of the report is that the collision force developed between the ship and the structure is following a sinusoidal curve of half a sine to its maximum value. The method is describing accurately the maximums for force and displacement but is falling short in describing loss of contact accurately after the maximum displacement is reached.

The virtual water mass method was used to perform calculations of forces, velocities and displacements of the fender structure in specific times deemed significant. The times distinguished in the method were the following:

- The beginning of collision (Braking stationary, ship's original speed)
- Start of joint movement (Ship and guiding structure joint speed)
- Maximum force
- Maximum Displacement
- Loss of contact

The calculations in Vrijer's research were calibrated with measurements of scaled prototypes. Upon comparison the effect of water on the ship's mass was accounted for by introducing a coefficient in the calculation of the mass of the system. The outcome of Vrijer's research is a simplified calculation method of the structures response which is to be used for this research project.

Vrijer's research breaks down the collision event into two stages. One is the impact stage and the other one is the movement stage. The suggested calculation method from this research is describing the movement stage. What can be derived with sufficient accuracy is the maximum force and the maximum displacement and the moment in time these appear. The results can be used for deriving the force - deflection curve which in its turn can be used for the collision energy calculation.

2.4.2. Overview of the Virtual Water Mass method

This paragraph discusses the method and the parameters involved. With this method the total influence of the water is only included in an extra mass term in the dynamic force equation. This extra mass, the schematic water mass is determined through model research.

A ship/fender system is assumed without the influence of water. The fender may spring in the perpendicular direction (y-axis) as an undamped system, and is assumed to be infinitely rigid in the parallel direction (x-axis). The ship can perform all the horizontal movements during the impact process: surging, swaying and yawing, in addition to its original movement. The horizontal movements surge, sway, and yaw, are described by dimensions x_1, x_2, x_6 directions, respectively, in figure 2.8.

The method uses a simplified representation of the ship as a box shaped floating object. The ship sails at a uniform forward (= longitudinal) velocity, drift (= transverse) velocity and yaw (= angular) velocity at a certain angle to the fender, collides against the fender and causes the fender to spring inwards, causing the ship to turn away, after which the ship is released from the fender.

Before the first contact between ship and fender, the ship sails at a uniform velocity, and the fender is at rest. At the moment of impact the fender will follow the movement of the fore part of the ship in the y-direction in a very short time: **the impact stage**. The fender then springs inwards, and the fore part of the ship and fender may move in the y-direction as a unit: **the movement stage**. After the ship is released from the fender, the ship and fender move separately.

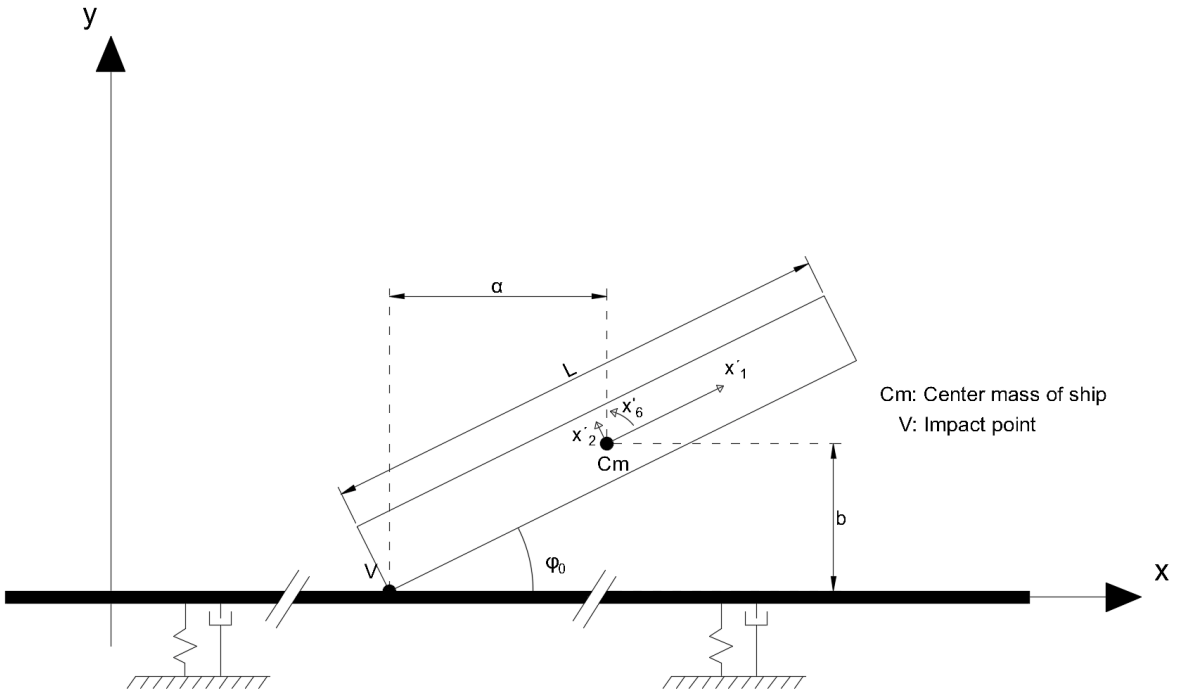

Figure 2.8: Virtual water mass scheme

The scheme of the method is presented in 2.8 and the variables of the method are presented in table 2.1.

The approach speed in the y-direction is calculated as follows:

$$\dot{y}_{v_0} = \dot{x}_{1_0} * \sin\phi + \dot{x}_{2_0} * \cos\phi + \frac{1}{2} * \alpha * \dot{x}_{6_0} \tag{2.5}$$

Table 2.1: Variables appearing in the virtual mass method

Ship Variables	*Symbol*	*Unit*
Mass	m	kg
Length	L	m
Breadth	B	m
Draught	D	m
Water depth	d	m
Approach speed longitudinal	$\dot{x}_{1_0}$	m/s
Approach speed transversal	$\dot{x}_{2_0}$	m/s
Approach speed rotational	$\dot{x}_{6_0}$	rad/s
Approach angle	ϕ_0	degrees
Structure variables	*Symbol*	*Unit*
Structure Mass	M	kg
Linear stiffness coefficient	k	N/m
Linear damping coefficient	c	Ns/m
Sliding Friction factor	$tg\beta$	[-]

At this point it useful to give expressions for the distance of the center mass of the ship from the impact point in the x-, y-directions.

$$\alpha = \frac{1}{2}(L * \cos\phi_0 - B * \sin\phi_0) \tag{2.6}$$

$$b = \frac{1}{2}(L * \sin\phi_0 + B * \cos\phi_0) \tag{2.7}$$

The assumption is that the for a very short time deceleration starts and the ship slows down. The fender structure at rest is accelerated. For this amount of time the ship and the structure move jointly at the point of collision at a new speed. At the beginning of the impact stage t_0 the ship is sailing and the fender is at rest, whilst at the end of the impact stage t_0', the fore part of the ship and fender are moving in the y-direction, together, at a new velocity. This new speed is given by:

$$\dot{y}_{v_0'} = c_{bt} * a_{btz} * \dot{y}_{v_0} \tag{2.8}$$

Where:

- $\dot{y}_{v_0'}$ = schematic initial speed, joint speed of ship and structure at time $t_{0'}$
- $\dot{y}_{v_0}$ = ship speed in y - direction at time t_0 (y - direction is perpendicular to the face of the structure)
- $a_{btz} = [\frac{M}{m}(1 - \frac{12\alpha}{L^2} * (tg\beta * b - \alpha) + 1]^{-1}$
- $c_{bt} = 1.1$ where $a_{btz} * c_{bt} \leq 1$

The virtual mass of the ship with the influence of the water is given by:

$$m_{bw} = a_{bwz} * c_{bw} * m \tag{2.9}$$

With:

$$a_{bwz} = \frac{1}{1 - 12 * \frac{a*(b*tg\beta - a)}{L^2}} \leq 1 \tag{2.10}$$

The coefficient a_{bwz} indicates what proportion of the total mass of the ship contributes to the movement stage of the fore part of the ship and structure in the y-direction and is always less than unity. The

coefficient c_{bw} is accounting for the influence of the water and is to be interpolated using the model research results of Vrijer, 1978 in figures 30 to 47.

The time at which the maximum force appears after impact is calculated as follows:

$$t_1 = \frac{1}{\omega\sqrt{1-\gamma^2}} * \arctan\frac{1-4\gamma^2\sqrt{1-\gamma^2}}{(3-4\gamma^2)\gamma} \quad [s] \tag{2.11}$$

With:

- $m' = m_{bw} + M$
- $\gamma = \frac{c}{2\sqrt{km'}}$
- $\omega = \sqrt{\frac{k}{m'}}$

Then, the maximum force between ship and structure is:

$$F(t_1) = m'e^{-\gamma\omega t_1}\dot{y}_{v'_0}((\frac{\gamma^2\omega^2}{\omega\sqrt{1-\gamma^2}} - \omega\sqrt{1-\gamma^2})\sin(\omega\sqrt{1-\gamma^2} * t_1) - 2\gamma\omega\cos(\omega\sqrt{1-\gamma^2} * t_1)) \quad [N] \tag{2.12}$$

The time at which the maximum displacement appears is:

$$t_2 = \frac{1}{\omega\sqrt{1-\gamma^2}}\arctan\frac{\sqrt{1-\gamma^2}}{\gamma} \quad [s] \tag{2.13}$$

Then, the maximum displacement of the structure is:

$$y(t_2) = e^{-\gamma\omega t_2}\dot{y}_{v'_0}\frac{1}{\omega\sqrt{1-\gamma^2}}\sin(\omega\sqrt{1-\gamma^2}) * t_2 \quad [m] \tag{2.14}$$

The ship-structure system can be written as the motion of a single-mass suspension system perpendicular to the guiding structure:

$$(m_{bw} + M)\ddot{y}_v + ky_v = 0 \tag{2.15}$$

Then the damping of the braking is added $(c\dot{y})$ and the effect of the virtual water mass is applied through the coefficient c_{bw}. This generates the following scheme and equation:

$$m'\ddot{y}_v + c\dot{y}_v + ky_v = 0 \tag{2.16}$$

In order to solve equation (2.16) the following data must be present:

- Properties of the resisting structure (e.g. mass M, spring stiffness k and damping c)
- Properties of the ship (e.g. virtual mass of ship $a_{bwz} * m$)
- Water data (e.g. virtual mass of water $a_{bwz} * c_{bw} * m$)
- Initial displacement (at time $t = 0$ the displacement is $y_v = 0$)
- Initial velocity

2.5. Comparison between EAU,2012 framework and simplified Virtual Water Mass method

In the EAU,2012 framework the design of the fender structure depends on the assumed absorbed kinetic energy of the ship by the structure whereas in the simplified Virtual Water Mass method the structure is to be designed using the maximum force and deflection derived by the calculations. By using the results of the calculation in the simplified Virtual Water Mass method, force - deflection curves can be produced and thus, derive the kinetic energy absorbed by the structure as the area below the curve. That way the two methods give a result for the collision energy.

Now that it is explained how the two methods can give a comparable result it is necessary to look into how this two methods compare at their inputs. Looking into which of the inputs are equal and which of these are different but comparable can shed light to how conclusions of one can be used to compliment the application of the other.

Starting with the common inputs, both methods need the same ship data. These are the mass of the ship, its geometry and its speed. Furthermore, the use of those inputs for both methods are similar. In both methods the ship speed serves as the initial velocity in the same sense (ship speed at the time of impact) and the mass of the ship is either reduced or increased by factors in an effort to approximate the effective mass of the ship, meaning the portion of the ship mass that contributes to the impact and causes the fender structure's response. In the EAU, 2012 framework these factors are the virtual mass and eccentricity coefficients $C_m \times C_e$ and in the Virtual Water Mass method these are the a_{bwz} coefficient and the c_{bw} coefficient, the first indicating the portion of the total mass of the ship contributing to the movement stage of the fore part of the ship and structure and the latter accounting for the influence of the water ($a_{bwz} \times c_{bw}$).

Thus, the two methods follow the same philosophy around the consideration of the mass impacting the structure. This being:

$$virtual\ water\ mass\ factor \times eccentricity\ factor \times ship\ mass \tag{2.17}$$

The shared philosophy makes them comparable. One, now has to lay down the definitions of these factors per method to understand the differences and derive conclusions about how these two methods work.

In both methods, the C_m and the c_{bw} account for the same thing. Their difference lies in how their value is derived. The C_m values are calculated through linear interpolation between values $1.5 - 1.8$ depending on the keel clearance of the vessel (PIANC, 2002), with an allowed for **longitudinal** approaches value of 1.1, whereas the c_{bw} values come from interpolations through graphs of model research results depending on case similarity. It is noteworthy that the values for both these factors agree with each other giving similar ranges.

The comparison becomes more interesting between the C_e and the a_{bwz} factors. While both are accounting for the proportion of the ship's mass that contributes to the movement stage of the fore part of the ship and structure, the way in doing so is not similar. What is common though, between the two factors, is that they both use the ship's geometry as input.

Looking into equation (2.3) for the eccentricity coefficient, what its value depends on is the angle α which as explained is the angle between distance r and the velocity vector of the ship. But, the case is different for a_{bwz} if we look into the equation 2.10. The a_{bwz} factor depends directly on the angle of approach of the ship ϕ_0 and at the same time on the sliding friction coefficient $tg\beta$. This means, that in the Virtual Water Mass method the eccentricity is accounted for by taking the structure properties into consideration as well, in contrast to the EAU, 2012 framework where it is overlooked.

Since the movement of the ship relative to the structure is indeed a sliding movement, this definition of eccentricity is closer to the physics describing the relative motion of the ship in respect to the structure. The constraint here is that that it is hard for engineer to come up with structure properties right at the start of the design process in order to use a_{bwz} as a staring point. It is thus, worth investigating how the

empirical C_e factor can be corrected to correspond better to the a_{bwz} one when the structure properties are yet unknown.

2.6. Conclusions on the available literature

The literature review conducted in Chapter 2 provides a thorough exploration of the existing methodology for calculating collision energy, with a specific focus on its application to maritime guiding structures. This review critically examines the adequacy of generally accepted berthing energy formulas when applied to scenarios involving ship collisions with guiding structures, revealing significant theoretical and practical gaps that necessitate a methodological overhaul.

Throughout the review, it becomes evident that the standard approach, which predominantly employs kinetic energy calculations derived for berthing scenarios, is insufficient for accurately modeling the dynamics of collisions at guiding structures. This inadequacy stems primarily from the improper application of the eccentricity coefficient and assumptions about the velocity vector's direction, which do not align with the actual conditions experienced during collisions. The review highlights that these traditional methods overly simplify the complex interactions between ships and structures, leading to potential inaccuracies in energy absorption calculations and, consequently, the structural design and safety assessments.

Moreover, the literature review identifies a critical oversight in current standards and guidelines, such as ROK-2.0 and EAU 2012, which do not differentiate between berthing and collision scenarios. This conflation results in a one-size-fits-all approach that fails to account for the unique characteristics and requirements of guiding structures. The review argues for the development of bespoke models that consider the specific impact angles, velocities, and structural interactions unique to collisions, which are distinct from berthing maneuvers.

The comparison carried out in Section 2.5 between the EAU, 2012 framework and the simplified Virtual Water Mass method underscores a crucial aspect of our study: the need for tailored calculation approaches that address specific collision dynamics at maritime guiding structures. While both methods provide valuable insights into the kinetic energy dynamics during ship collisions, this comparison reveals that each has its strengths and limitations when applied to real-world scenarios. The EAU, 2012 framework, with its focus on energy absorption by berthing structures, does not sufficiently capture the nuances of collisions involving guiding structures, which often feature different dynamics and impact scenarios. Conversely, the simplified Virtual Water Mass method, by accounting for the additional mass of water moved by the ship during a collision, offers a more realistic simulation of the physical interactions during such events.

.

3

The Refined Collision Energy Calculation Method

3.1. Introduction

This chapter introduces a novel methodological approach aimed at refining the calculation of collision energy, addressing specific deficiencies in existing framework, notably the inaccurate and often static interpretation of the angle α. The need for this refinement stems from critical inconsistencies observed between theoretical predictions and empirical data, highlighting the potential for significant enhancements in structural design.

This chapter is structured to first lay the theoretical groundwork for the proposed method (Section 3.2), detailing the scientific rationale and the conceptual underpinnings that support the new approach. Following this, Section 3.3 delves into the practical implementation of the method, illustrating through theoretical models and hypothetical scenarios how the revised definitions and calculations are applied.

By systematically addressing the limitations of the conventional EAU, 2012 method and introducing an alternative, this chapter sets the foundation for subsequent validation and application presented in Chapter 4.

3.2. The Refined Collision Energy Calculation Method

The impetus for developing a new methodology for calculating collision energy is rooted in the literature reviewed in Chapter 2, which examines the limitations of the existing kinetic energy calculation framework. The EAU, 2012 framework is predominantly configured for berthing scenarios and fails to adequately address the specific conditions found in ship-to-structure collisions when the ship is at sail and the structure is a guiding structure.

3.2.1. Theoretical Basis

The inadequacies in the existing framework are presented first:

- The EAU, 2012 definition of angle α is problematic due to its vagueness, especially concerning longitudinal ship speed. This ambiguity can lead engineers to select an angle that does not accurately reflect the ship's direction relative to the structure at the point of impact. As discussed in Chapter 2, this misinterpretation can result in substantial errors in the calculation of collision energy, as the angle chosen may not truly represent the actual interaction between the ship and the structure. The two most probable interpretations of angle α are presented in figure 3.1.

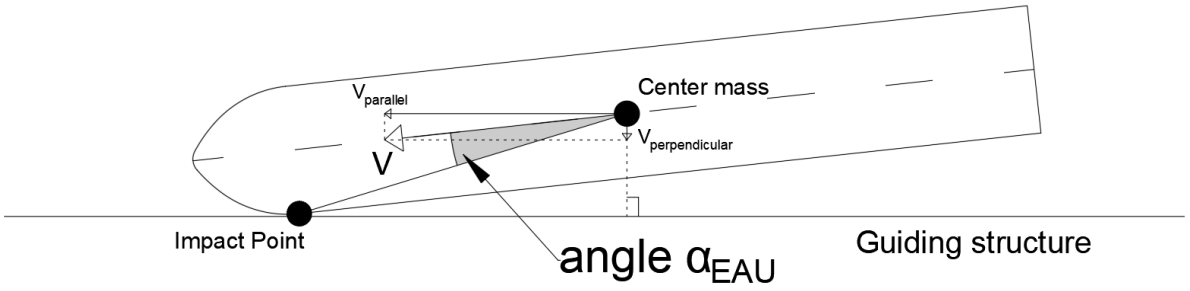

Figure 3.1: Erroneous angle α definition by EAU, 2012

- Ignoring Structural Properties: Unlike the Virtual Water Mass method, which incorporates structural properties into its calculations through the inclusion of a friction coefficient in the eccentricity expression (Chapter 2, Section 2.4.2), the EAU, 2012 framework neglects this.

3.2.2. Proposed Framework Improvement

The calculation method proposed in this thesis focuses primarily on refining the definition of angle α and validating this new approach through the Virtual Water Mass model that incorporates structural properties. This improved methodology aims to link angle α and subsequently the eccentricity coefficient direction directly to the angle of approach of the ship to the structure. In this manner, the guiding structure approaches can be represented accurately and a realistic collision energy value can be derived.

Refined Definition of Angle α

- The new definition of angle α is now determined as the angle between the perpendicular component of the ship's velocity to the structure and the line of distance **r** from the point of impact (figure 3.2). This dynamic definition allows for a more accurate representation of guiding approach scenarios by incorporating a direct link to the angle of approach.

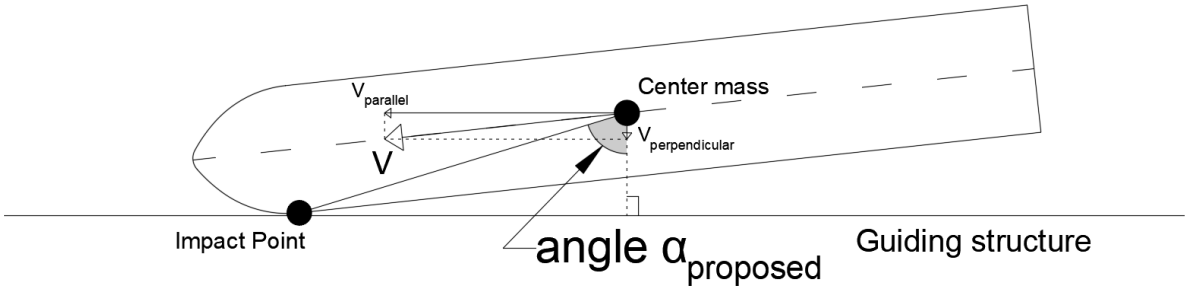

Figure 3.2: Proposed definition of angle α

Unlike the conventional method that ignores the approach angle, the new definition does not assume static or fixed angles but adjusts but adjusts regarding the ship direction in respect to the structure. At the same time it matches the philosophy of the contributing velocity component to the impact. That is the normal to the structure velocity component which is the one used by the framework in the kinetic energy equation (2.1).

Proposed Guiding Structure Approach Geometry

The new definition of angle α can be described through mathematical expression (3.1):

$$angle\ \alpha[^o] = 90^o - \phi_0[^o] - \sin^{-1}\frac{B}{2r}[^o] \tag{3.1}$$

where:

- $\phi_0[^o]$: angle of approach
- $B[m]$: Breadth of the ship
- $r[m]$: Distance of ship's centre of mass from point of impact on fender/dolphin

The implementation of the new definition of angle α into the collision energy calculations begins by revising the equations used to calculate the eccentricity coefficient and kinetic energy. This step involves altering the traditional equations where the angle was previously defined in a way that was ignoring the ship's approach angle to the structure. Now, the refined method incorporates the velocity vector's perpendicular component, in the definition of the angle, to reflect more realistic guiding structure collision dynamics. This is vital as it accounts for the actual orientation and motion of the ship at the point of impact, which significantly affects the calculated energy.

It is now possible to propose a definitive guiding structure approach geometry. This is presented in figure 3.3.

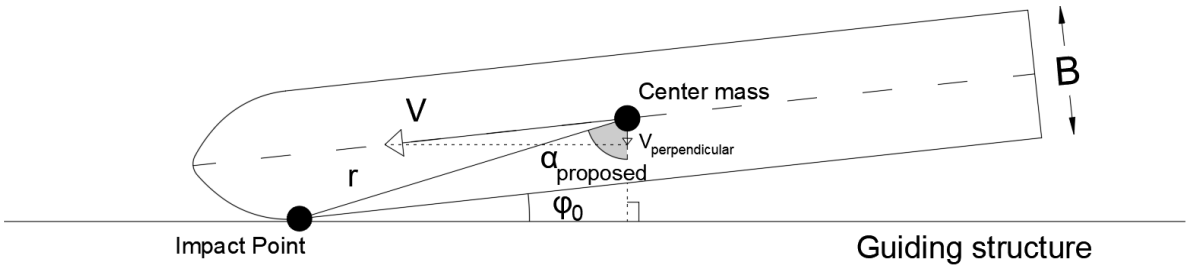

Figure 3.3: Proposed guiding structure approach geometry

3.3. Validation of the refined method

To validate the new definition of angle α, the values of the eccentricity coefficient and the kinetic energy it produces are compared to results derived by applying the EAU, 2012 framework and Virtual Water Mass method. As investigated in section 2.5, the Virtual Water Mass method shares the same philosophy of an effective mass of the vessel that is modified by two coefficients that account for the effect of the water and the eccentric impact. The difference is that the Virtual Water Mass method also takes into consideration the ship's rotational inertia and the friction between the ship and the structure on top of the geometry of ship and the approach.

3.3.1. Validation through comparison calculations

The comparison calculations are executed in the Chapter 4 for cases that have been discovered in the literature. For these cases, there are available measurements from model prototypes for the collision energy. This means that they can be used to validate analytical calculations made in the context of this research using the EAU, 2012 method, the proposed refined method and the Virtual Water Mass method.

The validation of the new approach is carried out by comparing the collision energy derived by the refined method to the one calculated with the EAU, 2012 method and the benchmark values provided by the Virtual Water Mass method. This comparison utilizes historical data and model research, where ship scenarios are recalculated using both definitions to highlight the discrepancies and improvements brought about by the new method.

3.3.2. Validation through case study

After the refined method for the collision energy calculation has been validated for its result accuracy, what is to be investigated is, if it produces the wanted results regarding the economical design. It remains to be seen if the lower collision energy translates into a structure with smaller dimensions. And if it does, the extent to which this effect is realised needs to be analyzed.

For this purpose, a real location is taken into consideration and comparison calculations between the EAU, 2012 framework and the proposed refined method are taking place once again. The case study

moves a few steps ahead the collision energy calculation up to the point of deriving the dimensions of the piles and the main girder the guiding structure consists of.

The Volkerak locks are going to serve as the case study location. Specifically the northeast lock entrance is investigated. The designs developed by the two methods will be compared and the possible material savings will be identified. The dimensions of the design are derived by doing strength material checks, pile - soil interaction effect on the strength of the pile and finally validation of the dimensions through modelling of the structure.

3.4. Conclusions

The refined calculation method introduced in Chapter 3 aims to provide a realistic approximation of the collision energy for the guiding structure approaches. The standard EAU, 2012 calculation method, falls short to provide a realistic result due to the ambiguity of the angle α variable the fails to describe the ship-to-guiding structure approach geometry.

The implementation plan outlined in this chapter involves revising the commonly used equations to calculate the eccentricity coefficient and kinetic energy. The new method integrates these revised equations into a comprehensive framework that better captures the nuances of collision scenarios. This involves comparing the new approach with established methods, such as the Virtual Water Mass method, to validate its applicability.

Moving forward, the refined method is tested through structure modelling. This allows for further assessment of the applicability of the method. The results of the method application will be showing if the method can contribute to a more economical and equally safe structure as derived with the existing framework.

4

Results and Validation

4.1. Introduction

This chapter focuses on the results derived from the application of the newly refined method for calculating the ship-to-guiding structure collision energy, as developed in Chapter 3. It emphasizes the empirical validation of the redefined angle α, showcasing how this modification enhances the accuracy and reliability of collision energy estimations.

In Chapter 3, a comprehensive methodology that incorporates a more accurate definition of angle α was established, aiming to correct the assumptions prevalent in the EAU, 2012 framework. The new approach was hypothesized to improve the predictive accuracy and robustness of collision energy calculations, particularly in ship-to-structure interaction scenarios.

Here, a series of validation tests and comparative analyses that underscore the effectiveness of the revised methodology is presented. By applying this method to simulated scenarios its enhanced capability to predict collision outcomes more reliably is demonstrated. This chapter details the testing process, the results obtained, and a comparative evaluation against traditional method and the Virtual Water Mass method, which includes structural properties in its calculations.

The findings presented here are crucial for validating the theoretical advancements made in Chapter 3 and for illustrating the practical implications of adopting this new method in engineering practices. This chapter will serve as a bridge to the subsequent implementation and broader integration of these methods.

4.2. Comparative Analysis

This section provides a comparative analysis between the newly developed methodology and the established collision energy calculation method. Performing detailed calculations historical data cases, this analysis highlights the discrepancies in predictions derived from the two methods. These calculations are executed for approaches that have been tested in published model research.

The cases are chosen in a way that they can provide valuable conclusions for this research project. The comparison of the calculations happens on a framework basis, meaning EAU, 2012 versus the proposed refined method, but also in a case to case basis. By comparing the cases to each other, conclusions regarding discrepancies between calculations can be derived. The inter-case comparison can show which of the variables introduced in the calculations is of most importance and what is its effect in the simplified proposed method.

4.2.1. Introducing the cases

The cases used for the calulations are derived from three different reports developed for TOW and Rijkswaterstaat. These are:

- Case A: Test 434A from Vrijer A., 1978, ”Belastingen op remmingwerken door schepen, varend

onder een hoek tegen het remmingwerk”

- Case B: Test R1 from Vrijburcht A., 1991, ”Loads on fender structures and dolphins by sailing ships”
- Case C: Calculation example table 11.1 from Vrijer A., 1983, ”Belasting op remmingwerken en dukdalven door varende schepen, berekeningen en modelonderzoek botskrachten”

Table 4.1: Case Data from model research reports

Case Data from model research

Ship characteristics						
Description	Case A		Case B		Case C	
Mass	m [kg]	16.7×10^6	m [kg]	12.8×10^6	m [kg]	11.6×10^6
Length	L [m]	229.50	L [m]	153.00	L [m]	153.00
Breadth	B [m]	22.70	B [m]	22.80	B [m]	22.70
Draught	d [m]	3.30	d [m]	3.90	d [m]	3.30
Longitudinal Speed	u [m/s]	2.40	u [m/s]	1.35	u [m/s]	1.509
Approach angle	ϕ [^{o}]	15	ϕ [^{o}]	15	ϕ [^{o}]	$4, 15, 30, 60, 80$

In the cases presented in these reports the ship is assumed of a rectangular shape for simplicity. So in the calculations of this chapter using these cases, the same is assumed. The actual results from the model research that is conducted for these reports are presented in Appendix C and are used to check that the Virtual Water Mass method has provided a correct output to be used as a benchmark value for the comparative analysis. The data for the ships coming from these cases in the reports are presented in table 4.1

4.2.2. Comparison Calculations for Case A

The situation of impact for Case A is presented in figure 4.1:

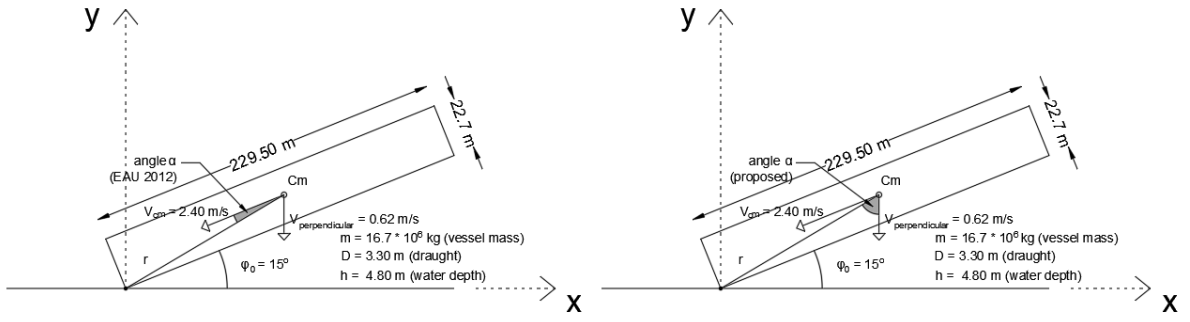

Figure 4.1: Impact Situation Case A

For the example case of the ”Vrijer A., 1978, Belastingen op remmingwerken door schepen, varend onder een hoek tegen het remmingwerk” report the definition of angle α as introduced in the EAU, 2012 and the alternate definition of angle α are presented in figure 4.1. The value of angle α is calculated by means of equation (3.1). The two cases yield the following eccentricity coefficient:

$$for\ \alpha_{EAU} = -5.64^o:\ c_{e_{EAU}} = \frac{k^2 + r^2 * \cos^2 \alpha}{k^2 + r^2} = 0.993 \tag{4.1}$$

$$for\ \alpha_{proposed\ definition} = 69.35^o:\ c_{e_{proposed}} = \frac{k^2 + r^2 * \cos^2 \alpha_{proposed}}{k^2 + r^2} = 0.348 \tag{4.2}$$

Where:

- Radius of gyration $k = (0.19 * c_b + 0.11) * L = 67.60\ m$
- Block coefficient $c_b = \frac{M}{L*B*D*\rho} = 0.97$

Having calculated the eccentricity coefficient for both definitions of the angle, the calculation of the collision energy as proposed by the EAU, 2012 - which is considered as the kinetic energy of the vessel right before impact adjusted for eccentricity and hydrodynamic effects - follows:

$$E_{EAU} = 0.5 * m_v * C_m * C_e * v^2_{perpendicular} = 4582.86\ kNm \tag{4.3}$$

$$E_{proposed\ definition} = 0.5 * m_v * C_m * C_e * v^2_{perpendicular} = 1604.86\ kNm \tag{4.4}$$

Where:

- Effective vessel mass $m_v = 16.67 * 10^6 kg$
- Virtual mass factor $C_m = 1.43$ (interpolated using the model research results in figures 30 to 47 of Vrijer, 1983a)

The kinetic energy to be absorbed by the structure due to collision turns out to be around 3 times smaller when calculated using the proposed definition for angle α in the eccentricity coefficient expression.

4.2.3. Comparison Calculations for Case B

The situation of impact for Case B is presented in figure 4.2:

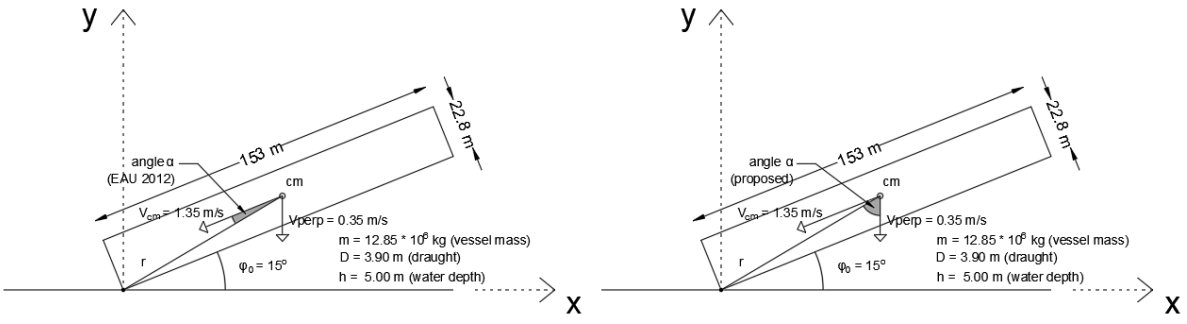

Figure 4.2: Impact Situation Case B

For the example case of the "Vrijburcht A., 1991, Loads on fender structures and dolphins by sailing ships" report the definition of angle α as introduced in the EAU, 2012 and the alternate definition of angle α are presented in figure 4.2. The value of angle α is calculated by means of equation (3.1). The two cases yield the following eccentricity coefficient:

$$for\ \alpha_{EAU} = -8.44^o:\ c_{e_{EAU}} = \frac{k^2 + r^2 * \cos^2 \alpha}{k^2 + r^2} = 0.98 \tag{4.5}$$

$$for\ \alpha_{proposed\ definition} = 66.52^o:\ c_{e_{proposed}} = \frac{k^2 + r^2 * \cos^2 \alpha_{proposed}}{k^2 + r^2} = 0.366 \tag{4.6}$$

Where:

- Radius of gyration $k = (0.19 * c_b + 0.11) * L = 44.16\ m$

- Block coefficient $c_b = \frac{M}{L*B*D*\rho} = 0.94$

Having calculated the eccentricity coefficient for both definitions of the angle, the calculation of the collision energy as proposed by the EAU, 2012 - which is considered as the kinetic energy of the vessel right before impact adjusted for eccentricity and hydrodynamic effects - follows:

$$E_{EAU} = 0.5 * m_v * C_m * C_e * v^2_{perpendicular} = 1088.05\ kNm \tag{4.7}$$

$$E_{proposed\ definition} = 0.5 * m_v * C_m * C_e * v^2_{perpendicular} = 405.26\ kNm \tag{4.8}$$

Where:

- Effective vessel mass $m_v = 12.85 * 10^6 kg$
- Virtual mass factor $C_m = 1.41$ (interpolated using the model research results in figures 30 to 47 of Vrijer, 1983b)

The kinetic energy to be absorbed by the structure due to collision turns out to be around 3 times smaller when calculated using the proposed definition for angle α in the eccentricity coefficient expression.

4.2.4. Calculations for Case C

The situation of impact for Case B is presented in figure 4.3

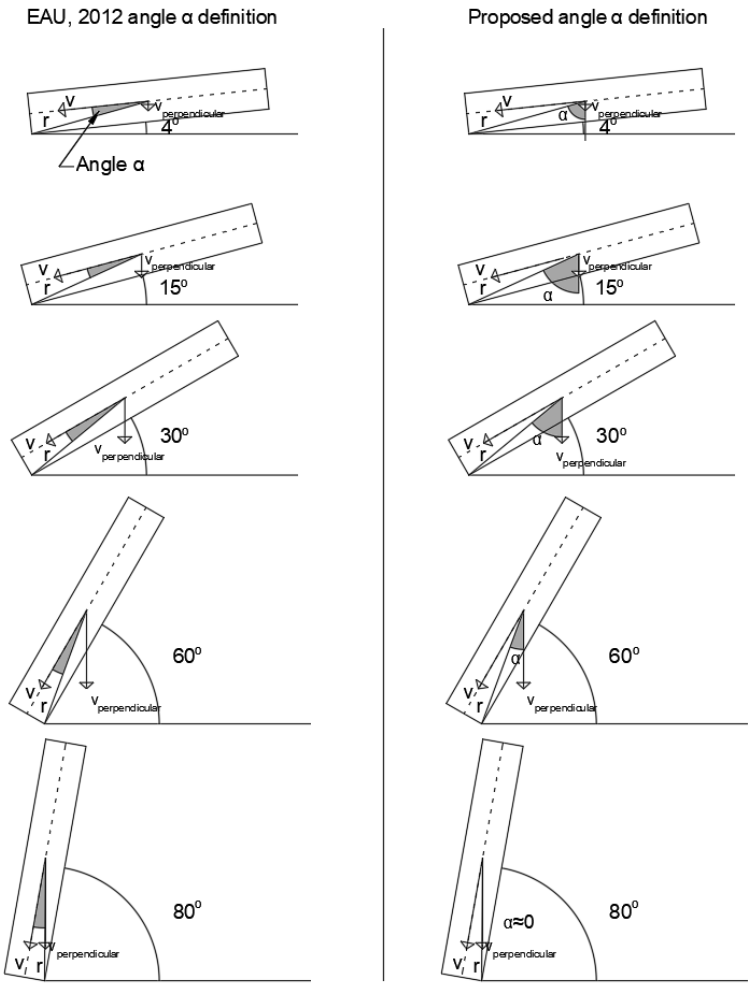

Figure 4.3: Impact Situation Case C

For the example case of the ”Vrijer A., 1983, Belasting op remmingwerken en dukdalven door varende schepen, berekeningen en modelonderzoek botskrachten” report the definition of angle α as introduced in the EAU, 2012 and the proposed definition of angle α are presented in figure 4.3. What is different in case C is that now the same vessel attempts 5 different approaches, with the approach angle changing in every calculation. The value of angle α is calculated by means of equation (3.1). The two cases yield the following eccentricity coefficients shown in table4.3:

Table 4.2: Collision energy calculated with EAU and proposed method

$\phi[^o]$	$E_{collision_{EAU}}[kNm]$	$E_{collision_{proposed}}[kNm]$
4	88.09	23.61
15	1212.69	390.25
30	4525.81	2118.82
60	10159.33	8585.78
80	12277.86	12278.23

Table 4.3: Eccentricity Coefficients for different ϕ

$\phi[^o]$	α_{EAU}	$C_{e_{EAU}}$	$\alpha_{proposed}$	$C_{e_{proposed}}$
4	8.44^o	0.984	85^o	0.264
15	8.44^o	0.984	74^o	0.317
30	8.44^o	0.984	58^o	0.461
60	8.44^o	0.984	28^o	0.832
80	8.44^o	0.984	0^o	1

What is interesting in the results presented in table 4.3 is the results for the 80^o angle approach. There the EAU, 2012 gives of course the static value for eccentricity of 0.984 but the calculation with the new definition of angle α gives an eccentricity of 1. This unveils the inability of the existing framework to accurately predict even the central impact. Of course, the error there is less than 2%, and in the collision energy result (4.2) the error is almost zero, but conceptually it is important to understand that the method missed this situation, too.

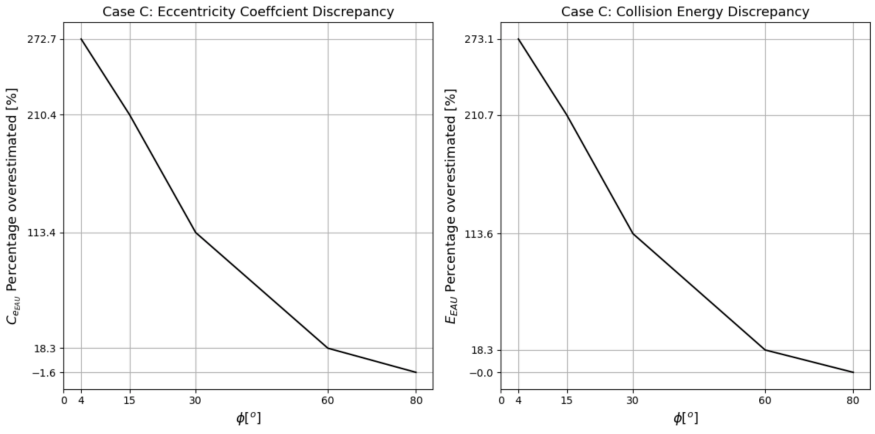

Figure 4.4: Discrepancy EAU, 2012 compared to Proposed method

The discrepancy between the EAU, 2012 calculated values and the proposed method is displayed in

figure 4.4

The reader should focus on the results presented for the angle of approach range $4^o \leq \phi_0 \leq 20^o$ (figure 4.4), because these are the expected approaches at the guiding structures, since these are designed for angles between 10^o - 15^o. And this is the area where the discrepancy is the largest. Meaning, that especially for the guiding structure approaches the existing framework performs the poorest, overestimating the kinetic energy by very large percentages.

4.3. Validation using simulation and model data

The refined methodology's validation is further supported through detailed simulations and the use of model data. This section compares the results obtained from the new calculations with those derived from the Virtual Water Mass method, which incorporates structural properties and has been used as a benchmark. The alignment of results from both methods confirms the effectiveness of the revised angle definition, proving that it can provide comparable outcomes without directly incorporating structural properties. Elements from Section 4.2 regarding the consistency and accuracy of the collision energy calculations using the new methodology will be integrated here, emphasizing how the revised definition of angle α aligns with empirical data across a variety of simulated scenarios.

Examining the behavior of the structure to the collision forcing by modelling the ship-structure interaction can prove to be very beneficial. The configuration of methods such as the Virtual Water Mass rely on inputs with definitions that do not allow for ambiguity compared to the ones of the kinetic energy approach. The progression of the resistance force of the structure is directly connected to the ship's direction and speed at impact and when the properties of the vessel and the structure are inputted correctly, the outcome for the maximum force and displacement is reliable. The progression curves are combined to produce a force - deflection curve, the area under which is the amount of the kinetic energy absorbed by the fender structure because of the impact. This collision energy calculation will be the ballpark figure to which the calculated collision energy with the proposed definition for angle α will be compared to for validity.

From the model research in the report of Vrijer A., 1978, "Belastingen op remmingwerken door schepen, varend onder een hoek tegen het remmingwerk" we obtain a simplified version of the Virtual Water Mass Method. Now, apart from the ship characteristics displayed in table 4.1, the structure characteristics need to be introduced (table 4.4). The simplified Virtual Water Mass method is reproduced in a python notebook for every case and the force-deflection curve is calculated. An example notebook is presented in Appendix C. The area under the force-deflection curve is the collision energy (or the kinetic energy of the ship absorbed by the structure due to collision). This energy serves as a baseline for comparing the validity of the collision energy calculated with the proposed definition for angle α.

Table 4.4: Data from model research reports - Fender structure

Data from model research

Fender structure characteristics						
Description	Case A		Case B		Case C	
Mass	M [kg]	1.1×10^6	M [kg]	0	M [kg]	1.1×10^6
Spring stiffness	k [N/m]	3.2×10^6	k [N/m]	2×10^6	k [N/m]	3.2×10^6
Damping factor	c [Ns/m]	1.0×10^6	c [Ns/m]	0.65×10^6	c [Ns/m]	0.405×10^6
Friction coefficient	tgβ [-]	0.16	tgβ [-]	0.40	tgβ [-]	0.16

4.3.1. Validation for Case A

For Case A, the collision energy calculated with the EAU,2012 method was $E_{EAU} = 4585.86\ kNm$. Whereas for the proposed definition it turned out to be $E_{proposed\ definition} = 1604.86\ kNm$.

Figure 4.5 illustrates the force-deflection curve for Case A, showing the relationship between the impact force applied by the ship and the resultant deflection of the structure. This curve is crucial as it quantifies the kinetic energy absorbed by the structure due to the collision. The area under this curve represents

the total collision energy, providing a visual representation of how the energy dissipates through the structure as it deforms under impact.

The model research by Vrijer, 1983a for Case A (or for test 434A in the model research) gives a collision energy of 900 kNm. Thus, the reproduction of the Virtual Water Mass method is accepted as a benchmark value.

The graph is used to validate the collision energy calculated using the new methodology against the Virtual Water Mass method. The curve helps in assessing the efficiency of the fender system in absorbing impact energy, which is vital for designing structures that can withstand such impacts without significant damage.

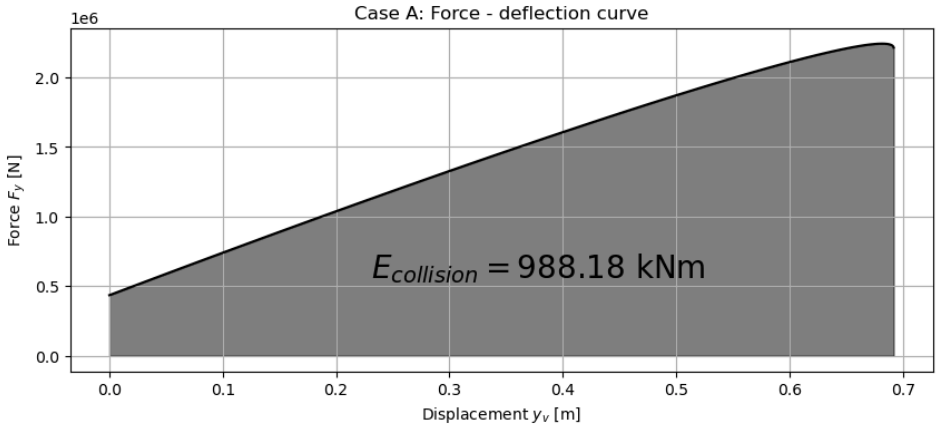

Figure 4.5: Force - Deflection curve and Collision Energy Case A

The eccentricity factor a_{bwz} of the Virtual Water Mass method is calculated for Case A as follows:

$$\alpha = \frac{1}{2} * (L * \cos\phi_0 - B * \sin\phi_0) = \frac{1}{2} * (229.50 * \cos 15 - 22.70 * \sin 15) = 107.90\ m \tag{4.9}$$

$$b = \frac{1}{2} * (L * \sin\phi_0 - B * \cos\phi_0) = \frac{1}{2} * (229.50 * \sin 15 - 22.70 * \cos 15) = 40.66\ m \tag{4.10}$$

$$a_{bwz} = \frac{1}{1 - 12 * \frac{\alpha * (b * tg\beta - \alpha)}{L^2}} = \frac{1}{1 - 12 * \frac{107.90 * (40.66 * 0.16 - 107.80)}{229.50^2}} = 0.286 \tag{4.11}$$

For the EAU, 2012 eccentricity and the proposed method one the values were $c_{e_{EAU}} = 0.993$ and $c_{e_{proposed}} = 0.348$ respectively.

4.3.2. Validation for Case B

For Case B, the collision energy calculated with the EAU,2012 method was $E_{EAU} = 1088.05\ kNm$. Whereas for the proposed definition it turned out to be $E_{proposed\ definition} = 405.26\ kNm$.

Figure 4.6 illustrates the force-deflection curve for Case A, showing the relationship between the impact force applied by the ship and the resultant deflection of the structure. This curve is crucial as it quantifies the kinetic energy absorbed by the structure due to the collision. The area under this curve represents the total collision energy, providing a visual representation of how the energy dissipates through the structure as it deforms under impact.

The graph is used to validate the collision energy calculated using the new methodology against the Virtual Water Mass method. The curve helps in assessing the efficiency of the fender system in absorbing impact energy, which is vital for designing structures that can withstand such impacts without significant damage.

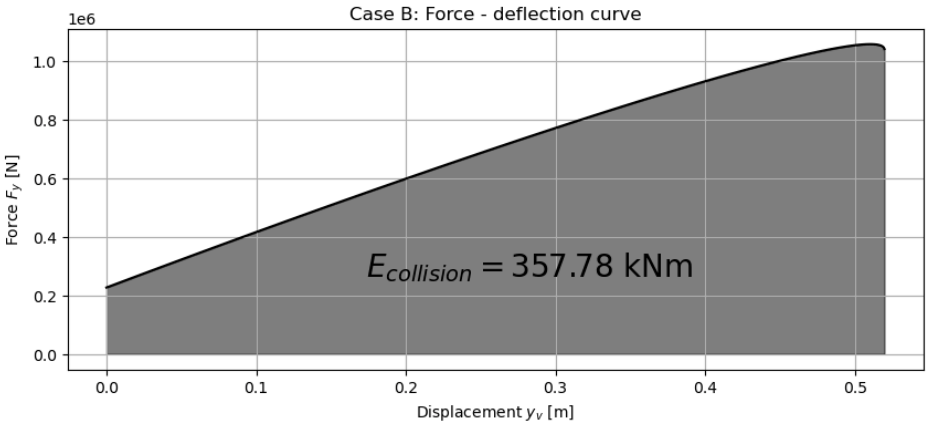

Figure 4.6: Force - Deflection curve and Collision Energy Case B

The model research by Vrijburcht, 1991 for Case B (or for test R1 in the model research) gives a collision energy of 339 kNm. Thus, the reproduction of the Virtual Water Mass method is accepted as a benchmark value.

The eccentricity factor a_{bwz} of the Virtual Water Mass method is calculated for Case A as follows:

$$\alpha = \frac{1}{2} * (L * \cos\phi_0 - B * \sin\phi_0) = \frac{1}{2} * (153 * \cos 15 - 22.80 * \sin 15) = 70.94\ m \tag{4.12}$$

$$b = \frac{1}{2} * (L * \sin\phi_0 - B * \cos\phi_0) = \frac{1}{2} * (153 * \sin 15 - 22.80 * \cos 15) = 30.81\ m \tag{4.13}$$

$$a_{bwz} = \frac{1}{1 - 12 * \frac{\alpha * (b * tg\beta - \alpha)}{L^2}} = \frac{1}{1 - 12 * \frac{70.94 * (30.81 * 0.40 - 70.94)}{153^2}} = 0.319 \tag{4.14}$$

The eccentricity factor has value $a_{bwz} = 0.319$, whereas for the EAU, 2012 eccentricity and the proposed one the values were $c_{e_{EAU}} = 0.984$ and $c_{e_{proposed}} = 0.366$ respectively.

4.3.3. Validation for Case C

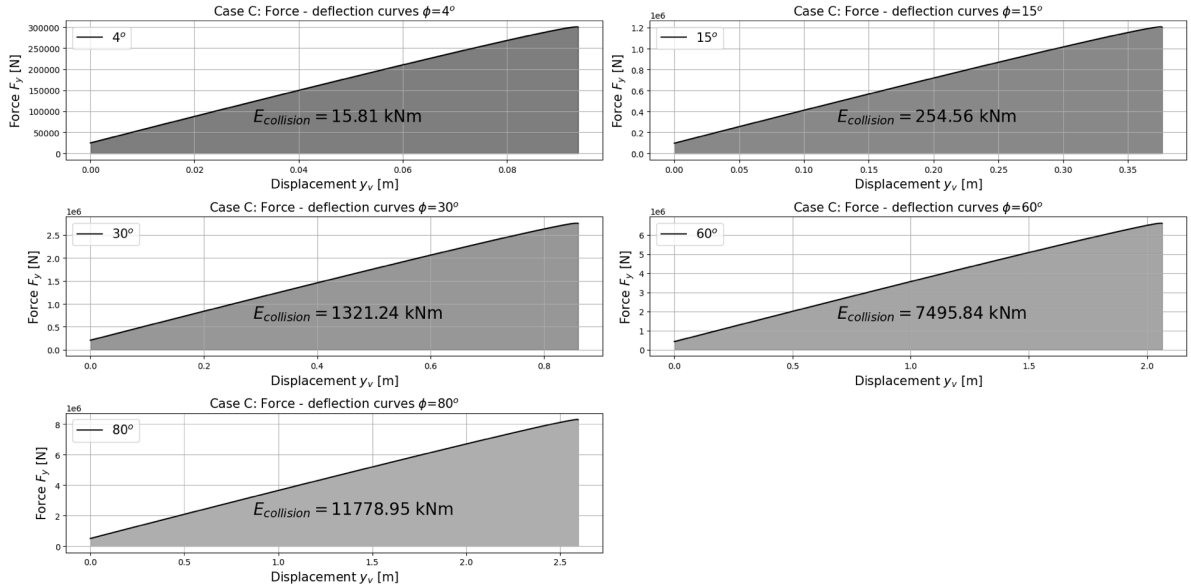

Figure 4.7: Force - Deflection curve and Collision Energy Case C

In Case C, the ship performs 5 approaches with different approach angle ϕ_0 each time. The collision energy using the EAU, 2012 method and the proposed one are shown for the 5 approaches in table 4.2, whereas for the Virtual Water Mass calculations the results are presented in figure 4.7.

The vessel attempted five different approaches, with angles of 4^o, 15^o, 30^o, 60^o, and 80^o, to examine how the collision energy calculations would vary with changes in the approach angle. This comprehensive analysis allowed for a detailed evaluation of the proposed definition of angle α across a spectrum of typical and extreme maritime collision conditions.

The eccentricity factors a_{bwz} for the 5 approaches are presented in table 4.5 along with the $C_{e_{EAU}}$ and $C_{e_{proposed}}$ that were calculated in section 4.2.4.

Table 4.5: Eccentricity Coefficients a_{bwz} for different ϕ

$\phi[^o]$	$C_{e_{EAU}}$	$C_{e_{proposed}}$	a_{bwz}
4	0.984	0.264	0.262
15	0.984	0.317	0.294
30	0.984	0.461	0.378
60	0.984	0.832	0.802
80	0.984	1	1

In the model research by Vrijer, 1983a in Table 11.1 a log is presented with the model research results for Case C. The table contains information regarding the maximum force and the maximum displacement for every approach angle. Since a curve cannot be reproduced from Vrijer's report and a clear value for the energy absorbed is not provided, the energy calculation will follow the general energy transfer principle for the structure response as shown in equation 4.15:

$$E = 0.5 * Force * Displacement \tag{4.15}$$

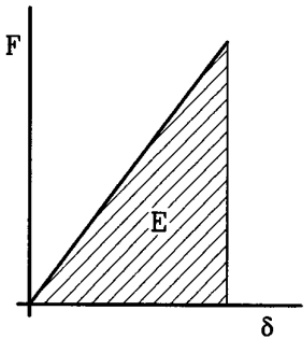

Figure 4.8: Force - Displacement Relationship (EAU,2012)

The relevant information from Table 11.1 of Vrijer, 1983a is reproduced here to calculate the collision energy from the model research results (table 4.6). The reproduction of the Virtual Water Mass method is again accepted safely as benchmark since it provides numbers close but a bit higher to the model research.

Table 4.6: Collision energy Case C, model research results by Vrijer, 1983a

$\phi[^o]$	$Maximum\ Force\ [kN]$	$Maximum\ Displacement\ [m]$	$E_{model}\ [kNm]$
4	290	0.089	12.91
15	1130	0.352	198.88
30	2580	0.803	1035.87
60	6600	2.06	6798.00
80	8160	2.54	10363.20

For each approach angle, collision energies were recalculated using both the conventional EAU, 2012 method and the proposed definition. The differences in calculated energies highlighted the sensitivity of collision energy estimates to the angle of approach, underscoring the importance of using a method that accurately reflects the dynamic interaction between the ship and the structure.

- Low Angles (4° and 15°): At these angles, the proposed method showed significantly lower collision energies, suggesting that the conventional method might overestimate the impact severity when the approach angle is small. This is a pivotal finding in the research as this angle range facilitates the guiding structure approaches.
- Moderate to High Angles (30°, 60°, 80°): As the angle increased, the discrepancy between the two methods decreased, particularly at 80 degrees, where the values almost converged. This indicates that the proposed method provides a more nuanced and accurate estimation of collision energy as the interaction becomes more direct and typical of high-energy impacts.

For **Case C** the discrepancies between the proposed method and the Virtual Water Mass method are presented in figure 4.9.

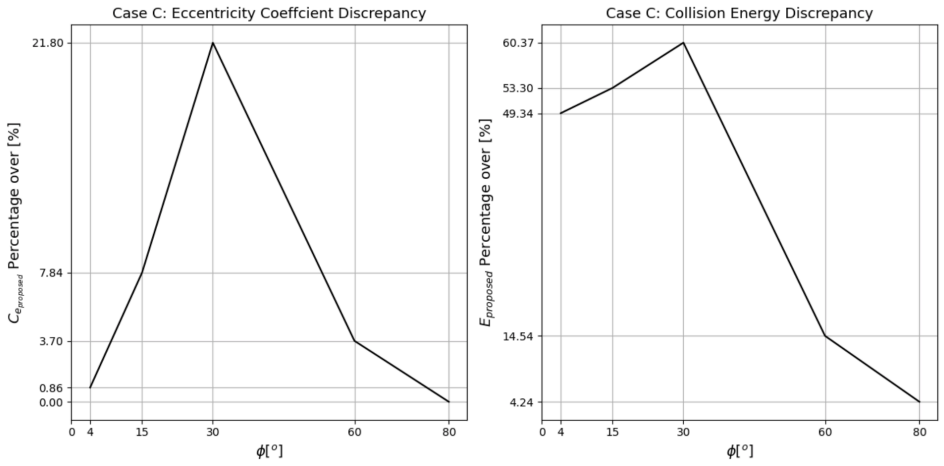

Figure 4.9: Case C Discrepancies Proposed method over Virtual Water Mass method

Figure 4.9 consists of two line charts illustrating the discrepancies in eccentricity coefficients and collision energies for Case C across various approach angles. Each chart is clearly labeled to show how these discrepancies change with the approach angle.

The left graph's x-axis represents the approach angle in degrees, ranging from 0 to 80 degrees, while the y-axis indicates the percentage discrepancy in the eccentricity coefficient over the a_{bwz} value. The trend in this graph reveals a significant peak at 30 degrees, where the discrepancy reaches approximately 21.8%. As the approach angle increases beyond 30 degrees, there is a sharp decline in the discrepancy, dipping to a zero value as the angle approaches 80 degrees.

Similarly, the right graph's x-axis shows the approach angle in degrees, and the y-axis displays the percentage discrepancy in collision energy over the $E_{virtual\ mass}$ value. This graph indicates an initial increase in discrepancy, peaking around 30 degrees with a value close to 60.37%. After reaching this peak, the discrepancy generally decreases as the angle increases, and it diminishes significantly as the approach angle extends beyond 60 degrees.

The discrepancy of the EAU, 2012 calculated collision energy over the values of the Virtual Water Mass method are presented in figure 4.10.

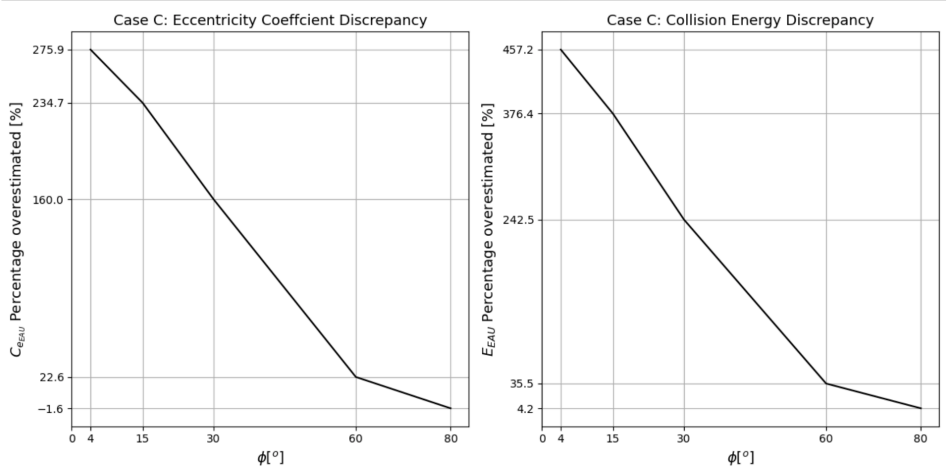

Figure 4.10: Case C Discrepancies EAU,2012 method over Virtual Water Mass method

The graph depicting the Eccentricity Coefficient Discrepancy for Case C shows a sharp decline in the percentage overestimation as the angle ϕ increases from 0 to 80 degrees. Initially, at 0 degrees, the eccentricity coefficient $C_{e_{EAU}}$ is overestimated by approximately 275.9%, indicating a significant discrepancy in the calculation method's prediction. As the angle increases, this overestimation dramatically decreases, reaching a near-zero overestimation (about -1.6%) at 80 degrees. This trend suggests that the EAU, 2012 method's accuracy in predicting the eccentricity coefficient improves as the angle of approach becomes more acute relative to the lock structure. Of course, the real meaning of the line is not exactly this. The decrease is circumstantial as the eccentricity coefficient by the EAU, 2012 is static and always has a value that better fits an eccentric impact. This is why the larger the angle of approach, the lower the discrepancy is. The graph highlights the need for revising how eccentricity coefficients are calculated at lower angles to reduce substantial initial overestimations.

The Collision Energy Discrepancy graph for Case C also demonstrates a substantial initial overestimation of collision energy by the EAU method, which diminishes as the angle ϕ increases. Starting at an overestimation close to 457.2% at 4 degrees, there is a pronounced decrease, with the discrepancy dropping to about 4.2% at 80 degrees. This data reflects how the traditional model tends to greatly overestimate the collision energy, particularly at lower angles.

4.3.4. Summarizing the validation results

This section provides a consolidated overview of the validation results obtained from the application of the corrected angle definition across three distinct cases—A, B, and C. These cases were carefully selected to test the proposed method under varying conditions and to highlight its capability to accurately predict collision energies in real-world scenarios.

The results summarized in table 4.8 clearly show how the proposed definition for angle α influences the calculated collision energies compared to traditional methods and the Virtual Water Mass method.

For **Case A** the calculated eccentricity coefficient with the correct definition of angle α, $C_{e_{proposed}} = 0.348$, is around 20% larger than the one calculated by the Virtual Water Mass method $a_{bwz} = 0.286$. This is a considerable discrepancy but still the lower limit one could get trying to apply a definition of C_e

Table 4.7: Case Data from model research reports: Summary

Case Data from model research						
Ship characteristics						
Description	Case A		Case B		Case C	
Mass	m [kg]	16.7×10^6	m [kg]	12.8×10^6	m [kg]	11.6×10^6
Length	L [m]	229.50	L [m]	153.00	L [m]	153.00
Breadth	B [m]	22.70	B [m]	22.80	B [m]	22.70
Draught	d [m]	3.30	d [m]	3.90	d [m]	3.30
Depth	h [m]	4.80	h [m]	5.00	h [m]	16.00
Longitudinal Speed	u [m/s]	2.40	u [m/s]	1.35	u [m/s]	1.509
Approach angle	ϕ [^{o}]	15	ϕ [^{o}]	15	ϕ [^{o}]	$4, 15, 30, 60, 80$
Fender structure characteristics						
Mass	M [kg]	1.1×10^6	M [kg]	0	M [kg]	1.1×10^6
Spring stiffness	k [N/m]	3.2×10^6	k [N/m]	2×10^6	k [N/m]	3.2×10^6
Damping factor	c [Ns/m]	1.0×10^6	c [Ns/m]	0.65×10^6	c [Ns/m]	0.405×10^6
Friction coefficient	tgβ [-]	0.16	tgβ [-]	0.40	tgβ [-]	0.16

that remains free of the structure properties. This discrepancy will be reflected on later in this section. The collision energy $E_{proposed\ definition} = 1604.86\ kNm$ is 62% larger than $E_{virtual\ mass} = 988.18\ kNm$.

For **Case B** the calculated eccentricity coefficient with the correct definition of angle α, $C_{e_{proposed}} = 0.366$, is around 14% larger than the one calculated by the Virtual Water Mass method $a_{bwz} = 0.319$. This is a considerable discrepancy but still the lower limit one could get trying to apply a definition of C_e that remains free of the structure properties. This discrepancy will be reflected on later in this section. The collision energy $E_{proposed\ definition} = 405.26\ kNm$ is 13% larger than $E_{virtual\ mass} = 357.78\ kNm$.

Table 4.8: Summarized results for all cases

$Case$	$C_{e_{EAU}}$	$C_{e_{proposed}}$	a_{bwz}	E_{EAU}	$E_{proposed\ definition}$	$E_{virtual\ mass}$
A	0.993	0.348	0.286	4582.86	1604.86	988.18
B	0.984	0.366	0.319	1088.05	405.26	357.78
C	-	-	-	-	-	-
4^o	0.984	0.264	0.262	88.09	23.61	15.81
15^o	0.984	0.317	0.294	1212.69	390.25	254.56
30^o	0.984	0.461	0.378	4525.81	2118.82	1321.24
60^o	0.984	0.832	0.802	10159.33	8585.78	7495.84
80^o	0.984	0.984	1	12277.86	12278.25	11778.95

An interesting remark on the summarized results can be made when looking into all the approaches of 15^o. These are Case A, B, and C-15^o. There, the effect of the structure properties are realised. The structure of Case B, not only has a larger friction coefficient of the one in cases A and C-15^o ($tg\beta_B = 0.40$, $tg\beta_{A,C} = 0.16$) but it is also a less stiff structure overall with $k_B = 2 * 10^6 N/m$ compared to the stiffness of $k_{A,B} = 3.2 * 10^6 N/m$ of the other two structures. The proposed definition for Case A and Case C-15^o calculates a collision energy 53 to 62% larger than what the Virtual Water Mass method calculates, whereas for Case B this percentage is 13%. This difference in the discrepancy finds its reason in the exclusion of the structure properties in the eccentricity coefficient and in the design process overall. The Virtual Water Mass method models the structure's response, being able

to include the structure properties and derive a more trustworthy result of the energy absorbed by the structure. But, since the proposed definition does not include structure properties, this is a point that is missed, the collision energy then is more overestimated, but still significantly less compared to the extreme EAU, 2012 overestimation.

4.4. Conclusions

The validation conducted in Chapter 4 through comparative analyses of historical data case studies, provides evidence supporting the efficacy of the refined methodology for calculating collision energy, with a particular focus on the redefined angle α.

The adjusted methodology consistently outperformed the EAU, 2012 method in predicting collision energies. Specifically, for Case A, the proposed method calculated a collision energy of 1604.86 kNm, significantly lower than the 4582.86 kNm estimated using the EAU, 2012 method, but closer to the 988.18 kNm obtained via the Virtual Water Mass method. In Case B, the new method estimated the collision energy at 405.26 kNm, compared to 1088.05 kNm (EAU, 2012) and 357.78 kNm (Virtual Water Mass). This consistency highlights the method's improved alignment with empirical data and model-based predictions. Although, when friction becomes important, an overestimation should be expected but not to the significantly exaggerated extent the EAU, 2012 framework shows.

The revised approach proved suitable for a variety of conditions, including different ship sizes, velocities, and impact angles. For example, in Case C, the discrepancies between the proposed method and the Virtual Water Mass method were clearly illustrated in Figure 4.9. The eccentricity coefficient calculated for Case C showed that at a 15-degree approach angle, the proposed method had a discrepancy of approximately 21.8%, which is the peak discrepancy. The $C_{e_{proposed}}$ performs better than the C_{eEAU} as proved by comparing figure 4.9 and figure 4.10. The refined definition allowed for the method to accurately describe the ship's approach to the guiding structure giving realistic results for both the eccentricity coefficient and the collision energy. This is a blind spot of the existing framework by the EAu, 2012 where all guiding structure approaches are translated into almost central collisions between the ship and the structure.

The calculated eccentricity coefficients using the new definition of angle α showed improvements over the standard method. For Case A, the proposed coefficient (0.348) was about 20% larger than the Virtual Water Mass method's coefficient (0.286), while for Case B, it was approximately 14% larger (0.366 vs. 0.319). These results indicate that the new definition provides a more accurate representation of the physical interactions during collisions, without compromising the structural properties.

5

Case study: Volkerak lock

This chapter presents a detailed case study focused on the application of the newly refined methodology for calculating collision energy at the Volkerak Lock. The objective of this study is to critically assess the effectiveness and accuracy of the proposed method by comparing it with traditional approaches under real-world conditions. The Volkerak Lock, a vital maritime infrastructure component, presents unique challenges and demands precise and reliable collision energy calculations to ensure structural integrity and safety. This case study aims to validate the theoretical improvements suggested in previous chapters by implementing them in a practical scenario, thereby demonstrating their relevance and applicability.

5.1. Location Description

The Volkerak Locks, strategically situated at the junction between the Rhine and Meuse rivers, play a pivotal role in facilitating inland waterway traffic in one of Europe's busiest waterways. Since their inception in 1967, these locks have been essential in connecting the ports of Rotterdam and Antwerp with Germany's hinterland, making them the largest locks in Europe at that time (Steenhuis, 2015). The locks manage the flow between Volkerak and the Hollands Diep, an estuary that provides vessels with access to the North Sea. This critical position underscores their importance not just for local but also for international maritime operations.

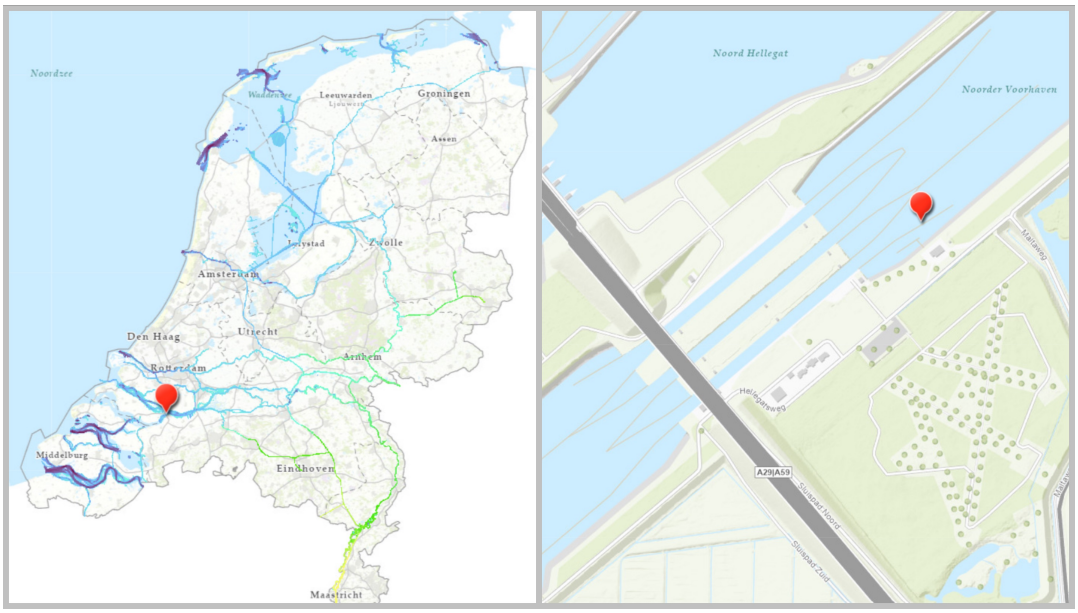

Figure 5.1: Volkerak Locks Location

The Volkerak Locks serve a significant volume of maritime traffic, with thousands of vessels passing through annually. Almost 150000 cargo ships pass the lock every year (Wongnitchakul, 2023). This heavy use emphasizes the need for precise and reliable infrastructure to manage the logistical demands of such a busy waterway. The locks not only support commercial and industrial shipping but also play a role in water management and environmental protection within the Rhine–Meuse–Scheldt delta (Aslan, 2023).

By situating the case study at the Volkerak Locks, this research taps into a location that exemplifies the complexities and challenges of modern maritime traffic and infrastructure management, providing a relevant and impactful context for testing the newly developed methodologies for collision energy calculation.

This setting, combined with its operational significance and the volume of traffic it handles, offers a robust framework for the practical application of theoretical advancements proposed in this thesis. The findings here could potentially influence future designs and operational standards not just locally but globally, given the international significance of the routes the Volkerak Locks service.

The Volkerak locks are positioned on the ”Hollandsch Diep naar de Schelde-Rijnverbinding, Krammer en Grevelingenmeer” waterway which carries a CEMT-VIb waterway class. The permissible ship dimensions in this waterway are 200 m length, 22.80 m width and 4.75 m draught while the allowed sailing speed for the waterway is 4.7 m/s (Euris Portal, 2024).

The bathymetry in the area is acquired by two sources one being the bathymetry map viewer by Rijkswaterstaat and the second being the chart viewer provided by Navionics. The bathymetry by Navionics is presented here as it is given in contours and is easier to read.

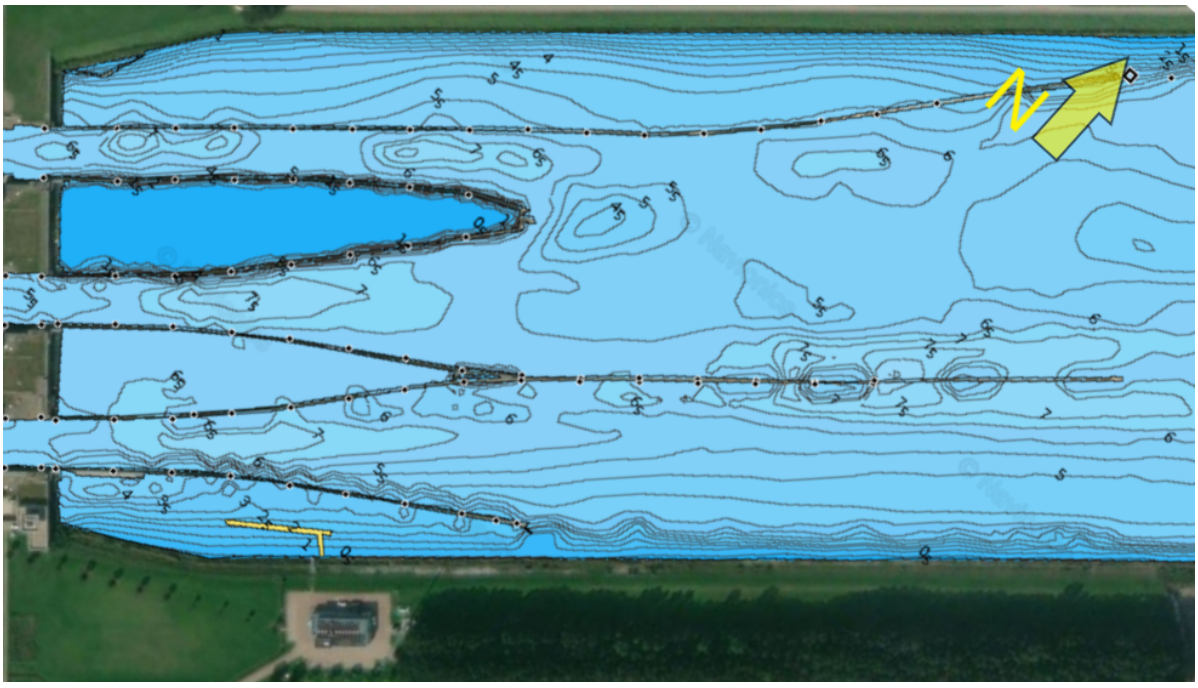

Figure 5.2: Guiding structure location bathymetry by Navionics Chart Viewer

5.2. Organizing the Volkerak lock comparison calculations

This chapter is organized as a side by side comparison calculation of the EAU, 2012 framework versus the adjusted proposed framework with the modified definition for angla α. The calculations of the case study are organised in the following steps:

1. Hand calculations: Kinetic energy approach
2. Hand calculations: Pile - soil interaction, pile diameter and length

3. Modelling: Optimizing for girder connected pile series

In order for the calculations to be carried out, some assumptions need to be made. These assumptions are related to the structure, the soil, the ship and the approach characteristics.

5.2.1. Structure characteristics

Starting with the model representing the guiding structure. The guiding structure consists of six equally sized vertical piles that are connected together with a main horizontal girder of equal size in diameter as the vertical piles schematized as shown in figure 5.3. The vertical members symbolized with letter S represent the vertical piles whereas the horizontal members represent the main girder. The K nodes represent the fixed supports for the vertical piles and the welded connections between the vertical piles and the main girder.

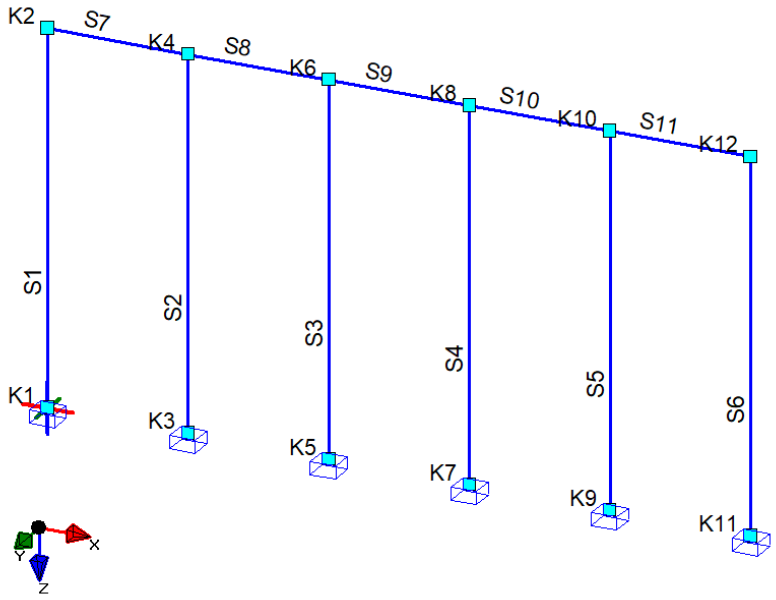

Figure 5.3: Structure Model

The material to be used for the pile is tube steel X70 with a young modulus of $E_{young} = 2.1 * 10^{11}\ N/m^2$, Poisson ratio of $v = 0.3$ and yield stress of $\sigma_{yield} = 483 * 10^6\ N/m^2$. The shape of the tubular pile is presented in figure 5.4 where D is the diameter of the pile and t is the thickness. For steel, the material safety factor is the unity $\gamma_{M0} = 1$.

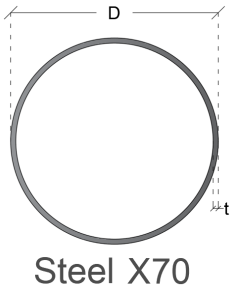

Figure 5.4: Steel Pile X70

The diameter of the pile is derived by performing iterative calculations for displacement convergence as instructed by the Blum method, later in this chapter. The structure is checked for stiffness and strength. The displacements of the structure appearing due to the force load exerted by the ship should be such that the kinetic energy of the ship is absorbed. The structure is then checked for strength where the moment load should not exceed the design moment of the piles.

5.2.2. Soil characteristics

For the soil in the area a CPT test is obtained from the DINOloket Data and Information of the Dutch Subsurface. The CPT test can be found in the appendix B. The soil properties are determined using the graph by Robertson, 1986 also found in the appendix B.

The friction ratio is found to be $1 - 1.5\%$. This indicates soil consisting of fine sand with the following properties:

- Saturated volumetric weight $\gamma_s = 20\ \frac{kN}{m^3}$
- Dry volumetric weight $\gamma_d = 18\ \frac{kN}{m^3}$
- Angle of internal friction $\phi_f = 35^o$
- Internal wall friction $\delta_f = -\frac{2}{3}\phi$

The passive soil pressure coefficient [1] is calculated:

$$K_{p,h,\sigma} = \frac{\cos^2 \phi_f}{(1 - \sqrt{\frac{\sin(\phi_f - \delta_f) * \sin \phi_f}{\cos - \delta_f}})^2} = 9.14 \tag{5.1}$$

5.2.3. Ship Characteristics

To define the design vessel depending on the waterway class, the information is given in Table 8 in Richtlijnen-Vaarwegen, 2020 (Appendix table A.1). The CEMT-VIb waterway class requires a design vessel with the following characteristics (5.5):

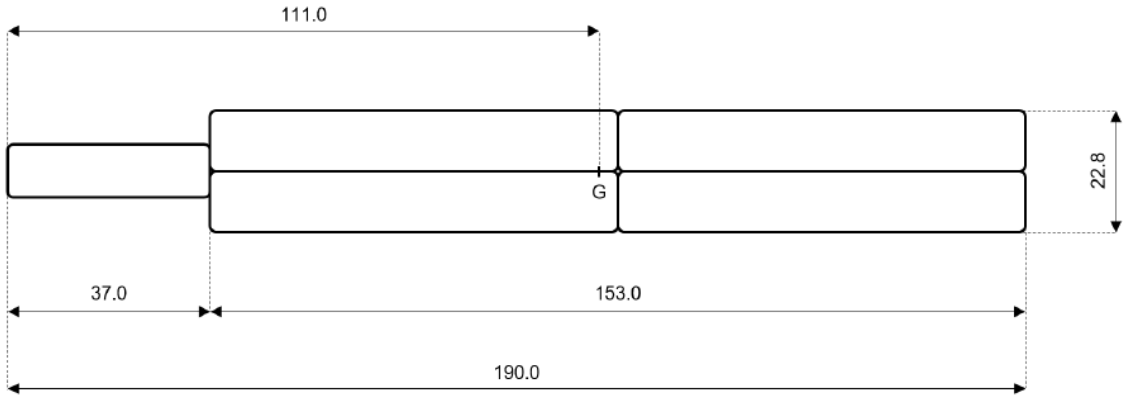

Figure 5.5: Typical 4-barge/ pusher convoy for CEMT-VIb, (Rijkswaterstaat, 2022)

- Length overall $L_{OA} = 190\ m$
- Breadth $B = 22.8\ m$
- Draught $d = 4.00\ m$
- Mass $m_s = 13.68 * 10^6\ kg$

For the design vessel the lenght overall is set to $L_{OA} = 200\ m$ and the breadth is set to a value of $B = 24\ m$ despite the instructions so that it follows the dimensions of the maximum allowed in the lock. The design vessel is presented in a conventional shape for illustration purposes in figure 5.6.

From the geometry of the vessel it is now possible to calculate the block coefficient C_b, the radius of gyration k and the virtual mass coefficient C_m. All three of these variables are calculated according to the EAU, 2012.

[1] The soil resistance only depends on the angle of internal friction and the volumetric weight of the soil. Almost always the effective (submerged) weight of the soil has to be used in combination with $\delta_f = -\frac{2}{3}\phi_f$, to calculate the $K_{p,h,\sigma}$, and arrive at the lateral bearing capacity.

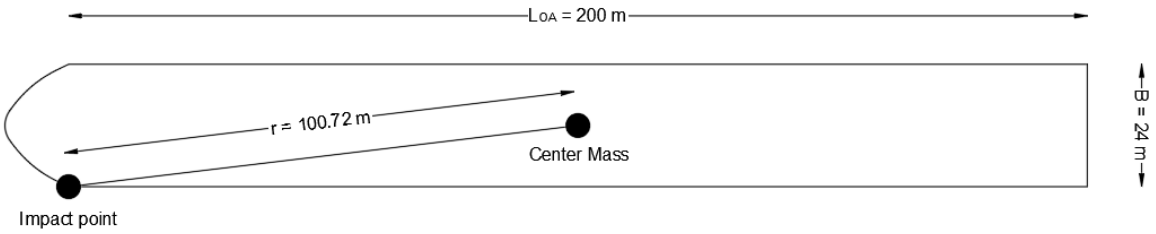

Figure 5.6: Design Vessel

$$C_b = \frac{m_s}{L_{OA} * B * \rho_w * d} = 0.71 \tag{5.2}$$

$$k = (0.19 * C_b + 0.11) * L_{OA} = 49.08m \tag{5.3}$$

$$C_m = 1.875 - 0.75 * \frac{h-d}{d} = 1.594 \tag{5.4}$$

5.2.4. Approach characteristics

According to clause 0653 by the ROK 2.0 for determining the collision energy on a guiding structure the ship speed must be calculated in accordance with table T0718 of the ROK 2.0 (appendix A) and an angle of approach with the guides relative to the axis of the waterway plus 5 degrees. For the Volkerak locks the guiding structures have a 10^o angle with the waterway axis, which according to this clause leads to an approach angle of 15^o between the ship's longitudinal axis and the guiding structure (figure 5.7). The ship's speed although the ROK-0653 clause instructs to derive it from table T0178, the ROK-0650 clause states that when the design is within a ship's length distance from the lock entrance, then maximum speed should be taken as $3\ m/s$. In this case the guiding structure falls within this description.

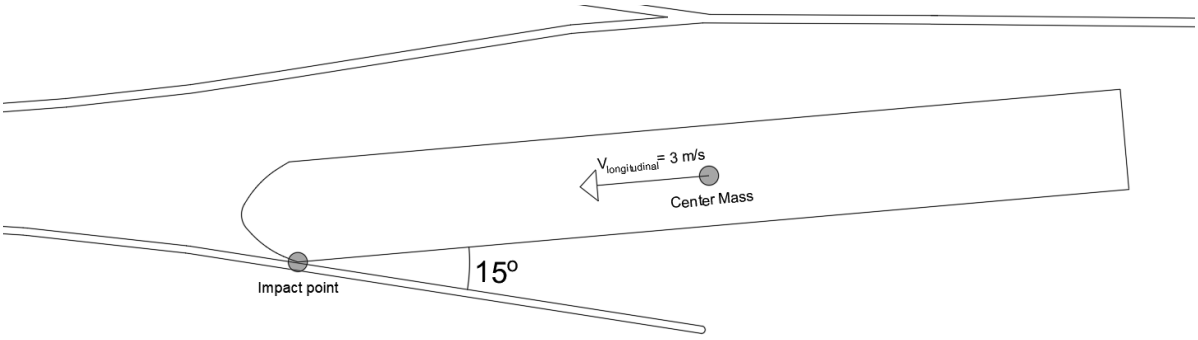

Figure 5.7: Approach at Volkerak locks

5.3. Hand calculations: Kinetic energy calculation

The calculations for the kinetic energy of the ship that is to be absorbed by the guiding structure follows the same steps as presented in section 4.2. First the kinetic energy calculation according to the EAU, 2012 is calculated and then the calculation with the modified definition of angle α follows.

5.3.1. Kinetic energy calculation according to EAU,2012

The situation for the approach at volkerak locks using the definition by the EAU, 2012 for the angle α is presented in figure 5.8.

The eccentricity coefficient $C_{e_{EAU}}$ is calculated as:

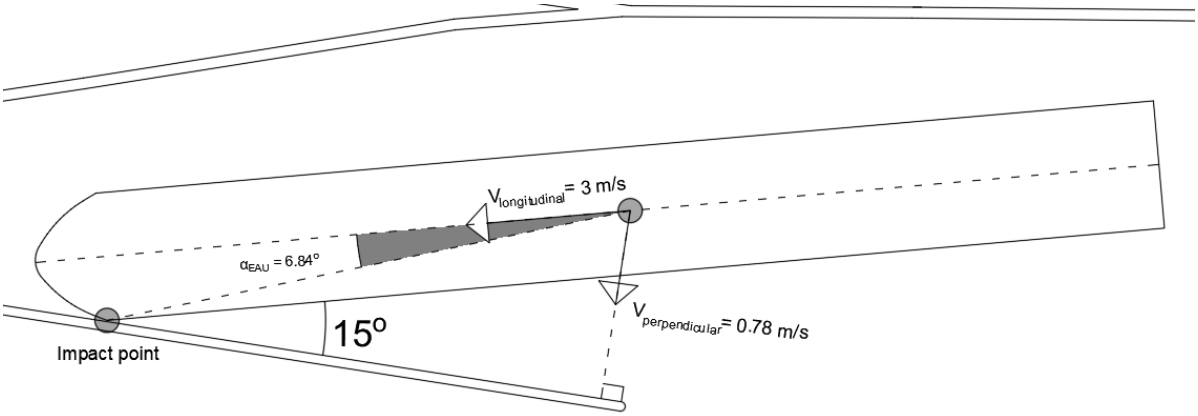

Figure 5.8: Volkerak locks EAU approach

$$C_{e_{EAU}} = \frac{k^2 + r^2 * cos^2\alpha_{EAU}}{k^2 + r^2} = 0.994 \tag{5.5}$$

And the kinetic energy emerging from this eccentricity is:

$$E_{EAU} = 0.5 * m_s * C_m * C_{e_{EAU}} * v^2_{perpendicular} = 6594\ kNm \tag{5.6}$$

5.3.2. Kinetic energy proposed calculation

The situation for the approach at Volkerak locks using the proposed definition for the angle α is presented in figure 5.9.

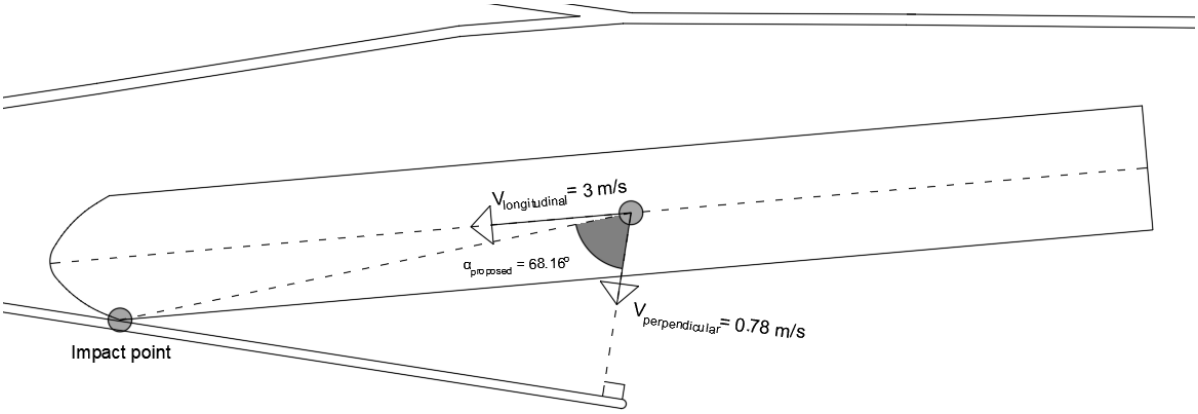

Figure 5.9: Volkerak locks proposed approach

The eccentricity coefficient $C_{e_{proposed}}$ is calculated as:

$$C_{e_{proposed}} = \frac{k^2 + r^2 * cos^2\alpha_{proposed}}{k^2 + r^2} = 0.493 \tag{5.7}$$

And the kinetic energy emerging from this eccentricity is:

$$E_{proposed} = 0.5 * m_s * C_m * C_{e_{proposed}} * v^2_{perpendicular} = 3270\ kNm \tag{5.8}$$

5.4. Hand calculations: Pile diameter and length

With the known kinetic energy impacting the structure it is possible to calculate the required dimensions for the piles. The calculation is carried out as instructed by the Blum method which is a commonly used method to compute the required embedded depth needed to provide enough passive soil resistance to lateral loads (Molenaar and Voorendt, 2016).

5.4.1. Relevant definitions

The assumptions taken into account for the preliminary pile dimensions follow the examples of Roubos, 2018 and the relevant definitions are displayed in figure 5.10:

- Still water level: $z_{SWL} = -(h + \eta_{HWL})$
- Force exerted at z_{SWL}
- Bed level: $z = 0$ (flat bed)
- Fixity strength level: z_M
- Fixity stiffness level: z_S
- Theoretical embedded depth z_{t_0} (used in calculations, not shown in figure 5.10)
- Practical embedded depth z_t

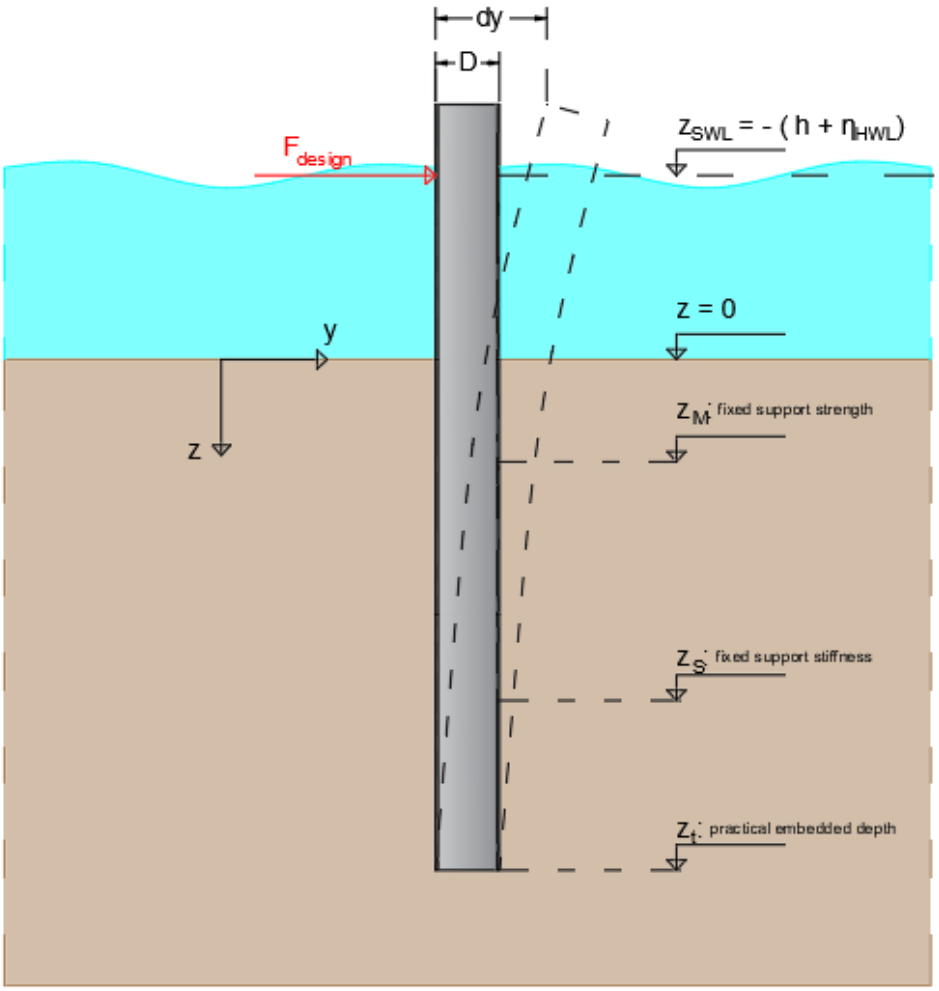

Figure 5.10: Pile assumptions

The calculation is kicked off by assuming that the load is absorbed in total by one pile. A diameter

is picked that gives displacement convergence in the Blum method. At this stage of the calculation the strength unity check for the pile is not fulfilled. The check is fulfilled when the whole structure is designed where all the piles are working towards energy absorption.

The comparison between the two calculation procedures using the two values calculated for the kinetic energy is presented in table 5.1. The main takeaway of this comparison is the pile diameter derived by each method. The acceptable diameter will be the one that allows for the pile to fulfill the unity check in the next stage of the calculations where the structure is represented by a pile series and the force load is distributed to more than just one pile. The unity check is fulfilled when the design moment M_d is smaller than the resistance moment of the pile M_{rd}. The resistance moment of the pile depends on its material strength and its cross section modulus (European Committee for Standardization, 2005).

$$Tube\ section\ modulus : W_{el} = \frac{\pi * (D^4 - (D-t)^4)}{32 * D} \tag{5.9}$$

$$Resistance\ moment : M_{rd} = W_{el} * \sigma_{yield} \tag{5.10}$$

$$Unity\ check : \frac{M_d}{M_{rd}} \leq 1 \tag{5.11}$$

5.4.2. Pile dimensions for kinetic energy according to EAU, 2012

In 5.3 the kinetic energy according to the EAU, 2012 is calculated to be:

$$E_{EAU} = 6594\ kNm \tag{5.12}$$

To apply the Blum method, an initial displacement and a diameter need to be assumed. The displacement is used to derive the force load by means of the equation:

$$E = \frac{1}{2} * F * \delta \tag{5.13}$$

where:

- F [kN] = force load
- δ [m] = displacement of the pile head

Here, the diameter chosen is $D = 2.02$ m. The force load derived by assuming a displacement of $\delta = 1.08\ m$ is $F = 12241\ kN$. Now, according to Blum, the theoretical embedded depth t_0 needed so that the pile can undertake the force load, is calculated implicitly by means of:

$$F = \gamma' * K_{p,h,\sigma} * \frac{t_0^3}{24} * \frac{t_0 + 4 * D}{t_0 + z_{SWL}} => t_0 = 14.54\ m \tag{5.14}$$

where:

- F [kN] = maximum load that can be resisted
- γ' [kN/m^3] = effective volumetric weight $(\gamma_s - \gamma_w)$
- $K_{p,h,\sigma}$ [-] = passive soil pressure coefficient
- t_0 [m] = theoretical embedded depth
- D [m] = width of the pile perpendicular to the load
- z_{SWL} [m] = still water level

Because all (shear) forces are known, the moment diagram can be determined, using the following equation:

$$M_z = F * (z_{SWL} + z) - \gamma' * K_{p,h,\sigma} * (z + 4 * D) * \frac{z^3}{24} \tag{5.15}$$

where:

- M_z [kNm] = moment at depth z
- z [m] = depth

Next step is to calculate for the level of fixity for the pile strength. This is the point when the moment load reaches its maximum value. The maximum moment M_{max} occurs at depth z_M, where $\frac{\delta M}{\delta z} = 0$. This depth is found by solving the following equation implicitly[2]:

$$z_M^2 * (z_M + 3 * D) = \frac{t_0^3}{4} * \frac{t_0 + 4 * D}{t_0 + z_{SWL}} \tag{5.16}$$

Substituting the known variables the result is:

$$z_M = 7.60\ m \tag{5.17}$$

Substituting z_M in equation 5.15 gives the maximum moment:

$$M_{max} = 158130\ kNm \tag{5.18}$$

Last step is to calculate the displacement that the force produces and check if it matches the one assumed in the beginning of the calculation.

$$\delta = \frac{F * (z_{SWL} + 0.65 * z_t)^3}{3EI} \tag{5.19}$$

where:

- δ [m] = displacement of the pile head
- F [kN] = load
- z_{SWL} [m] = level of the unsupported part
- z_t [m] = practical embedded depth ($1.2 * t_0$)
- E_{young} [kN/m^2] = Young's modulus of the pile material
- I [m^4] = moment of inertia of the pile

All variables are known, thus, equation 5.19 can be straightforwardly solved for δ, giving value:

$$\delta = 1.08\ m \tag{5.20}$$

The displacement converges. Thus, the solution is accepted. What cannot be fulfilled at this stage of the calculations is the unity check for the resistance moment as the moment load on the pile is very large. This is why modelling of the structure is necessary. When the load is applied on the steel frame structure then the moment load is different. This is because the load is distrubuted to more than just one pile. At the modelling stage, decisions regarding the design of the structure will be made in order to fulfill the unity check.

[2]For the strength considerations in the above, the position of the fixed support of the pile is at a distance z_M below ground level.

5.4.3. Pile dimensions for proposed kinetic energy

In 5.3 the kinetic energy according to proposed refined definition of angle α is calculated to be:

$$E_{EAU} = 3270\ kNm \tag{5.21}$$

With an assumed displacement of $\delta = 0.92$ m, the forcing load according to equation 5.13 is calculated:

$$F = 7109\ kN \tag{5.22}$$

The chosen diameter here is $D = 1.62$ m. Now, the same calculation steps are followed to apply the Blum method and derive the necessary values for the pile design. Starting with the theoretical embedded depth:

$$F = \gamma' * K_{p,h,\sigma} * \frac{t_0^3}{24} * \frac{t_0 + 4 * D}{t_0 + z_{SWL}} => t_0 = 12.45\ m \tag{5.23}$$

The depth where the moment load reaches its maximum is:

$$z_M^2 * (z_M + 3 * D) = \frac{t_0^3}{4} * \frac{t_0 + 4 * D}{t_0 + z_{SWL}} => z_M = 6.38\ m \tag{5.24}$$

The maximum moment then is:

$$M_{z_{max}} = F * (z_{SWL} + z_M) - \gamma' * K_{p,h,\sigma} * (z_M + 4 * D) * \frac{z_M^3}{24} => M_{z_{max}} = 85709\ kNm \tag{5.25}$$

The displacement that the force produces is:

$$\delta = \frac{F * (z_{SWL} + 0.65 * z_t)^3}{3EI} = 0.92\ m \tag{5.26}$$

Since the displacement converges, the solution is accepted.

5.4.4. Comparing results

The resutls of both calculations according to the EAU, 2012 and the proposed refined definition of angle α are presented in table 5.1. The results from this culculation step will serve as the starting point for modelling the structure.

At first glance, it looks like the EAU, 2012 calculation gives a larger quantity of steel to be used in the structure. This is hinted, not only by the larger diameter of the pile, but also by the larger required embedded depth.

The unity check is expected to be fulfilled at the modelling stage where the forcing load is distributed to more than just one pile. The design choices at the modelling stage regarding the spacing of the piles and the girder connecting them will contribute to the beneficial for the structure distribution of the load to the members.

Table 5.1: Pile strength calculations comparison

Pile strength calculations comparison		
Variable	EAU, 2012	Proposed
E_d [kNm]	6594	3270
dy [m]	1.08	0.92
F_d [kN]	12241	7109
D [mm]	2020	1620
t [mm]	40	40
z_M	7.82	6.38
z_S	14.91	12.45
$L_{stiffness}$ [m]	18.84	17.21
$L_{strength}$ [m]	15.1	13.88
M_d [kNm]	158130	85709
M_{rd} [kNm]	58334	36968
$Unity\ Check$	2.70	2.30

5.5. Modelling: Optimizing for girder connected pile series

The structure is now modelled as presented in figure 5.3. In this step the response of the total structure is studied. This will allow to make conclusions regarding the cooperation of the piles and the main girder. Now the configuration of the total structure takes part in the energy absorption instead of just the outermost pile.

For the mono-pile the energy absorption is calculated as indicated in equation 5.13, whereas for the pile series connected with the girder (figure 5.11) the energy absorption calculation is as follows:

$$E_{series} = 0.5 * F_{design} * \Sigma_1^i (dy_1 + dy_2 + ... + dy_i) \tag{5.27}$$

In similar organization, as in the mono-pile case, here the model is created for both methods of calculation. The embedded lengths derived by the Blum method are used to set up the model. For each method, two models are necessary. A model for the structure's stiffness and a model for the structure's strength. This is because the Blum method calculates a level of fixity where the required stiffness is achieved and a level of fixity where the moment load reaches is maximum and the structure's strength is tested. The fixity length for strength is smaller because it only needs to meet the failure criterion, whereas the fixity length for stiffness must ensure minimal deflection and provide long-term stability under normal service load (Carter, 2016, Ruigrok, 2010). Details on the Blum method can be found in Appendix B.

The force of the impacting ship is then applied to the outermost pile for an iteration (Node K2) and the middle of member pile (Member S9) in the schematization of figure 5.3. The force exerted on the tip of the outermost pile is the least favorable load for the piles, whereas when the force is exerted in the middle of member S9, this is the least favorable load for the main girder. This is because for the first case the largest part of the kinetic energy of the ship has to be absorbed by just one pile (Section S1), whereas in the latter case it is the only point of the structure that the girder is expected to bend the most since its bending at the rest of the nodes is confined by the rest of the piles.

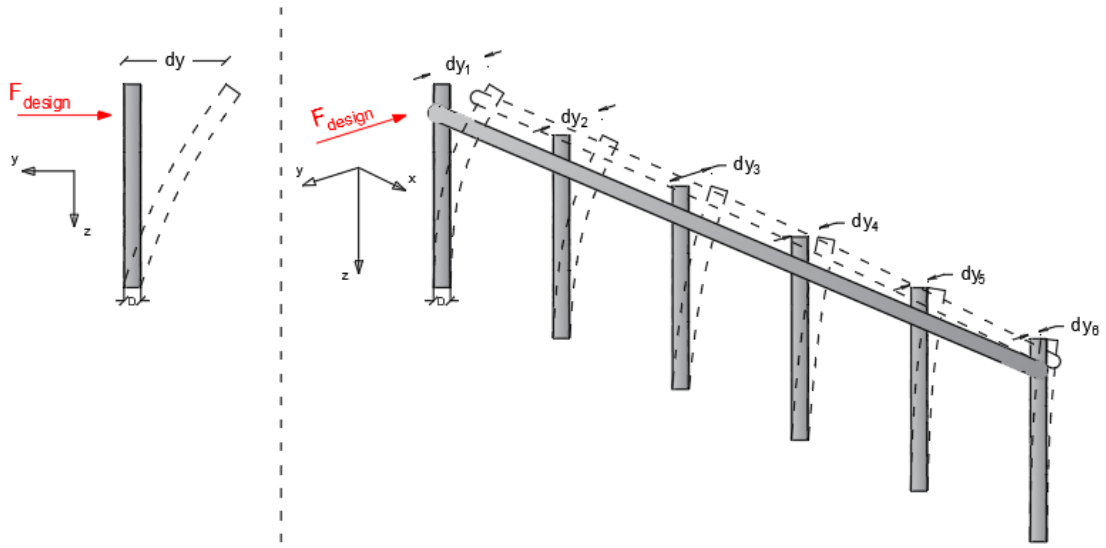

Figure 5.11: Mono-pile vs. Frame Sketch

5.5.1. Modelling the structure for the EAU, 2012 calculation

The models created for the EAU, 2012 calculations follow the schematization presented in figure 5.3 with pile diameter of $D = 2020\ mm$, thickness of $t = 40\ mm$.

Stiffness and strength model

To derive the deflections that are caused by the force load, the stiffness model is used shown in 5.12 whereas, the strength model of 5.13 is used to derive the moments that are caused by the force load.

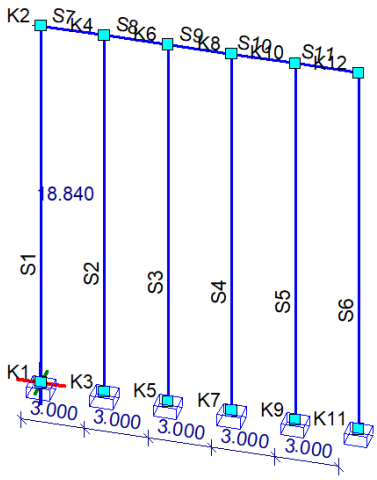

Figure 5.12: Stiffness model, calculations with EAU, 2012

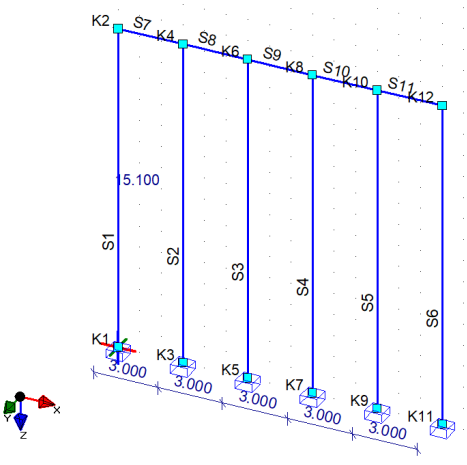

Figure 5.13: Strength model, calculations with EAU, 2012

The stiffness model brings a fixity length of 18.84 m, whereas, the strength model brings a fixity length of 15.1 m. The piles are positioned within 3 m from each other in order for the strength criteria to be fulfilled.

Pile S1 loading

Figure 5.14 illustrates a structural model subjected to an applied load at node K2. The load magnitude is 12241 kN, acting in the negative y-direction. Figure 5.15 depicts the nodal displacements resulting from the applied load shown in figure 5.14. The displacements are presented in green values at each node. Node K2 experiences the highest displacement of 0.2571 m in the y-direction, indicating a significant response to the applied load at K2. Other nodes also show varying degrees of displacement, with node K12 displaying a displacement of 0.1096 m which is the smallest value. This distribution of displacements provides insight into how the structure deforms under the given load.

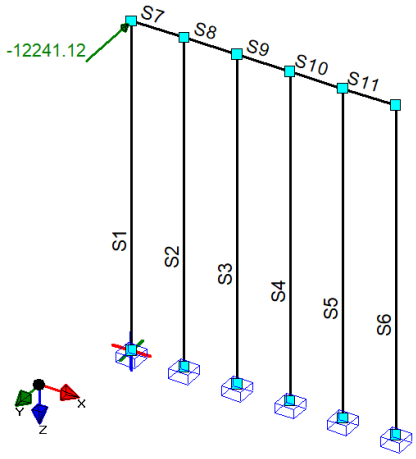

Figure 5.14: Node K2 force load

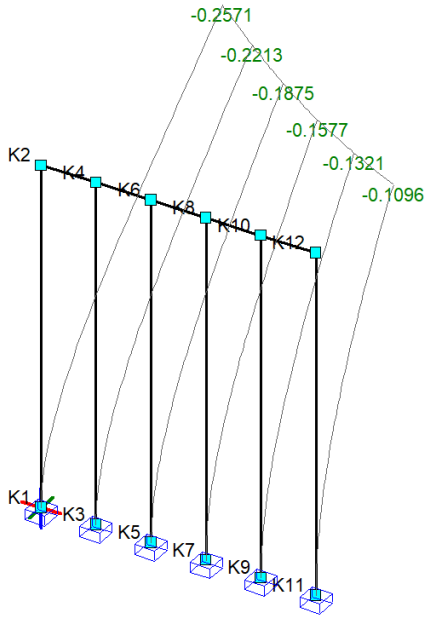

Figure 5.15: Nodal displacement - Load K2

Using the displacements of figure 5.15, the energy absorbed by the pile series can be calculated using equation 5.27.

$$E_{EAU_1} = 0.5 * 12241\ kN * (0.2571 + 0.2213 + 0.1875 + 0.1577m + 0.1321 + 0.1096)\ = 6520\ kNm \quad (5.28)$$

The value of 6520 kNm compares well with the value of 6594 kNm calculated in section 5.3. It's a difference of 1.12 %. If precision is an objective then calibrating the force load can give an even more precise result. For the purpose of this study, the result is considered acceptable. The structure can absorb the energy load.

After it is ensured that the structure has the necessary stiffness to produce the displacements that will allow for the kinetic energy to be absorbed, the next step is to check the structure for its strength. The moments caused by the load can be seen in figure 5.16.

The highest moment load is found, as expected, on the first pile where the load is exerted. Thus, the largest part of it is distributed on S1. The unity check for pile S1 gives:

$$U.C._{S_1} = \frac{M_{S_1}}{M_{rd_{el}}} = \frac{54884\ kNm}{58334\ kNm} = 0.95 \quad (5.29)$$

The unity check is fulfilled, thus, the design can be accepted regarding the vertical piles. The horizontal girder is to be checked next, by applying the load in the middle of member S9 in the model.

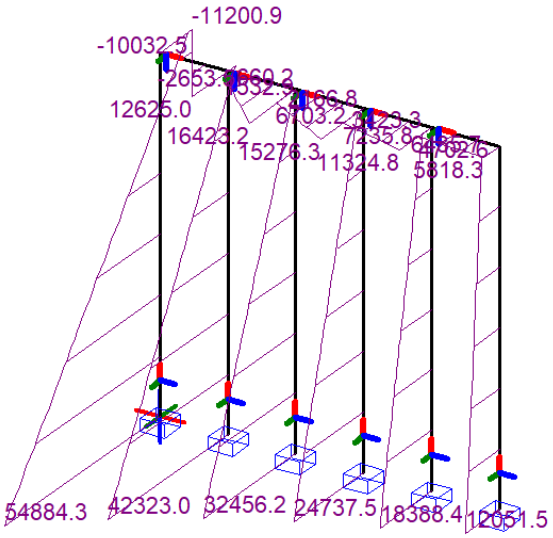

Figure 5.16: Moments - Load K2

Member S9 loading

Figure 5.17 shows a structural model with an applied load in the middle of member S9. The load has a magnitude of 12241 kN, acting in the negative y-direction. All nodes show deflections of the same order of magnitude with nodes K6 and K8 experiencing the largest deflection of 0.1826 m and nodes K2 and K12 the smallest which has the value of 0.1720 m. This distribution of displacements illustrates the deformation pattern of the structure when the load is applied at the middle of member S9.

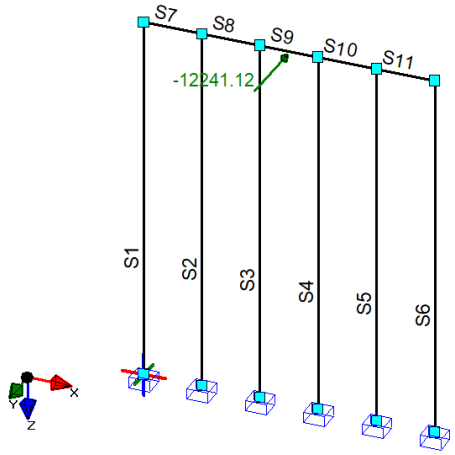

Figure 5.17: Member S9 force load

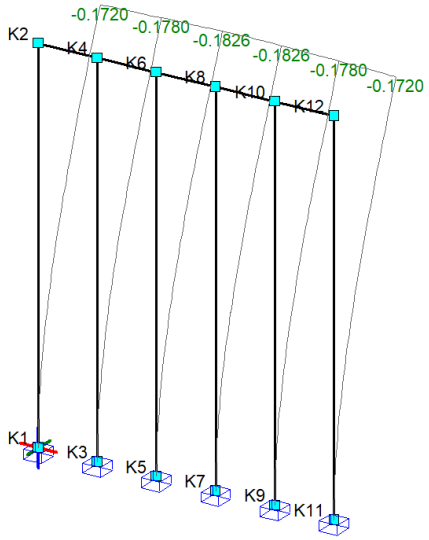

Figure 5.18: Nodal Displacement - Load S9

The energy absorbed when the load is applied in middle of member S9 is:

$$E_{EAU_2} = 0.5 * 12241\ kN * (0.1720 + 0.1760 + 0.1826 + 0.1826 + 0.1760 + 0.1720)\ m = 6498\ kNm \quad (5.30)$$

The value of 6498 kNm compares well with the value of 6594 kNm calculated in section 5.3. It's a difference of 1.46 %. If precision is an objective then calibrating the force load can give an even more precise result. For the purpose of this study, the result is considered acceptable. The structure can absorb the energy load.

The next step is to check the horizontal girder for its strength. The moments caused by the load can be seen in figure 5.19.

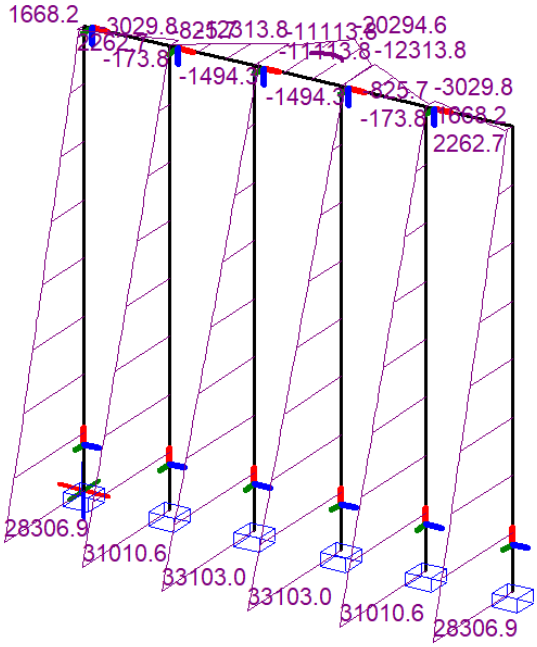

Figure 5.19: Moments - Load S9

The unity check for the girder gives:

$$U.C._{S_9} = \frac{M_{S_9}}{M_{rd_{el}}} = \frac{20295\ kNm}{58334\ kNm} = 0.35 \tag{5.31}$$

The load even when applied mid-length on the girder, is still distributed for the largest part to the vertical piles. A unity check of 0.35 hints that the diameter of the girder could be smaller. The diameter to be chosen should be as such that the load distributed to the vertical piles does not cause strength failure.

5.5.2. Modelling the structure for the proposed refined energy calculation

The models created for the proposed refined energy calculation follows the schematization presented in figure 5.3 with pile diameter of $D = 1620\ mm$, thickness of $t = 40\ mm$.

Stiffness and strength model

To derive the deflections that are caused by the force load, the stiffness model is used shown in 5.20 whereas, the strength model of 5.21 is used to derive the moments that are caused by the force load.

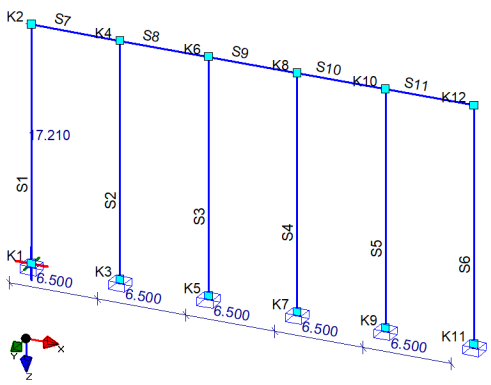

Figure 5.20: Stiffness model, proposed calculation

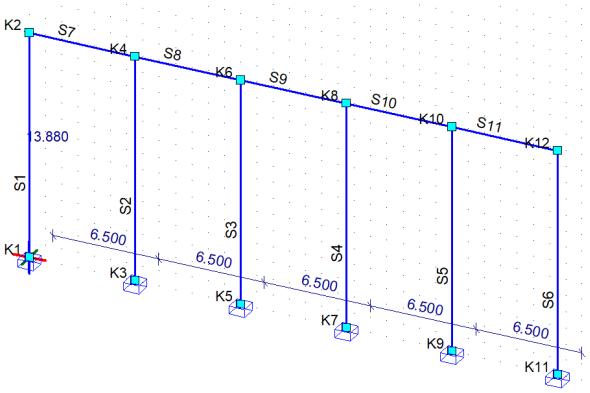

Figure 5.21: Strength model, proposed calculation

The stiffness model brings a fixity length of 17.21 m, whereas, the strength model brings a fixity length of 13.88 m. The piles are positioned within 6.5 m from each other in order for the strength criteria to be fulfilled.

Pile S1 loading

Figure 5.22 illustrates a structural model subjected to an applied load at node K2. The load magnitude is 7109 kN, acting in the negative y-direction. Figure 5.23 depicts the nodal displacements resulting from the applied load shown in figure 5.22. The displacements are presented in green values at each node. Node K2 experiences the highest displacement of 0.3602 m in the y-direction, indicating a significant response to the applied load at K2. Other nodes also show varying degrees of displacement, with node K12 displaying a displacement of 0.0225 m which is the smallest value. This distribution of displacements provides insight into how the structure deforms under the given load.

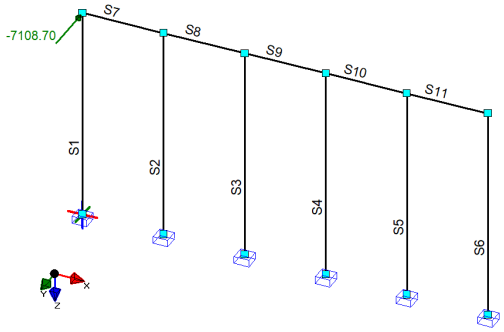

Figure 5.22: Node K2 force load

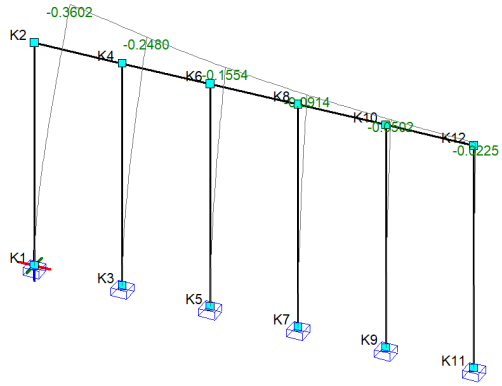

Figure 5.23: Nodal displacement - Load K2

Using the displacements of figure 5.23, the energy absorbed by the pile series can be calculated using equation 5.27.

$$E_{EAU_1} = 0.5 * 7109\ kN * (0.3602 + 0.2480 + 0.1554 + 0.0914 + 0.0502 + 0.0225)\ m = 3297\ kNm \quad (5.32)$$

The value of 3297 kNm compares well with the value of 3270 kNm calculated in section 5.3. It's a difference of 0.8 %. If precision is an objective then calibrating the force load can give an even more precise result. For the purpose of this study, the result is considered acceptable. The structure can absorb the energy load.

After it is ensured that the structure has the necessary stiffness to produce the displacements that will allow for the kinetic energy to be absorbed, the next step is to check the structure for its strength. The moments caused by the load can be seen in figure 5.24.

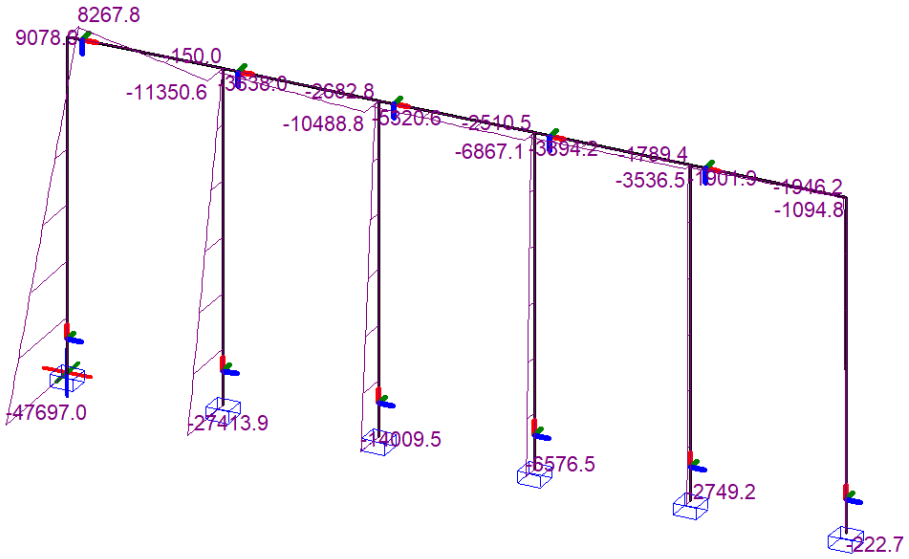

Figure 5.24: Moments - Load K2

The highest moment load is found, as expected, on the first pile where the load is exerted. Thus, the largest part of it is distributed on S1. The unity check for pile S1 gives:

$$U.C._{S_1} = \frac{M_{S_1}}{M_{rd_{el}}} = \frac{47697\ kNm}{36968\ kNm} = 1.29 \tag{5.33}$$

The unity check criteria is not fulfilled. But, in the case of the Circular Hollow Section (CHS) of X70 steel with diameter 1620 mm and thickness 40 mm, the following apply according to Eurocode 3 (EN1993-1-1):

Slenderness parameter

$$\lambda = \frac{D}{2 * t * \epsilon} \tag{5.34}$$

where:

- D [mm] = Cross section diameter
- t [mm] = Cross section thickness
- ϵ = Material factor for the steel calculated as $\sqrt{\frac{235MPa}{f_y MPa}}$

Substitution of the known variables gives:

$$\epsilon = \sqrt{\frac{235\ MPa}{485\ MPa}} = 0.697 \tag{5.35}$$

$$\lambda = \frac{1620}{2 * 40 * 0.697} = 29.05 \tag{5.36}$$

Classification limits

According to Table 5.2 of Eurocode 3 (EN 1993-1-1), the classification limits for circular hollow sections under axial compression or bending are given for various classes:

- **Class 1**: $\lambda \leq 50\epsilon = 50 * 0.697 = 34.85$
- **Class 2**: $\lambda \leq 70\epsilon = 70 * 0.697 = 48.79$
- **Class 3**: $\lambda \leq 90\epsilon = 90 * 0.697 = 62.73$

Since the slenderness $\lambda = 29.05$ is less the hollow circular tube with a diameter of 1620 mm, wall thickness of 40 mm, and made from X70 steel is classified as class 1. This means the section is capable of developing full plastic bending without local buckling, allowing for the use of plastic design in accordance with Eurocode 3.

The unity check is performed now for the plastic resistance moment $M_{rd_{pl}}$:

$$U.C._{S_1} = \frac{M_{S_1}}{M_{rd_{pl}}} = \frac{47697\ kNm}{48241\ kNm} = 0.99 \tag{5.37}$$

Since the plastic deformation is allowed, the design is accepted. Overall, the first pile in the series is allowed to show plastic deformation while the rest of the piles are experiencing moment loads that are below their elastic moment capacity.

Member S9 loading

Figure 5.25 shows a structural model with an applied load in the middle of member S9. The load has a magnitude of 7109 kN, acting in the negative y-direction. All nodes show deflections of the same order of magnitude with nodes K6 and K8 experiencing the largest deflection of 0.1881 m and nodes K2 and K12 the smallest which has the value of 0.1201 m. This distribution of displacements illustrates the deformation pattern of the structure when the load is applied at the middle of member S9.

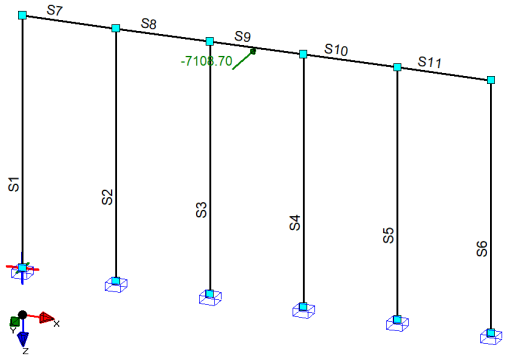

Figure 5.25: Member S9 force load

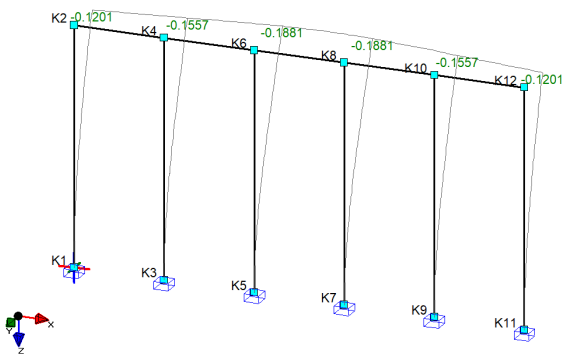

Figure 5.26: Nodal Displacement - Load S9

The energy absorbed when the load is applied in middle of member S9 is:

$$E_{EAU_2} = 0.5 * 7109\ kN * (0.1201 + 0.1557 + 0.1881 + 0.1881 + 0.1557 + 0.11201)\ m = 3298\ kNm \tag{5.38}$$

The value of 3298 kNm compares well with the value of 3270 kNm calculated in section 5.3. It's a difference of 0.9 %. If precision is an objective then calibrating the force load can give an even more precise result. For the purpose of this study, the result is considered acceptable. The structure can absorb the energy load.

The next step is to check the horizontal girder for its strength. The moments caused by the load can be seen in figure 5.27.

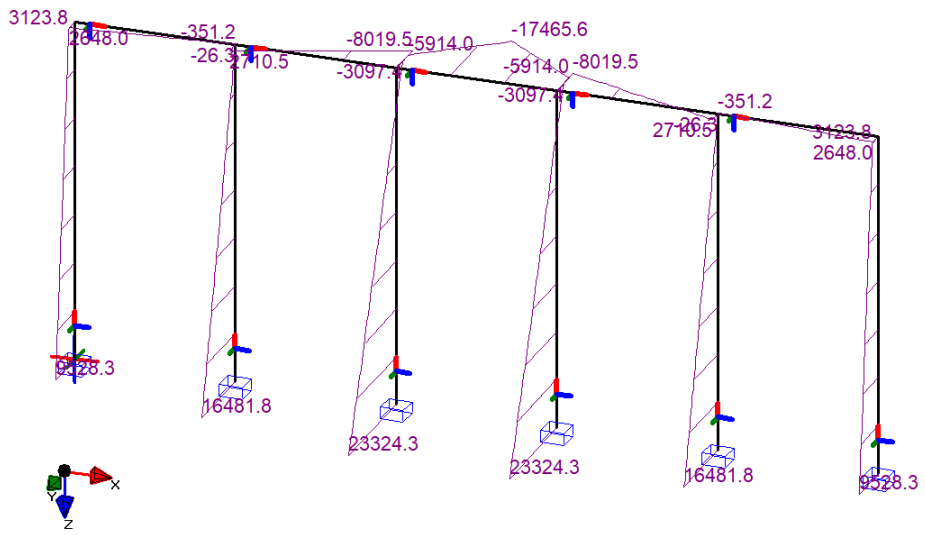

Figure 5.27: Moments - Load S9

The unity check for the girder gives:

$$U.C._{S_9} = \frac{M_{S_9}}{M_{rd_{el}}} = \frac{17466\ kNm}{36968\ kNm} = 0.47 \tag{5.39}$$

The load even when applied mid-length on the girder, is still distributed for the largest part to the vertical piles. A unity check of 0.47 hints that the diameter of the girder could be smaller. The diameter to be chosen should be as such that the load distributed to the vertical piles does not cause strength failure.

5.6. Calculating the collision energy with the Virtual Water Mass method

For the structure derived with the refined calculation method, a stiffness coefficient and a damping coefficient are approximated.

Stiffness of the Vertical Pile

The length of the vertical piles plays a key role in determining their stiffness. The lateral stiffness of a cantilevered pile subjected to a horizontal force at the top is given by:

$$K_{\text{pile}} = \frac{3EI}{L_{\text{pile}}^3}$$

Where:

- $E = 200000$ MPa (Young's modulus of X70 steel).
- $I = 6105 * 10^{10}$ mm^4 (previously calculated moment of inertia).
- $L_{\text{pile}} = 17.21$ m $= 17210$ mm (height of the pile).

Now, substituting values:

$$K_{\text{pile}} = \frac{3 * 200,000 * 6.105 * 10^{10}}{(17210)^3}$$

$$K_{\text{pile}} = \frac{3.663 * 10^{16}}{5.016 * 10^{12}} = 7.3 * 10^3 \text{ N/mm}$$

So, the lateral stiffness of each vertical pile is approximately $7.3 * 10^3$ N/mm.

The girder, spanning 32.5 m, has the same cross-sectional properties as the piles. The total stiffness of the girder depends on how it behaves as a beam spanning multiple supports.

For simplicity, if a fixed-ended beam is assumed, the stiffness for a beam of length L_{girder} with a moment of inertia I is:

$$K_{\text{girder}} = \frac{48EI}{L_{\text{girder}}^3}$$

Where:

- $L_{\text{girder}} = 32.5\,\text{m} = 32,500\,\text{mm}$ (length of the girder).

Substituting values:

$$K_{\text{girder}} = \frac{48 * 200,000 * 6.105 * 10^{10}}{(32,500)^3}$$

$$K_{\text{girder}} = \frac{5.859 * 10^{17}}{3.43 * 10^{13}} = 1.7 * 10^4 \text{ N/mm}$$

So, the stiffness of the girder is approximately $1.7 * 10^4$ N/mm.

The overall stiffness of the frame is influenced by the combination of the vertical piles and the horizontal girder. Assuming the girder and piles work together in a sway frame configuration, the total stiffness K_{frame} can be approximated as a combination of the pile and girder stiffnesses.

If the piles and the girder are combined as a system, the following relation for the lateral stiffness of the frame can be used (Karnovsky et al., 2021):

$$K_{\text{frame}} = \left(\frac{1}{K_{\text{pile}}} + \frac{1}{K_{\text{girder}}} \right)^{-1}$$

Since we have **6 piles**, the total pile stiffness is:

$$K_{\text{pile, total}} = 6 * K_{\text{pile}} = 6 * 7.3 * 10^3 = 4.38 * 10^4 \text{ N/mm}$$

Thus, the combined stiffness of the frame is:

$$K_{\text{frame}} = \left(\frac{1}{4.38 * 10^4} + \frac{1}{1.7 * 10^4} \right)^{-1}$$

Performing the calculation:

$$K_{\text{frame}} = \left(\frac{1}{4.38 * 10^4} + \frac{1}{1.7 * 10^4} \right)^{-1} = 1.24 * 10^4 \text{ N/mm} = 12.4 * 10^6 \text{N/m}$$

Estimating the Damping coefficient

To estimate the damping coefficient, the mass of the piles and the girder need tobe estimated first.

The mass per unit length of a hollow circular pile (and the girder, which shares the same properties) is given by:

$$\text{Mass per unit length} = \rho * A$$

Where:

- ρ is the density of steel, typically around $7850\,\text{kg/m}^3$ (Liu and Li, 2024).
- A is the cross-sectional area of the hollow tube.

For a hollow circular section (European Committee for Standardization, 2005):

$$A = \frac{\pi}{4}\left(d_{\text{outer}}^2 - d_{\text{inner}}^2\right)$$

Using:

- $d_{\text{outer}} = 1.62\,\text{m}$
- $d_{\text{inner}} = 1.54\,\text{m}$
- $t = 40\,\text{mm} = 0.04\,\text{m}$

The cross-sectional area A is:

$$A = \frac{\pi}{4}\left(1.62^2 - 1.54^2\right) = \frac{\pi}{4} * (2.6244 - 2.3716) = \frac{\pi}{4} * 0.2528 = 0.1986\,\text{m}^2$$

$$\text{Mass per unit length} = 7850 * 0.1986 = 1,559\,\text{kg/m}$$

Assuming each pile is 17.21 m long and there are 6 piles, the total mass for the piles is:

$$\text{Total mass of piles} = 6 * 1,559 * 17.12 = 160,404\,\text{kg}$$

The girder, which is 32.5 m long, has the same cross-sectional area and mass per unit length:

$$\text{Mass of the girder} = 1,559 * 32.5 = 50,668\,\text{kg}$$

Thus, the total mass of the structure is:

$$M = 160,404 + 50,668 = 211,072\,\text{kg}$$

The natural frequency ω_n for a structure can be approximated as:

$$\omega_n = \sqrt{\frac{K}{M}}$$

Where K is the stiffness of the structure (from previous calculations) and M is the mass.

From earlier calculations, we know that:

$$K = 12,400,000\,\text{N/m}$$

Substituting the mass and stiffness:

$$\omega_n = \sqrt{\frac{12,400,000}{211,072}} = \sqrt{58.74} = 7.66\,\text{rad/s}$$

The damping ratio ζ is typically a material and system property. For steel structures, a typical assumed damping ratio is between 0.01 and 0.05 for lightly damped systems Jiang et al., 2024. A damping ratio of $\zeta = 0.02$ (2%) is assumed.

The damping coefficient C is related to the damping ratio ζ, the mass M, and the natural frequency ω_n by the formula (Moore, 2024):

$$C = 2\zeta M\omega_n$$

Substituting the known values:

$$C = 2 * 0.02 * 211,072 * 7.66 = 64,580\,\text{Ns/m}$$

Collision energy by Virtual Water Mass method

Now that the stiffness and damping coefficients of the structure is approximated and with a conservative assumption for the value sliding friction coefficient factor ($tg\beta = 0.8$) the Virtual Water Mass method calculation can be run in Python to produce the force - deflection curve for the structure (figure 5.28). The collision energy absorbed by the structure due to the ship impact is the area below the force - deflection curve.

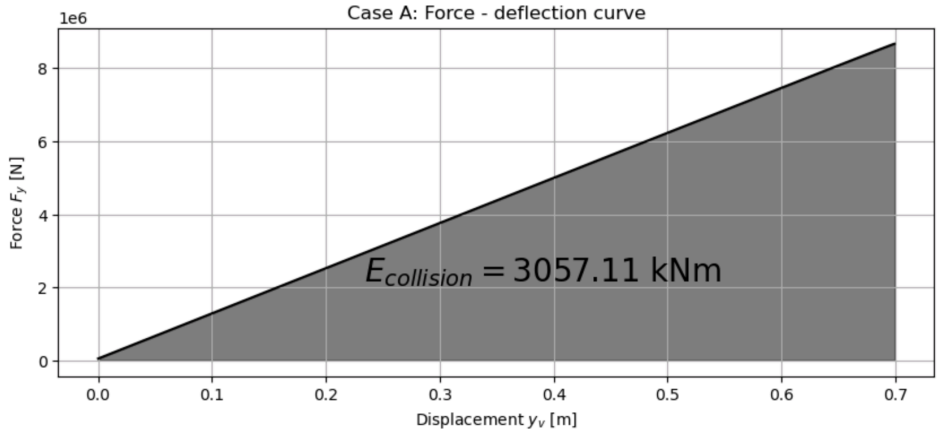

Figure 5.28: Virtual Water Mass Collision Energy

The collision energy calculated by the refined method ($E_{proposed} = 3270$ kNm) corresponds well with the benchmark value of 3057 kNm calculated with the Virtual Water Mass method.

5.7. Conclusions

This chapter examined the application of a newly refined collision energy calculation method within the context of the Volkerak Locks. The objective was to assess the structural behavior of the guiding structure under vessel impact, comparing the standard EAU, 2012 method with the proposed adjustments for angle α.

The kinetic energy load calculated with the refined method was validated by performing the Virtual Water Mass method calculation that has been used to provide benchmark values in the validation of the refined method in Chapter 4.

The structure was modelled using the calculations from both methods (EAU, 2012 and refined). A smaller kinetic energy load is achieved with the refined method leading to a structure with smaller pile diameters. Despite the slightly higher displacements, the structure remained within acceptable limits.

In terms of material savings, the refined method allowed for the use of smaller pile diameters (1620 mm versus 2020 mm in the EAU, 2012 model), reducing the total material used while maintaining structural integrity. The results suggest that adopting this calculation method can lead to a more balanced design approach, optimizing both safety and material use.

The application of this refined method in the Volkerak Locks case study demonstrates that it offers potential improvements in both material efficiency and cost-effectiveness, while still ensuring compliance with safety standards.

6

Discussion, Conclusions and Recommendations

6.1. Introduction

This chapter synthesizes the findings of the research with a focus on evaluating the effectiveness of the refined collision energy calculation method developed in this thesis. The aim is to critically analyze how the method addresses the initial research questions posed in Chapter 1, particularly its application to real-world scenarios, as demonstrated through the case study at the Volkerak locks.

The ensuing sections of this chapter will therefore cover the application of the refined method, assess its limitations, and propose comprehensive approaches for future research that could address these limitations and expand the method's applicability. Each section aims to build upon the previous content, ensuring a cohesive narrative that effectively addresses all facets of the research questions and provides a clear path forward for both theoretical advancement and practical application.

6.2. Covering the research questions

In this section, the research questions articulated in Chapter 1 are methodically addressed, providing a discussion on the findings and insights derived from the newly developed collision energy calculation method. The sub-questions are addressed first, leading to the coverage of the main reasearch question.

Sub-questions:

- **What is the level of conservatism in the established energy calculation method based on berthing?**

In the literature review of this research the shortcoming of the vague definition of the angle variable in the eccentricity coefficient expression used in the kinetic energy approach by the established EAU, 2012 method is explained. The findings of the literature review were that the conventional method realistically calculates the berthing energy but when it is applied unmodified in the ship-to-guiding structure collision energy calculation, it can produce a very large unrealistic value.

The reason for this was that the definition of the angle variable in the eccentricity coefficient is phrased in a way that might lead the engineer to choose the angle between the line that connects the center mass of the ship to the point of impact and the total ship velocity vector instead of the perpendicular to the structure one which contributes to the impact.

When the definition is followed unmodified, especially for the sailing ship that maintains a purely longitudinal speed on its approach to the guiding structure, the eccentricity coefficient returns values close to unity which resemble a central impact, rather than a sliding movement that is observed in such approaches.

The comparison between the EAU, 2012 calculation method and the Virtual Water Mass method gave

some more insight on the level of conservatism of the EAU, 2012 calculation when the definition of the angle variable of the eccentricity coefficient is applied unmodified. Especially, for the allowed angles of approach between 9^o and 14^o the overestimation is around 400 % and 377 %, respectively.

It is important to state that the conservatism of the established method is unintentional. Although, it produces an exaggerated collision energy estimation, this result does not come because of load or material safety factors. These have been kept the same for both ways of calculations (EAU, 2012 vs. Virtual Mass Method) per given case. This means that the conservatism is coincidental and not strategically thought through.

- **How do collision dynamics in guiding structure approaches differ from berthing dynamics, and what are the underlying reasons that call for a distinct methodology for quantifying collision energy?**

The main difference between the dynamics of collision happening in berthing and guiding structure approaches lies in the velocity configuration. In berthing, the ship, after coming to a halt or decreasing significantly it's forward speed, is assisted by bow thrusters which determine its motion as it closes on the berth. The movement of the ship is more translational, rather perpendicular to the structure (See berthing approach according to PIANC, 2024 in figure 2.5).

In guiding structure approaches, the ship maintains a sailing speed and the problem is dominated by a forward movement. The observed situation is that the impact of the ship on the structure is a sliding phenomenon. The ship touches the structure and keeps sailing after it bounces off on it. This happens because the normal to the structure component of the ship's velocity is around 4 to 6 times smaller than the component parallel to the structure. This ratio is derived by the allowed by the Richtlijnen-Vaarwegen, 2020 angles for the guiding structures layout which should fall in the range of 9^o to 14^o angle between the guide and the waterway axis.

In the guiding structure approaches, the framework ignores the approach angle of the ship when it accounts for the eccentric impact. This brings out an erroneous result where, regardless of the approach angle of a ship, the impact is always considered almost central. This happens because the angle α in the eccentricity coefficient expression (2.3) ignores the direction of the ship in respect to the structure, as it considers the longitudinal component of the ship's velocity. Fact that contradicts the purpose of the eccentricity coefficient which is to modify the normal component of the total kinetic energy.

An example of this shortcoming is presented in Chapter 4 where for Case C, for the same ship attempting guiding structure approaches under different angles of attack, according to the EAU, 2012, angle α and subsequently the eccentricity coefficient appear to have the same value for all approaches (see figure 4.3 and table 4.3)

The deficiency described causes higher eccentricity coefficient values that lead to inflated values of collision energy that demand a heftier structural design requiring more material and increasing the overall project cost.

So, the underlying reasons that call for a distinct methodology for quantifying collision energy are two. One related to the fact that the established method fails to describe the collision dynamics on a guiding structure approach because of its vagueness of the angle α definition, and the second, that the consequence of this ambiguity leads to over-conservative designs that lead to waste of financial and material resources.

- **How does the refined method compare to the existing one and what is the impact of application on the design of the new guiding structures? Is it possible that the suggested method by this research leads to a more economical design regarding material usage?**

The final sub-question of this study addresses the practical application of the proposed refined collision energy calculation. The focus is to validate the hypothesis that the refined calculation not only maintain the ease of application similar to the established one but also produces a more realistic result.

The refined method is as simple to use as the established one. By just, correcting for the eccentricity coefficient input in the kinetic energy approach (equation 2.2) to describe the ship's approach to the guiding structure, it is possible to derive a more realistic result regarding the collision energy. This is

demonstrated both in the comparative calculations in Chapter 4 and the case study in Chapter 5. All other inputs in the refined method remain similar to the ones instructed by the EAU,2012.

The impact of application to the design is realized through the case study of chapter 4. There, the refined calculation results in a structure that consists of piles with smaller diameter compared to the result produced by the EAU, 2012 calculation. This is because the refined calculation does not overestimate the collision energy to the same extent that the established one does. Thus, application of the refined calculation leads to less conservative but still safe designs.

A significant advantage highlighted in the case study is the reduction in material usage. The refined calculations led to a decrease in the required diameters of tube steel. This reduction directly translates into lower costs for materials, which is a critical factor in the economic planning of structures. By optimizing material usage, the refined method contributes to substantial cost savings and, by extension, a lower environmental impact through reduced resource consumption. So, the answer to the last part of this research sub-question is positive.

Main Research Question:

How can the berthing energy calculation method be adjusted to describe collision on guiding structures and produce a realistic calculation of the kinetic energy?

The main research question focuses on refining the berthing energy calculation to accurately represent collisions with guiding structures. The refined methodology addresses the significant difference in velocity dynamics between berthing and guiding structure approaches, especially by re-defining the angle α used in the eccentricity coefficient. In guiding structure collisions, where sliding impacts dominate, the standard EAU, 2012 method overestimates collision energy by using an angle variable that does not accurately reflect the actual dynamics of the ship's approach.

By modifying the angle α to account for the normal velocity vector and adjusting the eccentricity coefficient accordingly, the refined method provides a more realistic kinetic energy calculation. This change leads to less conservative, but still safe, designs that avoid the material and cost inflation associated with overestimated collision energies in the established method. This refined approach was validated through comparative calculations and a case studie, which demonstrated its practicality

6.3. Limitations of the refined method

While the refined collision energy calculation method has demonstrated substantial benefits in terms of accuracy and economic efficiency, it is imperative to acknowledge its limitations. This understanding helps in setting realistic expectations and identifying areas for future research and development.

6.3.1. Ignoring structure properties

A consistent point of discussion throughout this research is how the structure properties are not part of the collision energy preliminary hand calculations. The proposed refined method, although it provided more realistic results that comply with published model research and measurements, it still can overestimate the collision energy more than 50 %. This might be an improvement from the exaggerated overestimation of the EAU, 2012 (e.g. 400 % as as calculated for Case C in Chapter 4) but it means that there is room left for further improvement.

Another limitation is identified in the iterative process of the design phase. Starting the hand calculations with an overly large estimation of the collision energy will yield structure dimensions that are exaggerated. Thus, more iterations in the design need to be executed so that the suitable structure and the accurate energy absorption occurs. This is time consuming, and since it provides large differences in the dimensions it might bring the engineer to confusion regarding the validity of the calculation steps they are performing.

6.3.2. Complexity in Parameter Estimation

One more notable limitation is the potential complexity involved in accurately estimating the necessary parameters. The refined method relies on precise input data regarding ship dynamics and structural interactions, which may not always be readily available. Accurately determining factors such as the

angle of approach in dynamic marine environments can be challenging and subject to variability due to changing sea conditions and ship behaviors.

The method's effectiveness is also predicated on certain assumptions that may not hold true under all circumstances. For instance, the simplifications used to model ship behavior and the interaction with water masses might not capture all relevant dynamics, especially under unusual or extreme conditions. This could lead to discrepancies between predicted and actual outcomes, potentially affecting the reliability of the method in critical applications.

6.4. Recommendations for future research

The development and implementation of the refined collision energy calculation method have set a new benchmark for the design and assessment of maritime structures. To further enhance its effectiveness and applicability, the following recommendations for future research are proposed.

- **Implementation of Sensor Measurements on Guiding Structures:**

To enhance the accuracy of input data used in collision energy calculations, it is recommended to implement advanced sensor technology on guiding structures at lock entrances. These sensors should be capable of measuring real-time deflections caused by impacting ships. This data would provide valuable insights into the actual dynamics during collisions, allowing for more accurate validation and refinement of the calculation models. Additionally, the continuous collection of empirical data could help in calibrating the models to better reflect the real-world scenarios.

- **Integration of Automatic Identification System (AIS) Data:**

AIS was originally developed as an aid to navigation, but the range of application is now well expanded.Data generated and transmitted from the vessel can be used for predictive analysis as well as post event analysis. Since the mandatory implementation of AIS, a variety of new applications have been developed using the derived data generated from the AIS data. Technological advances in data and applications have increased the amount of data collected, as well as the variety of types of data (Lee et al., 2019). Applications such as vessel tracking (Mazzarella et al., 2015) , extraction of knowledge (Pallotta et al., 2013), vessel behavior identification (Vespe et al., 2016), anomaly detection on vessel movements (Ristic et al., 2008), ship surveillance, tracking and security (Ou and Zhu, 2008), discovery of traffic patterns (Xiao et al., 2015), traffic simulation (van Dorp and Merrick, 2011), accident analysis (Goerlandt et al., 2017), ship routing development (Chen et al., 2015), near miss detection (Zhang et al., 2016), collision risk assessment (Qu et al., 2011), exhaust emission estimation (Jalkanen et al., 2014), ecological impact analysis (Merchant et al., 2012), and maritime spatial planning (Shelmerdine, 2015) have also been proposed.

Incorporating AIS data to track ship movements at lock entrances can significantly improve the understanding of ship behavior and dynamics in these critical areas. Although AIS data might have limitations in accuracy at slow velocities typically observed at lock entrances, it can still provide useful information regarding the direction and orientation of ships, which are crucial for accurately determining the approach angle in collision scenarios. Future research should explore methods to enhance the resolution of AIS data or supplement it with other navigational tools to overcome the accuracy limitations.

- **Development of Iterative Software Tools:**

There is a need for the development of sophisticated software tools that integrate the structural characteristics directly into the collision energy calculations. An iterative software tool or a Python calculation notebook could be developed to link energy calculations dynamically with structural properties. This tool would allow engineers to simulate various collision scenarios and automatically adjust design parameters based on the calculated results. Such a tool would not only streamline the design process but also ensure that the structures are optimized for both safety and cost-efficiency.

6.5. Research conclusions

This research focused on addressing the shortcomings in the current EAU, 2012 framework used for calculating collision energy in guiding structures. It demonstrated that the conventional method, which was designed for berthing situations, inaccurately captures the dynamics of ship-to-guiding structure

collisions. Specifically, the existing framework overestimates collision energy due to its treatment of the eccentricity coefficient and the misapplication of the angle α.

The refined method introduced in this thesis recalibrates the calculation of the eccentricity coefficient, particularly by redefining the angle variable to reflect the ship's actual approach to the guiding structure. This adjustment addresses the key issue where the EAU, 2012 framework treats all impacts with guiding structures as nearly central when a ship approaches with purely longitudinal speed. By focusing on the normal velocity component of the ship's movement, the refined method produces more realistic values for collision energy.

The findings were validated through both comparative analysis and a case study of the Volkerak locks. In the comparative analysis, historical data were used to compare the refined method with the standard EAU, 2012 method and the Virtual Water Mass method. The results consistently showed that the refined method more accurately reflects the actual collision dynamics, reducing overestimations of collision energy by significant margins. This reduction in estimated energy directly translates to material savings in the structural design.

The case study further confirmed the practical benefits of the refined method. By applying the refined calculations, the design required smaller pile diameters and less material overall, while still maintaining the necessary structural integrity. For instance, the refined calculation resulted in a reduction of pile diameter from 2020 mm to 1620 mm, and the spacing between piles was extended from 3 m to 6.5 m. These adjustments demonstrate the method's potential for reducing material costs and improving design efficiency without compromising safety.

In conclusion, the refined collision energy calculation method provides a more accurate and efficient approach for designing guiding structures. It corrects the over-conservatism of the EAU, 2012 framework and offers significant benefits in terms of both material usage and cost. This research establishes a foundation for adopting the refined method in future designs, particularly for high-traffic inland waterways where such structures are critical. Further research can build on this work by incorporating real-time data collection and exploring additional refinements to the method.

Bibliography

Aslan, Y. (2023). Understanding the relationship between lock complex effectiveness and system performance: A study of the volkerak complex.

Atiq, M. S., Shajib, A. et al. (2023). Analysis of marine fender systems minimizing the impact of collision damage. *Kazi Naimul, Analysis of Marine Fender Systems Minimizing the Impact of Collision Damage (May 11, 2023)*.

Berendsen, E. (2022). Impact resistance of ship hull to berthing loads: Quantifying critical fender impact.

Brolsma, J., Hirs, J., & Langeveld, J. (1977). On fender design and berthing velocities. *Proceedings of the PIANC 24th International Navigation Congress, Leningrad, Russia*, 6–14.

Brolsma, J., & Roelse, K. (2011). Waterway guidelines 2011. *ISBN 9789036900690*.

BS-6349-4. (2014). Code of practice for design of fendering and mooring system. *BSI*.

Cajiao, J., & Phelan, J. (2022). Eccentricity coefficient in berthing energy calculations. *Ports 2022* (pp. 325–335).

Carter, D. P. (2016). The evolution of analysis methods for laterally loaded piles through time. *SpringerLink*. https://link.springer.com

Chen, J., Lu, F., & Peng, G. (2015). A quantitative approach for delineating principal fairways of ship passages through a strait. *Ocean Engineering*, *103*, 188–197.

Demenet, P.-F. (2018). The kinetic energy method revisited. *Journal of Applied Water Engineering and Research*, *6*(1), 1–16.

EAU. (2012). *Recommendations of the committee for waterfront structures harbours and waterways: Eau 2012*. Ernst & Sohn.

Euris Portal. (2024). Waterway segment nl0014300047 [Accessed: [10-05-2024]]. https://www.eurisportal.eu/waterway/segments?id=NL0014300047

European Committee for Standardization. (2005). *Eurocode 3: Design of steel structures - part 1-1: General rules and rules for buildings*. CEN.

Fontijn, H. (1975). An approximative method for the determination of the hydrodynamic coefficients of a ship in case of swaying and yawing on shallow water. *Communications on hydraulics, 1975-04*.

Glerum, A., & Vrijburcht, A. (2000). Design of locks.

Goerlandt, F., Goite, H., Banda, O. A. V., Höglund, A., Ahonen-Rainio, P., & Lensu, M. (2017). An analysis of wintertime navigational accidents in the northern baltic sea. *Safety science*, *92*, 66–84.

Jalkanen, J.-P., Johansson, L., & Kukkonen, J. (2014). A comprehensive inventory of the ship traffic exhaust emissions in the baltic sea from 2006 to 2009. *Ambio*, *43*, 311–324.

Jiang, C., Xiang, X., & Xiang, G. (2024). A joint multi-model machine learning prediction approach based on confidence for ship stability. *Complex & Intelligent Systems*, 1–18.

Kang, E.-J., Lee, H.-T., Kim, D.-G., Yoon, K.-K., & Cho, I.-S. (2022). Grouping pilots' maneuvering types according to berthing velocity using agglomerative clustering algorithm. *Journal of Marine Science and Engineering*, *10*(10), 1452.

Karnovsky, I. A., Lebed, O., Karnovsky, I. A., & Lebed, O. (2021). Matrix stiffness method. *Advanced Methods of Structural Analysis*, 451–498.

Lee, E., Mokashi, A. J., Moon, S. Y., & Kim, G. (2019). The maturity of automatic identification systems (ais) and its implications for innovation. *Journal of Marine Science and Engineering*, *7*(9), 287.

Lindijer, G. (1981). Rekenmodellen voor het botsen van schepen tegen remmingwerken: Theoretische benaderingen voor de invloed van het water. *M1374*.

Liu, Z., & Li, G.-Q. (2024). Thermophysical properties of high–strength steel wires at high temperatures. *Fire Safety Journal*, *146*, 104165.

Mazzarella, F., Arguedas, V. F., & Vespe, M. (2015). Knowledge-based vessel position prediction using historical ais data. *2015 Sensor Data Fusion: Trends, Solutions, Applications (SDF)*, 1–6.

Merchant, N. D., Witt, M. J., Blondel, P., Godley, B. J., & Smith, G. H. (2012). Assessing sound exposure from shipping in coastal waters using a single hydrophone and automatic identification system (ais) data. *Marine pollution bulletin*, *64*(7), 1320–1329.

Molenaar, W., & Voorendt, M. (2016). Manual hydraulic structures. *Collegedictaat CIE3330*.

Moore, D. (2024). *Viscous damped free vibrations* [Accessed: September 6, 2024]. LibreTexts. https://eng.libretexts.org/Bookshelves/Mechanical_Engineering/Mechanics_Map_(Moore_2nd_Edition)/16:Vibrations_with_One_Degree_of_Freedom/16.02:Viscous_Damped_Free_Vibrations

Neşer, G., & Ünsalan, D. (2006). Dynamics of ships and fenders during berthing in a time domain. *Ocean engineering*, *33*(14-15), 1919–1934.

Ou, Z., & Zhu, J. (2008). Ais database powered by gis technology for maritime safety and security. *The Journal of Navigation*, *61*(4), 655–665.

Pallotta, G., Vespe, M., & Bryan, K. (2013). Vessel pattern knowledge discovery from ais data: A framework for anomaly detection and route prediction. *Entropy*, *15*(6), 2218–2245.

PIANC. (2002). *Wg 33, guidelines for design of fender systems* (tech. rep.). PIANC.

PIANC. (2024). *Wg 211, fender guidelines 2024* (tech. rep.). PIANC.

Qu, X., Meng, Q., & Suyi, L. (2011). Ship collision risk assessment for the singapore strait. *Accident Analysis & Prevention*, *43*(6), 2030–2036.

Richtlijnen-Vaarwegen. (2020). Richtlijnen vaarwegen 2020.

Rijkswaterstaat. (2022). 4-barge pusher convoy 190 preparation [Accessed: [01-08-2022]]. https://open.rijkswaterstaat.nl/open-overheid/@253312/4-barge-pusher-convoy-190-preparation/

Ristic, B., La Scala, B., Morelande, M., & Gordon, N. (2008). Statistical analysis of motion patterns in ais data: Anomaly detection and motion prediction. *2008 11th International Conference on Information Fusion*, 1–7.

Robertson, P. K. (1986). Use of piezoeter cone data. *Proc. of Insitu'86, Speciality Conference*.

ROK-2.0. (2021). Richtlijn ontwerp kunstwerken: Rok 2.0. *RTD 1001: 2021 2.0 Rijkswaterstaat Technisch Document*.

ROM. (2011). Rom 2.0-11. recomendaciones para el proyecto y ejecución en obras de atraque y amarre. *Ministerio de Fomento: Madrid, Spain*.

Roubos, A. (2018). *Flexible dolphins* (Vol. CRW C1005). Kennisplatvorm CROW.

Roubos, A., Groenewegen, L., & Peters, D. J. (2017). Berthing velocity of large seagoing vessels in the port of rotterdam. *Marine Structures*, *51*, 202–219.

Ruigrok, J. (2010). Laterally loaded piles, models and measurements. *TU Delft Repository*. https://repository.tudelft.nl/record/uuid:dbcf881e-9cdb-4689-9dbf-018b098d7481

Shelmerdine, R. L. (2015). Teasing out the detail: How our understanding of marine ais data can better inform industries, developments, and planning. *Marine Policy*, *54*, 17–25.

Steenhuis, M. (2015). The deltaworks: Heritage and new space for a changing world. *Water & heritage. Material, conceptual and spiritual connections. Sidestone Press, Leiden*, 331–350.

van Dorp, J. R., & Merrick, J. R. (2011). On a risk management analysis of oil spill risk using maritime transportation system simulation. *Annals of Operations Research*, *187*, 249–277.

Vasco Costa, F. (1965). Analytic study. *Proceedings of NATO Advanced Study Institute on Analytical Treatment of Problems of Berthing and Mooring Ships, Technical University Lisbon, Portugal*.

Vespe, M., Gibin, M., Alessandrini, A., Natale, F., Mazzarella, F., & Osio, G. C. (2016). Mapping eu fishing activities using ship tracking data. *Journal of Maps*, *12*(sup1), 520–525.

Vrijburcht, A. (1991). Loads on fender structures and dolphins by sailing ships. *Rijkswaterstaat communications 49*.

Vrijburcht, A. (2000). Ontwerpen van schutsluizen. *ISBN 90-369-3305-6*.

Vrijer, A. (1978). Belastingen op remmingwerken door schepen, varend onder een hoek tegen het remmingwerk. *M1374*.

Vrijer, A. (1983a). Berekeningen en modelonderzoek botskrachten. *Waterloopkundig laboratorium, delft hydraulîcs laboratory*.

Vrijer, A. (1983b). Rekenmethodes en procedure voor het ontwep. *Waterloopkundig laboratorium, delft hydraulîcs laboratory*.

Wongnitchakul, A. (2023). The living barriers: The architectural adaptation of existing flood barriers on zeeland's new biodiversity synergy.

Xiao, F., Ligteringen, H., Van Gulijk, C., & Ale, B. (2015). Comparison study on ais data of ship traffic behavior. *Ocean Engineering*, *95*, 84–93.

Zhang, W., Goerlandt, F., Kujala, P., & Wang, Y. (2016). An advanced method for detecting possible near miss ship collisions from ais data. *Ocean Engineering*, *124*, 141–156.

A

Guideline tables and relevant information

A.1. Framework: Designing with the ROK-2.0

The Guidelines for the Design of Structures (ROK: Richtlijnen Ontwerp Kunstwerken) is a framework within the RWS (Rijkswaterstaat) working method. It is a collection of general requirements that the design and execution of a new structure must meet. These are, therefore, design preconditions that are set for the verifications to be carried out (modelling with control calculation or inspections). The ROK-2.0 also applies to new parts of existing structures when these parts are replaced, or to widening works when structures are expanded.

A.1.1. Relevant definitions

The ROK-2.0 defines the following six categories of structures:

- Bridge
- Tunnel
- Wet structure
- Movable bridge
- Noise barrier
- Traffic support structure

The relevant category for this research is the one that includes guiding structures. This is the “wet structure” category. It is a civil-engineering construction that is part of a waterway with the purpose of regulating water levels, passage of ships, flood protection, intersection of waterways or drainage of water. The subcategory of “wet structure” that is relevant here is locks. The definition in the ROK-2.0 follows:

Wet structure – Lock: A structure with a movable water barrier that forms connection between two waterways

A.1.2. Relevant clauses regarding the collision energy

For calculating the collision energy the relevant clauses of ROK-2.0 are included in section 1.6 and are presented next.

ROK-0485: Encountering a resilient structure

Resilient structures such as protective bollards, berthing and guiding structures must be calculated for a collision energy that is determined in accordance with EAU 2012, 6.15.4.

ROK-0649: Water displacement calculation for collision energy

Resilient structures such as protective piles, berthing and guiding structures must be calculated with a water displacement G [ton] for ships allowed on the waterway, taking into account:

- Inland vessels
  - Maximum load capacity according to RWV 2020 table 8 (Appendix A.1 A.2)
- Motorships: load capacity multiplied by 1.15
- Pusher barge combinations and coupled connections: load capacity multiplied by 1.14
- Seagoing vessels
  - For R/S1-3 ships, a water displacement according to the dimensions in table 12 of Richtlijnen-Vaarwegen, 2020 with a block coefficient of 0.9.
  - For larger seagoing vessels: apply dead-weight tonnage (DWT).

ROK-0650: Collision speed on protective piles for determining collision energy

Protective bollards must be calculated with an approach speed of ships equal to sailing speeds in accordance with ROK-2.0 table T0718 (table A.1). If a protective bollard is located within the length of the ship in question of a lock, the approach speed may be limited to 3 m/s. A protective bollard is hit perpendicularly.

CEMT Class	I	II	III	IV	Va	Vb to VII
Speed [m/s]	4.1	4.8	5.1	5.3	5.5	4.5

Table A.1: ROK T0718: Maximum sailing speed to be observed per CEMT-class waterway

ROK-0651: Impact load protective bollard

The impact load on a protective bollard must be regarded as a special load (emergency situations). Normally a protective bollard is normally not subjected to an impact load from shipping.

ROK-0652: Approach speed for berthing structures for determining collision energy

Berthing facilities for inland shipping must be calculated with a perpendicular approach speed of 0.25 m/s.

ROK-0653: Collision speed for guiding structures for determining collision energy

Guiding structures must be calculated with a ship speed in accordance with the table T0718 of the ROK and an angle of approach of the ship with the guide of 5 degrees plus the angle of the guides relative to the axis of the waterway. The speed may be limited to 1.2 times the permitted sailing speed. Within distance from the lock equal to a ship's length, the sailing speed of the ship under consideration may be limited to 3 m/s.

ROK-0654: Further aspects of design of resilient structures for collision energy

Resilient structures such as protective poles, mooring, and guiding structures must be designed in such a way that they comply with the following aspects:

- The impact load of the ships is between the Guiding Low Water Levels (MLWS) and the design conform of Richtlijnen-Vaarwegen, 2020 table 39.
- For the impact load, the particle load factor by 1,0 is applicable.
- When steel is used, the material factor on the yield strength $\gamma_m = 1,4$ in UGT; conform EN-NEN 1990.
- In the presence of bed protection, the confinement (restriction of movement) of the resilient structure must be taken into account, unless the required freedom of movement is guaranteed
- Cohesive soil layers must be modeled with saturated strength values.

- The calculation values of the soil properties must be derived in accordance with CUR Report 166.
- With an impact load on the construction, the resilient structure must absorb the total load by means of elastic deformation (structure + soil); plastic deformation is thus not permitted.
- Corrosion must be calculated in accordance with ROK paragraph 7.14, where the structure must meet the requirements set in ROK-0485 from the beginning to the end of the service life.
- If steel is used, a toe test must take place on local buckling and fold of the resilient structure.

ROK-0655: Rotational speed for determining collision energy

Berthinhg and guiding structures with continuous dolphins in or near turning basins must be dimensioned on a rotation speed of ships that follows from a thorough nautical study. Usually, ω = 0 [rad/s], but in turning basins, the rotation speed is a determining factor.

ROK-0804: Collision energy parallel to the day-side of the berthing and guiding structures

Berthing and guiding structures must be calculated for a frictional force parallel to the clear side of the structure at a value of 50 % of the impact load. This load must be handled due to friction caused by the hull with the purlins.

ROK-0805: Further aspects of design of resilient structures for collision energy

Berthing and guiding works must be calculated in such a way that they meet the following aspects:

- During an impact load from a normally maneuvering ship, it must be prevented that the ship gets damaged. For the ship impact load which a ship can withstand without damage, a maximum of 200 $kN/m2$ for CEMT I to 1200 kN/m^2 for CEMT VI applies, according to the experience data (source: RWS). For transit shipping vessels, a maximum ship impact load of 700 kN/m^2 applies. (PIANC, 2002).
- In the case of BGT, if the structure can be walked on under governing conditions, the displacement on the level where the edge remains must be limited to a maximum of 500 mm.

Table 8: Classification of the inland shipping fleet, Rijkswaterstaat 2010

CEMT Class	Motor freighters (Motorvessels)							Push convoys (Barges)			
	RWS Class	Characteristics reference ship**				Classification		RWS Class	Characteristics normative push convoy**		
		Name	Width	Length	Draft (loaded)	Load power	Width and length		Combination	Width	Length
			m	m	m	t	m			m	m
	M0	Other				1-250	B<= 5.00 of L <= 38.00				
I	M1	Rush hour	5.05	38.5	2.5	251-400	B= 5.01-5.10 en L>=38.01	BO1		5.2	55
II	M2	Kempenaar	6.6	50-55	2.6	401-650	B=5.11-6.70 en L>=38.01	BO2		6.6	60-70
III	M3	Hagenaar	7.2	55-70	2.6	651-800	B=6.71-7.30 en L>=38.01	BO3		7.5	80
	M4	Dortmund Ems (L < = 74m)	8.2	67-73	2.7	801-1050	B=7.31-8.30 en L=38.01-74.00	BO4		8.2	85
	M5	Verl. Dortmund Ems (L > 74 m)	8.2	80-85	2.7	1051-1250	B=7.31-8.30 en L>=74.01				
IVa	M6	Rhine-Herne Ship (L <= 86m)	9.5	80-85	2.9	1251-1750	B=8.31-9.60 en L=38.01-86.00	BI	Europa I push convoy	9.5	85-105
	M7	Verl. Rhine-Herne (L > 86 m)	9.5	105	3.0	1751-2050	B=8.31-9.60 en L>=86.01				
IVb											
Va	M8	Large Rhine ship (L <=111m)	11.4	110	3.5	2051-3300	B= 9.61-11.50 en L=38.01-111.00	BII-1	Europa II push convoy	11.4	95-110
	M9	Extended Large Rhine ship (L >111m)	11.4	135	3.5	3301-4000	B= 9.61-11.50 en L>=111.01	BIIa-1	Europa IIa push convoy	11.4	92-110
								BIIL-1	Europe II Long	11.4	125-135
Ex								BII-2l	2-barge pusher long	11.4	170-190
Through	M10	Size Ship 13.5 ' 110 m	13.50	110	4.0	4001-4300	B=11.51-14.30 and L=38.01-111.00	BII-2b	2-box push convoy wide	22.8	95-145
	M11	Size Ship 14.2 ' 135 m	2.20 pm	135	4.0	4301-5600	B=11.51-14.30 and L>= 111.01				
	M12	Rijnmax ship	17.0	135	4.0	>= 5601	B>= 14.31 and L>= 38.01				
VIb								BII-4	4-bin push convoy (incl. 3-bin long)	22.8	185-195
VIc								BII-6l	6-box pusher long (including 5-bin long)	22.8	270
VIc								BII-6b	6-box push convoy wide (incl. 5-bin wide)	34.2	195

* In classes I, IV, V and higher, the clearance heights have been adjusted for 2 or 3 and 4-layer container shipping, respectively. (air draft relative to MHWS)

** The characteristics of the reference vessel have a margin of ± 1 meter in length and in width of ± 10 cm

Figure A.1: Table 8 RWV 2010 (Brolsma and Roelse, 2011), page 1

Push convoys (Barges)			Couplings (Convoys)							Passage height*
	Classification		RWS Class	Characteristics normative coupling**				Classification		
Draft (loaded)	Load power	Width and length		Combination	Width	Length	Draft (loaded)	Load power	Width and length	incl. 30 cm shock height
m	t	m			m	m	m	t	m	m
1.9	0-400	B<=5.20 and L= all	C1l C1b	2 spires long 2 spires wide	5.05 10.1	77-80 38.5	2.5 2.5	<= 900 <= 900	B<= 5.1 and L=all B=9.61-12.60 en L <= 80.00	5.25* 5.25*
2.6	401-600	B=5.21-6.70 en L=all								6.1
2.6 2.7	601-800 801-1250	B=6.71-7.60 en L=all B=7.61-8.40 en L=all								6.4 6.6 6.4
3.0	1251-1800	B=8.41-9.60 en L=all								7.0* 7.0*
			C2l	Class IV + Europe I long	9.5	170-185	3.0	901-3350	B=5.11-9.60 en L=all	7.0*
3.5 4.0 4.0	1801-2450 2451-3200 3201-3950	B=9.61-15.10 en L<=111.00 B=9.61-15.10 en L<=111.00 B=9.61-15.10 and L=111.01-146.00								9.1* 9.1* 9.1*
3.5-4.0	3951-7050	B=9.61-15.10 en L>=146.01	C3l	Class Va + Europe II long	11.4	170-190	3.5-4.0	3351-7250	B=9.61-12.60 en L>=80.01	9.1*
3.5-4.0	3951-7050	B=15.11-24.00 and L<=146.00	C2b C3b	Class IV + Europe I wide Class Va + Europe II wide	19.0 22.8	85-105 95-110	3.0 3.5-4.0	901-3350 3351-7250	B=12.61-19.10 en L<=136.00 B>19.10 and L<=136	7.0* for class IV couples only 9.1*
3.5-4.0	7051-12000 (7051-9000)	B=15.11-24.00 and L=146.01-200	C4	Class Va + 3 Europe II	22.8	185	3.5-4.0	>=7251	B>12.60 and L>=136.01	9.1*
3.5-4.0	12001-18000 (12001-15000)	B=15.11-24.00 and L>=200.01								9.1*
3.5-4.0	12001-18000 (12001-15000)	B>=24.01 en L=all								9.1*

Note: 1: A reference vessel is a vessel whose dimensions determine the dimensioning of the waterway and the structures in it.

2: New construction or waterway widening is based on the largest reference vessel within a CEMT class.

3: Class M3, M4, M6, M8, M10 and M11 may only be used for the renovation of existing waterways, locks and bridges.

4: The smallest dimensions of a reference vessel form the lower limit for classifying a waterway in a certain standardized class.

Figure A.2: Table 8 RWV 2010 (Brolsma and Roelse, 2011), page 2

B

Volkerak locks case study supplement

In this section, a supplement for the case study is provided. Here, the necessary background information for the case study comprehension along with the detailed analytical calculations are presented.

B.1. Soil Characteristics

The soil characteristics are derived using the CPT information publically available on DINOloket. There, a point near the structure is chosen on the map, and the platform returns the CPT.

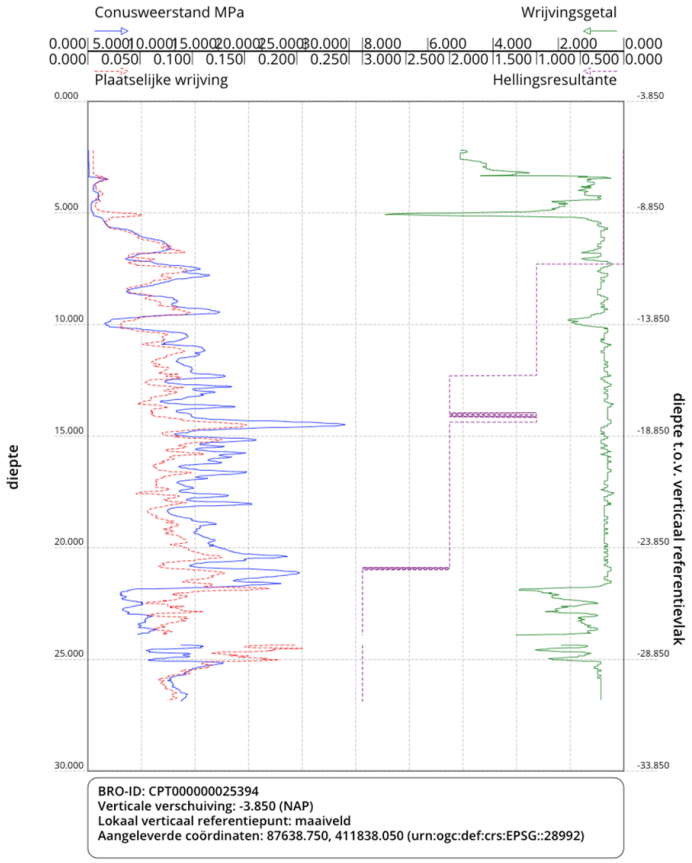

Figure B.1: CPT Volkerak Lock

From the CPT, soil properties are determined using the the graph by Robertson et al. (1986). Deeper than the 9 m the friction ratio is in the range 1-1.5 %. This indicates soil consisting of fine sand.

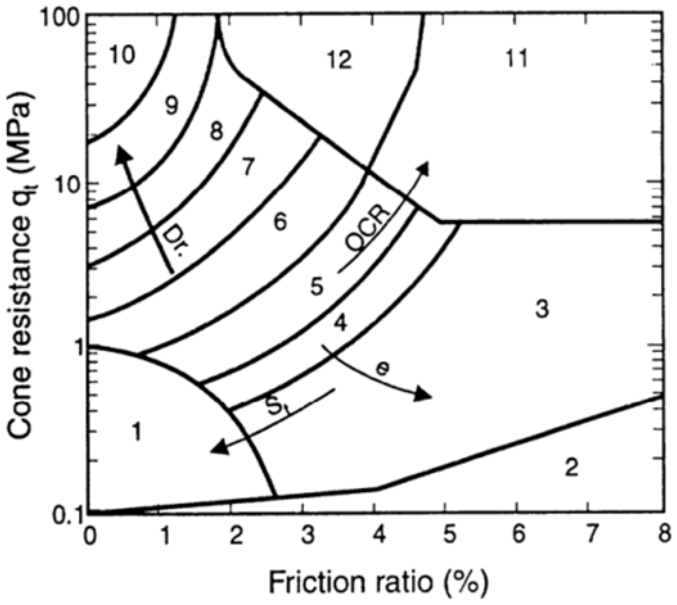

Zone	*Soil Behavior Type*
1	*Sensitive fine grained*
2	*Organic material*
3	*Clay*
4	*Silty Clay to clay*
5	*Clayey silt to silty clay*
6	*Sandy silt to clayey silt*
7	*Silty sand to sandy silt*
8	*Sand to silty sand*
9	*Sand*
10	*Gravelly sand to sand*
11	*Very stiff fine grained**
12	*Sand to clayey sand**

** Overconsolidated or cemented*

Figure B.2: Robertson, 1986

B.2. Blum method for pile - soil interaction

According to the Manual of Hydraulic Structures by Molenaar and Voorendt, 2016, a commonly used method to compute the required embedded depth (inheidiepte) needed to provide enough passive soil resistance to lateral loads, is Blum's method (Die Bautechnik, Heft 5,1932). Blum used the following assumptions for his theory:

1. the embedded part of the foundation pile is regarded as an elastically supported beam;
2. the soil response is perfectly plastic;
3. the soil reaction on the deeper part of the pile is substituted by a concentrated force known as the Ersatzkraft (R3), see Figure 44-2; [1]

[1] It is assumed that the elastic range of the soil is extremely small. As soon as there is a displacement u the soil response is either immediately at is maximum (passive, σh,max) or minimum (active, σh,min). Hence the stiffness of the soil is assumed to be very large. It is to be expected that the displacements as a result of the load will be somewhat underestimated.

4. for stiffness considerations the pile is thought to have a fixed support at the depth were the concentrated force R3 is acting on the pile.

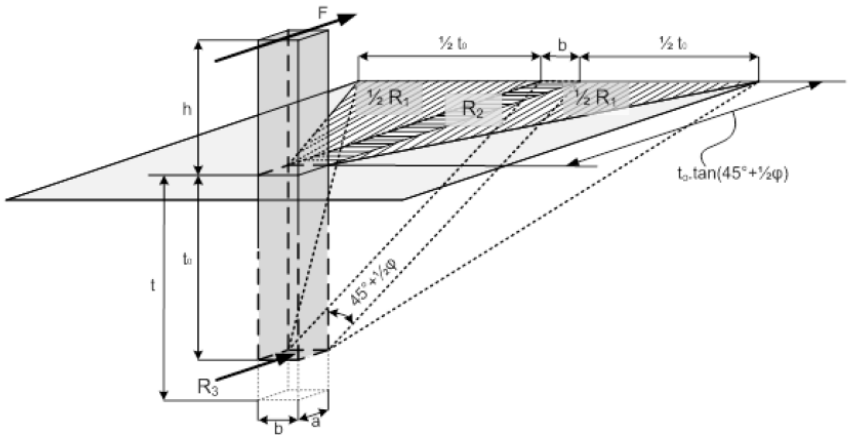

Figure B.3: Soil wedge behind laterally loaded pile (Molenaar and Voorendt, 2016)

where:

- F [kN] = load
- $R1$ [kN] = resultant force of the soil wedges on both sides next to the soil wedge directly behind the pile (two half pyramids)
- $R2$ [kN] = resultant force of the soil wedge directly behind the pile (a triangle with width b)
- $R3$ [kN] = substitute force ('Ersatzkraft')
- a [m] = width of the pile in the direction of the load
- b [m] = width of the pile perpendicular to the load
- h [m] = length of the unsupported part of the pile
- t_0 [m] = theoretical embedded depth
- t [m] = practical embedded depth $t = 1,2t_0$
- ϕ [°] = angle of internal friction

The maximum load the soil wedge behind the pile is able to resist can be computed by taking the sum of the moments at depth t_0 below bed level, in this way the concentrated force R3 does not enter into the equations (see Figure B.4).

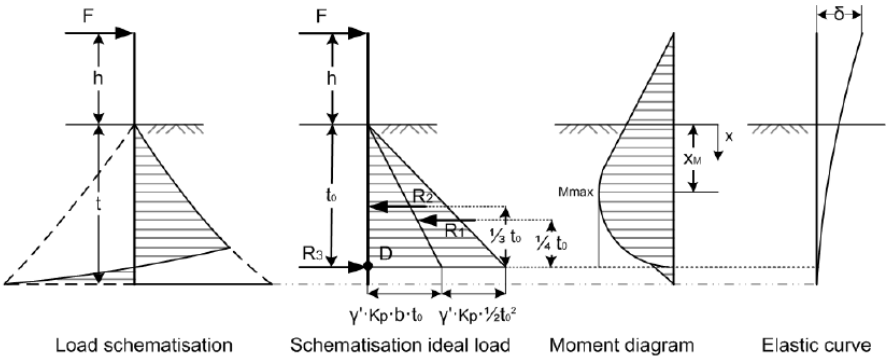

Figure B.4: Blum's schematization (Molenaar and Voorendt, 2016)

By moment equilibrium at point D the maximum force is derived as:

$$F_{max} = \gamma' * K_p * \frac{t_0^3}{24} * \frac{t_0 + 4 * b}{t_0 + h} \tag{B.1}$$

where:

- F_{max} [kN] = maximum load that can be resisted
- b [m] = width of the pile perpendicular to the load
- K_p [-] = passive soil pressure coefficient [2]
- γ' [kN/m3] = effective volumetric weight $(\gamma_s - \gamma_w)$
- δ [°] = (pile) wall friction; generally $\delta = -\frac{2}{3}\phi$

Because all (shear) forces are known, the moment diagram can be determined, using the following equation:

$$M_x = F * (h + x) - \gamma' * K_p * (x + 4 * b) * \frac{x^3}{24} \tag{B.2}$$

where:

- M_x [kNm] = moment at depth x
- F [kN] = load
- x [m] = distance below bed level

The maximum moment M_{max} occurs at depth X_M, where $\frac{\delta M}{\delta x} = 0$. This depth is found by solving the following equation iteratively[3]:

$$x_M^2 * (x_M + 3 * b) = \frac{t_0^3}{4} * \frac{t_0 + 4 * b}{t_0 + h} \tag{B.3}$$

When loaded in a direction perpendicular to its axis, a foundation pile will bend. The displacement of the part of the pile embedded in soil results in a passive resisting force. The graph of the bending moments in the pile, according to Blum's strength considerations, shows a curved development, see Figure B.5. The pile could also be modelled as a cantilevering beam with concentrated load (horizontal). For this last schematization the bending moment diagram and the formula for the maximum displacement are well known:

$$\delta = \frac{F * L_i^3}{3EI} \tag{B.4}$$

where EI is the stiffness of the cantilever; in this case, the pile stiffness.

[2] The soil resistance only depends on the angle of internal friction and the volumetric weight of the soil. Almost always the effective (submerged) weight of the soil has to be used in combination with $\delta = -\frac{2}{3}\phi$, to calculate the K_p, and arrive at the lateral bearing capacity.

[3] For the strength considerations in the above, the position of the fixed support of the pile is at a distance X_M below ground level.

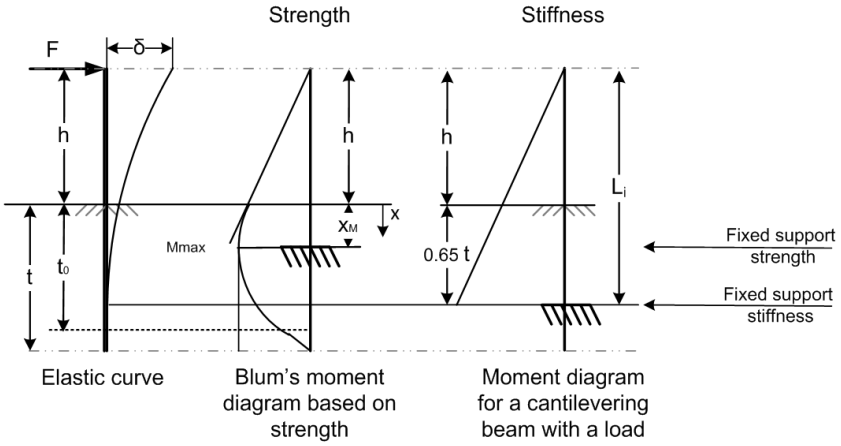

Figure B.5: Moment diagrams for laterally loaded piles (Molenaar and Voorendt, 2016)

Equating the statical moments of both moment diagramas, Blum found the following expression for the displacement of the pile head as a result of a lateral load F:

$$\delta = \frac{F * (h + 0.65 * t)^3}{3EI} \tag{B.5}$$

where:

- δ [m] = displacement of the pile head
- F [N] = load
- h [m] = length of the unsupported part
- t [m] = practical embedded depth
- E [N/m^2] = Young's modulus of the pile material
- I [m^4] = moment of inertia of the pile
- L_i [m] = $h + 0,65 * t$

Hence the overall pile stiffness, the spring stiffness k of the pile, which includes a contribution of both soil and pile material, when the maximum load is acting, can be estimated as follows:

$$k_{pile} = \frac{F_{max}}{\delta} = \frac{3EI}{(h + 0.65 * t)^3} \tag{B.6}$$

As long as the soil can be schematized as one layer, Blum's schematization results in a reasonable approximation of the maximum absorbable lateral load on a foundation pile (Molenaar and Voorendt, 2016). However when the soil profile consists of multiple layers, then the displacements better be analysed using a finite element model or an elasto-plastic spring model.

B.3. Pile - Soil Interaction Optimization Calculation Process Supplement

The energy calculated in section 5.3 and the preliminary pile diameters calculated in section 5.4, work as the starting point for this calculation step. In this step, the practical embedded depth that is needed for the deflection limits to not be surpassed, are derived.

The calculation process is kicked off by assuming an allowed pile deflection. This maximum deflection is the upper limit of deflection for which the unity check is fulfilled for the specific pile diameter.

Practical embedded depth

With the energy calculation and the allowed deflection, the force for which the pile is designed is known by means:

$$F_{max} = \frac{2 * E_{collision}}{\delta} \tag{B.7}$$

Then, the wanted pile stiffness is derived by:

$$k_{pile} = \frac{F_{max}}{\delta} \tag{B.8}$$

The stiffness of the pile is also expressed as:

$$k_{pile} = \frac{3EI}{(h + 0.65 * t)^3} \tag{B.9}$$

By means of equation B.9 it is possible to solve for the practical embedded depth t.

Length of fixity (Strength)

With the maximum force known, it is possible to solve for the theoretical embedded depth t_0 using equation B.1. The theoretical embedded depth is then used in equation B.3 to calculate the position where the maximum moment appears, which defines the level of fixity.

$$L_{fixity_{strength}} = h + x_M \tag{B.10}$$

Length of fixity (Stiffness)

$$L_{fixity_{stiffness}} = h + 0.65 * t \tag{B.11}$$

Unity Check

The maximum moment can be calculated by equation B.2 and then the unity check is performed where for steel:

$$\frac{M_d}{M_{rd}} \leq 1 \tag{B.12}$$

where:

- M_d: Design moment
- M_{rd}: Resistance design moment

C

Example Notebook

Calculation Virtual Water Mass method

```
%matplotlib inline
import numpy as np
import matplotlib.pyplot as plt
import pandas as pd

#in this step we define the design ship
m = 11.6 * 10**6 #mass of ship [kg]
L = 153 #length of the ship [m]
B = 22.7 #beam of the ship [m]
d = 3.30 #draught of the ship [m]
h = 4.80 #water depth [m]
x1_dot0 = 1.509 #longitudinal approach speed [m/s]
x2_dot0 = 0.0 #transversal approach speed [m/s]
phi_dot0 = 0 #rotational approach speed [rad/s]
phi0 = np.array((4,15,30,60,80)) * np.pi / 180 #approach angle [rad]

#in this step we define the design ship
m = 11.6 * 10**6 #mass of ship [kg]
L = 153 #length of the ship [m]
B = 22.7 #beam of the ship [m]
d = 3.30 #draught of the ship [m]
h = 4.80 #water depth [m]
x1_dot0 = 1.509 #longitudinal approach speed [m/s]
x2_dot0 = 0.0 #transversal approach speed [m/s]
phi_dot0 = 0 #rotational approach speed [rad/s]
phi0 = np.array((4,15,30,60,80)) * np.pi / 180 #approach angle [rad]

#in this step we define the guiding structure
M = 1.1 * 10**6 #mass of the structure [kg]
k = 3.2 * 10**6 #linear stiffness of the structure [N/m]
c = 0.405 * 10**6 #linear damping of the structure [Ns/m]
tgb = 0.16 #friction factor

#to be determined using the above
a = 0.5 * (L * np.cos(phi0) - B * np.sin(phi0)) #distance from contact point to cm x-
    direction [m] (the ship is considered to have a rectangular shape)
b = 0.5 * (L * np.sin(phi0) + B * np.cos(phi0)) #distance from contact point to cm y-
    direction [m] (the ship is considered to have a rectangular shape)
yv0_dot = x1_dot0 * np.sin(phi0) + x2_dot0 * np.cos(phi0) + 0.5 * a * phi_dot0 #speed of
    point of impact at time zero [m/s]

#virtual mass initial speed to be determined here
a_btz = (M/m * (1 - (12 * a / L**2) * (tgb * b - a)) + 1)**(-1) #coefficient
yv0_dot_v = a_btz * yv0_dot #virtual mass initial speed
F0 = c * yv0_dot_v

#virtual mass calculation
```

```
a_bwz = 1 / (1 - 12 * (a * (b * tgb - a) / L**2)) #check that a_bwz<=1
c_bw = np.array((1.43,1.43,1.43,1.07,1)) #value to be interpolated using figures 30 to 47 of the report
m_bw = a_bwz * c_bw * m #virtual mass [kg]
for i in range(len(a_bwz)):
    if a_bwz[i] < 1:
        a_bwz[i]
    else:
            a_bwz[i]=1
#calculating the time t1 for maximum force
m_acc = m_bw + M #system mass ship + structure
gamma = (c / (2 * np.sqrt(k * m_acc)))
omega = np.sqrt(k / m_acc)
omega_d = np.sqrt(omega**2 - gamma**2)
t1 = (1 / (omega * np.sqrt(1 - gamma**2))) * np.arctan((1 - 4 * gamma**2 * np.sqrt(1 - gamma**2))/((3 - 4 * gamma**2) * gamma)) #time of maximum force [s]

#calculating the maximum force between ship and structure
F_t1 = m_acc * np.exp(- gamma * omega * t1) * yv0_dot_v * (((gamma**2 * omega**2)/(omega * np.sqrt(1 - gamma**2)) - omega * np.sqrt(1 - gamma**2)) * np.sin(omega * np.sqrt(1 - gamma**2) * t1) - 2 * gamma * omega * np.cos((omega * np.sqrt(1 - gamma**2) * t1)))

#calculating the time t2 for maximum displacement
t2 = (1 / (omega * np.sqrt(1 - gamma**2))) * np.arctan(np.sqrt(1 - gamma**2) / gamma)

#calculating the maximum displacement
y_t2 = np.exp(- gamma * omega * t2) * yv0_dot_v * (1 / (omega * np.sqrt(1 - gamma**2))) * np.sin(omega * np.sqrt(1 - gamma**2) * t2)

#loss of contact at time t3 calculated here
t3 = (1 /omega_d) * np.arctan(2 * gamma * np.sqrt(1 - gamma**2) / (1 - 2 * gamma**2))

#displacement progression
t = np.linspace(0,t2,100)
yv = np.zeros((100,5))
for i in range(5):
    yv[:,i] = np.exp(-gamma[i] * omega[i] * t[:,i]) * (yv0_dot_v[i] / omega_d[i]) * np.sin(omega_d[i] * t[:,i])
    print(f"Maximum displacement is {np.max(yv[:,i]):.3} m at time {t[:,i][yv[:,i]==np.max(yv[:,i])][0]:.3} s ")
plt.figure(figsize=(10,4))
plt.plot(t, yv);

#velocity progression with differentiation of yv
yv_dot = -gamma * omega * np.exp(-gamma * omega * t) * (yv0_dot_v / omega_d) * np.sin(omega_d * t) + np.exp(- gamma * omega * t) * (yv0_dot_v / omega_d) * np.cos(omega_d * t) * omega_d
#plt.figure(figsize=(10,4))
#plt.plot(t, yv_dot);

#acceleration progression by differenciating yv_dot
yv_ddot = np.exp(- gamma * omega * t) * yv0_dot_v * ((gamma**2 * omega**2 / omega_d) * np.sin(omega_d * t) - 2 * gamma * omega * np.cos(omega_d * t))

#force progression
Fy = M * yv_ddot + c * yv_dot + k * yv
for i in range(5):
    print(f"Maximum force is {np.max(Fy[:,i]):.0f} N at time {t[:,i][Fy[:,i]==np.max(Fy[:,i])][0]:.3f} s ")
display(np.min(Fy) * 10**(-3))
display(np.max(Fy) * 10**(-3))
display(t[Fy==np.max(Fy)])
plt.figure(figsize=(10,4))
plt.plot(t, Fy);

#force-deflection curve
from scipy.integrate import trapz
I = np.zeros(5)
color = ['r','b','g','m','y']
plt.figure(figsize=(20,10))
for i in range(5):
```

```
    r = np.round(np.random.rand(),1)
    g = np.round(np.random.rand(),1)
    b = np.round(np.random.rand(),1)
    yc = i + np.random.rand(100)*0.25
    I[i] = trapz(Fy[:,i],yv[:,i])
    print(f"For  = {phi0[i]* 180 / np.pi:.0f} the collision energy is {I[i] * 10**(-3):.2f} kNm")
    plt.subplot(3,2,i+1)
    plt.plot(yv[:,i],Fy[:,i], label=f"{phi0[i]* 180 / np.pi:.0f}$^o$", color='k');
    plt.fill_between(yv[:,i], Fy[:,i],color=f"{i/10}", alpha=0.5)
    plt.text(np.max(yv[:,i]) / 3, np.max(Fy[:,i]) / 4, f"$E_{{collision}}=${I[i] * 10**(-3):.2f} kNm", dict(size=20))
    plt.ylabel('Force $F_y$ [N]',dict(size=15))
    plt.xlabel('Displacement $y_v$ [m]',dict(size=15))
    plt.legend(prop={'size': 15})
    plt.title(f"Case C: Force - deflection curves $\phi$={phi0[i]* 180 / np.pi:.0f}$^o$",dict(size=15))
    plt.tight_layout()
    plt.grid();
plt.savefig('phi_var.png')

#Discrepancy plot
c_e = np.array((0.264,0.317,0.461,0.832,1))
desc_c = ((c_e-a_bwz)/a_bwz)*100
E_prop = np.array((23.61, 390.25, 2118.82, 8585.78, 12278.25))
desc_E = ((E_prop-I * 10**(-3))/(I * 10**(-3)))*100
y0 = np.zeros(6)
x0 = [0, 4, 15, 30, 60,80]
plt.figure(figsize=(12,6))
plt.subplot(121)
plt.plot(phi0 * 180 / np.pi,desc_c,color='k')
#plt.plot(x0,y0,color='r')
plt.xticks([0, 4, 15, 30, 60,80])
plt.yticks(desc_c)
plt.grid()
plt.title('Case C: Eccentricity Coeffcient Discrepancy',dict(size=13))
plt.ylabel('$C_{e_{proposed}}$ Percentage over [%]',dict(size=13))
plt.xlabel('$\phi [^o]$',dict(size=13));
plt.subplot(122)
plt.plot(phi0 * 180 / np.pi,desc_E,color='k')
#plt.plot(x0,y0,color='r')
plt.xticks([0, 4, 15, 30, 60,80])
plt.yticks(desc_E)
plt.grid()
plt.title('Case C: Collision Energy Discrepancy',dict(size=13))
plt.ylabel('$E_{proposed}$ Percentage over [%]',dict(size=13))
plt.xlabel('$\phi [^o]$',dict(size=13))
plt.tight_layout();

#Discrepancy plot
c_e_EAU = np.array((0.984,0.984,0.984,0.984,0.984))
desc_c2 = ((c_e_EAU-c_e)/c_e)*100
E_EAU = np.array((88.09, 1212.69, 4525.81, 10159.33, 12277.86))
desc_E2 = ((E_EAU-E_prop)/E_prop)*100
y0 = np.zeros(6)
x0 = [0, 4, 15, 30, 60,80]
plt.figure(figsize=(12,6))
plt.subplot(121)
plt.plot(phi0 * 180 / np.pi,desc_c2,color='k')
#plt.plot(x0,y0,color='r')
plt.xticks([0, 4, 15, 30, 60,80])
plt.yticks(desc_c2)
plt.grid()
plt.title('Case C: Eccentricity Coeffcient Discrepancy',dict(size=13))
plt.ylabel('$C_{e_{EAU}}$ Percentage overestimated [%]',dict(size=13))
plt.xlabel('$\phi [^o]$',dict(size=13));
plt.subplot(122)
plt.plot(phi0 * 180 / np.pi,desc_E2,color='k')
#plt.plot(x0,y0,color='r')
plt.xticks([0, 4, 15, 30, 60,80])
plt.yticks(desc_E2)
```

```
plt.grid()
plt.title('Case C: Collision Energy Discrepancy',dict(size=13))
plt.ylabel('$E_{EAU}$ Percentage overestimated [%]',dict(size=13))
plt.xlabel('$\phi [^o]$',dict(size=13))
plt.tight_layout();

#discrepancy plot
desc_c3 = ((c_e_EAU-a_bwz)/a_bwz)*100
#E_EAU = np.array((88.09, 1212.69, 4525.81, 10159.33, 12277.86))
desc_E3 = ((E_EAU-I * 10**(-3))/(I * 10**(-3)))*100
plt.figure(figsize=(12,6))
plt.subplot(121)
plt.plot(phi0 * 180 / np.pi,desc_c3,color='k')
#plt.plot(x0,y0,color='r')
plt.xticks([0, 4, 15, 30, 60,80])
plt.yticks(desc_c3)
plt.grid()
plt.title('Case C: Eccentricity Coeffcient Discrepancy',dict(size=13))
plt.ylabel('$C_{e_{EAU}}$ Percentage overestimated [%]',dict(size=13))
plt.xlabel('$\phi [^o]$',dict(size=13));
plt.subplot(122)
plt.plot(phi0 * 180 / np.pi,desc_E3,color='k')
#plt.plot(x0,y0,color='r')
plt.xticks([0, 4, 15, 30, 60,80])
plt.yticks(desc_E3)
plt.grid()
plt.title('Case C: Collision Energy Discrepancy',dict(size=13))
plt.ylabel('$E_{EAU}$ Percentage overestimated [%]',dict(size=13))
plt.xlabel('$\phi [^o]$',dict(size=13))
plt.tight_layout();
```

List of Figures

List of Tables